



PHD THESIS

---

**Improve the Understanding of  
Uncertainties in Numerical Analysis of  
Moored Floating Wave Energy  
Converters**

---

Submitted by Andrew William Vickers to the University of Exeter as a Thesis  
for the degree of Doctor of Philosophy in Earth Resources in June 2012.

This Thesis is available for Library use on the understanding that it is copyright  
material and that no quotation from this Thesis may be published without  
proper acknowledgement.

I certify that all material in this thesis which is not my own work has been  
identified and that no material has previously been submitted and approved for  
the award of a degree by this or any other University.

Signature.....

July 30, 2013

## Abstract

The wave energy industry, still in its infancy compared to similar activities offshore, must look to the oil and gas industry for guide lines on design criteria for survival, safety and operational optimisation for installations at sea. Numerical analysis tools for prediction of the response of floating moored structures have become an important part of the design task for the offshore industry offering a low cost and low risk option compared to scale tank testing. However, rather than having only a task of station keeping and survival, the moorings for a wave energy converters (WECs) would also be required to provide the ability of not adversely affecting the power capture task. The main aim of this work is to gain an understanding and reduce the uncertainties in the numerical modelling of WECs.

Experimental work designed and performed under the HydraLab III project of which the author was a member were used to evaluate the response characteristics of a 1:20 scale “generic WEC” device with a 3 point mooring system. The investigation was enhanced through further tests implemented by the author at Heriot-Watt wave tank using a single WEC device. The outcomes from these experiments were used to aid in the implementation of the aim identified above.

Two numerical model categories were set up to understand the uncertainties apparent to the mooring simulations. The first category included only the calculation of the mooring line response using experimental data to inform the motion of the floating body. The second category included the motion response of the floating body coupling the complex behaviour to the moored system. The mooring tension results for the first category shows an error between the numerical prediction and the experimental results up to 16 times that of the experimental value. This was mainly during slack conditions where the mooring line tension was lower than the pretension in the line at still water. During the higher tension events the average error was 26%. For the second category it was found that the numerical predictions of the WEC motion response in six degree of freedom (6DOF) were generally over predicted. The tension predictions for the coupled simulations identified an error of between 1.4 and 4.5%.

The work presented here contributed to the understanding of uncertainties in numerical simulations for WEC mooring designs. The disparity between the simulation and experimental results re-enforced the requirement for a better understanding of highly dynamic responding moored coupled systems. From this work it is clear that the numerical models used to approximate the response of moored WECs could provide a good first design step. Whilst this work contributed to the understanding of uncertainties and consequently reduced some of these, further work is recommended in chapter 6 to investigate the definition of some of the mechanical and hydrodynamic properties of the mooring line. It is also suggested that external functions should be included

---

that would allow to model the coupled effect of Power-Take-Off (PTO) system. It is intended to conduct future work deriving a fully dynamic mooring simulation including the effects of PTO.

## Acknowledgements

This thesis represents research I have carried out over the last four years within the Renewable Energy Group at the University of Exeter, Cornwall campus. It has been the most challenging and rewarding experience I have ever been through and I would like to thank all those who have made it possible.

I would like to thank my primary and secondary supervisors Dr Lars Johanning and the late Prof George Smith. Without their guidance and dedication I would have been lost in the early stages of my work. As my project progressed they were there to guide me through and fought to make themselves available when I needed them. Sadly Prof George Smith passed away before getting the chance to read this thesis and I can only hope that the final product would have met his approval.

I would also like to thank David Parish and Dr Ian Ashton who were always there to help both professionally and personally, mentoring me through my PhD. They both helped me with many aspects of my work and were always on hand to bounce ideas off of.

My PhD project was one of many that were part of the SuperGen Marine Energy Research Consortium. As a result of this I had the privilege to meet many different researchers from many different backgrounds. Many of these researchers have also helped me to complete my project in one way or another and I would like to thank everyone involved with SuperGen.

I could not have made it through the difficult time in my studies without the love and support of my family and I would like to thank them all for putting up with me over last four years.

The final stages of this project have been the most stressful and challenging. I was however, blessed when I met my partner Lucy Cruse who has helped me so much over the last few years, keeping me positive and uplifting me on a daily basis. Within the final months of the thesis and after a very difficult and dangerous pregnancy and birth we had our son Owen Andrew Michael Vickers, who is to become the next great chapter in my life.

# CONTENTS

<b>1</b>	<b>Introduction</b>	<b>16</b>
1.1	Introduction . . . . .	17
1.2	Wave Energy Converters . . . . .	18
1.3	Moorings . . . . .	20
1.3.1	Motion independent device (MID) and Motion dependent device (MDD) . . . . .	22
1.4	Design Criteria for a floating moored system . . . . .	26
1.4.1	First order oscillating forces on small structures . . . . .	27
1.4.2	Radiation and added mass . . . . .	35
1.5	Theoretical Response Amplitude Operators (RAOs) . . . . .	36
1.5.1	Mean drift forces on a small structure . . . . .	37
1.6	Experimental Mooring line damping . . . . .	38
1.6.1	HydraLab III . . . . .	43
<b>2</b>	<b>Numerical modelling</b>	<b>46</b>
2.1	Introduction to Numerical model of a moored structure . . . . .	47
2.1.1	Simple Analytical Models . . . . .	49
2.1.2	Dynamic analysis . . . . .	51
2.2	Dynamic time domain modelling . . . . .	53

---

2.2.1	Environment . . . . .	54
2.2.2	The mooring system model . . . . .	55
2.2.3	Floating body response . . . . .	63
2.2.4	Experimental RAOs . . . . .	65
2.2.5	Numerical RAOs and QTFs using diffraction theory . . . . .	65
2.2.6	Numerical RAOs using 6D buoy approximation . . . . .	70
2.2.7	Mean drift forces . . . . .	70
<b>3</b>	<b>Mooring properties</b>	<b>72</b>
3.1	Introduction to mooring line property characterisation . . . . .	73
3.2	Attachment method . . . . .	73
3.3	Preliminary Tests . . . . .	75
3.3.1	Outcome of Preliminary tests . . . . .	78
3.4	Chosen load extension test method . . . . .	78
3.4.1	Test schedule . . . . .	79
3.4.2	Discussion of load extension results . . . . .	79
<b>4</b>	<b>Mooring line tension prediction</b>	<b>83</b>
4.1	Introduction to Mooring line tension prediction study . . . . .	84
4.1.1	Wave Basins . . . . .	85
4.1.2	Generic WEC . . . . .	93
4.1.3	Motion capture system . . . . .	95
4.1.4	Mooring systems . . . . .	96
4.1.5	WEC Instrumentation setup . . . . .	99
4.2	Test methodologies . . . . .	101
4.2.1	Decay tests . . . . .	101
4.3	Time domain analysis of mooring system . . . . .	103
4.3.1	Vessel representation of the floating body . . . . .	104
4.3.2	Mooring approximation . . . . .	105
4.3.3	Marker buoy approximation . . . . .	105
4.3.4	Simulation condition . . . . .	106
4.3.5	Wave field . . . . .	106
4.3.6	Simulation scheme . . . . .	107

---

4.4	Discussion on comparison between experimental and numerically predicted mooring loads . . . . .	110
<b>5</b>	<b>Motion and tension prediction</b>	<b>124</b>
5.1	Introduction to coupled simulation study . . . . .	125
5.2	Experimental RAOs . . . . .	125
5.2.1	RAO tests with different amplitudes . . . . .	127
5.2.2	Different mooring arrangements . . . . .	129
5.2.3	Power take-off system . . . . .	131
5.3	Numerical RAOs . . . . .	132
5.4	Time domain simulation of coupled system . . . . .	134
5.4.1	Floating body . . . . .	135
5.4.2	Wave environment . . . . .	139
5.5	Discussion on comparison between experimental and numerically predicted tension and response of coupled system . . . . .	140
5.5.1	Regular Wave Comparison . . . . .	140
5.5.2	Irregular wave comparison . . . . .	143
<b>6</b>	<b>Conclusions</b>	<b>158</b>
6.1	Further work . . . . .	162
<b>A</b>	<b>Heriot-Watt test results</b>	<b>167</b>
<b>B</b>	<b>Trondheim MarinTek test results</b>	<b>172</b>
<b>C</b>	<b>RAOs</b>	<b>182</b>
C.1	RAOs . . . . .	183
<b>D</b>	<b>Geometric data file for Trondheim WEC</b>	<b>185</b>
D.0.1	Functions defining Shapes . . . . .	186
<b>E</b>	<b>Numerical RAOs of simple cylinders</b>	<b>195</b>
E.0.2	Simple Cylinder . . . . .	196
E.0.3	Modified simple cylinder . . . . .	196

# LIST OF FIGURES

1.1	Annual mean wave power in the UK MetOffice (2008) . . . . .	17
1.2	Example of Wave Energy Devices . . . . .	19
1.3	Tank power capture measurements on a free-floating slope IPS buoy (Parkin and Taylor (2005)) . . . . .	21
1.4	Illustrative figure of largest natural period against water depth (Haver (2010))	23
1.5	Magnification response with different damping ratios (Chakrabarti. (2001))	23
1.6	Selection criteria for load theories Chakrabarti. (2001) . . . . .	29
1.7	Regimes of flow around a smooth, circular cylinder in oscillatory flow. $Re =$ $10^3$ Sumer and Fredsøe (2006) . . . . .	30
1.8	Regimes of flow around a smooth, circular cylinder in steady current.Sumer and Fredsøe (2006) . . . . .	31
1.9	Inertia coefficient vs KC number for various Reynold numbers Chakrabarti. (2001) . . . . .	32
1.10	Drag coefficient vs KC number for various Reynold numbers Chakrabarti. (2001) . . . . .	33
1.11	Sketch of the incident, diffracted and reflected wave fronts for a vertically placed cylinder Sumer and Fredsøe (2006) . . . . .	36
1.12	Definition of steady drift load contributions Chakrabarti (2005) . . . . .	38
1.13	Small scale test results . . . . .	41



1.14	Experimental mooring arrangements . . . . .	42
1.15	Time histories results for Orkney experiments . . . . .	43
1.16	Stiffness results Johanning and Smith (2008b) . . . . .	43
1.17	Schematic of WEC device . . . . .	44
2.1	Difference in mooring line behaviour . . . . .	49
2.2	Flow chart for preliminary design approach(Johanning and Smith (2005)) . . . . .	50
2.3	Example flow chart of a possible dynamic analysis . . . . .	52
2.4	Diagram showing the regimes of applicability of the different regular wave theories(Chakrabarti. (2001)) . . . . .	56
2.5	Analog model of Viscoelastic Synthetic Fibre Rope Flory et al. (2004) . . . . .	58
2.6	OrcaFlex model of mooring lines . . . . .	58
2.7	Flow chart of WAMIT showing the subprograms POTEN and FORCE with their associated input and output files . . . . .	66
2.8	Definition of beta as the wave direction for Wamit simulations . . . . .	68
2.9	Panel definition of cylinder . . . . .	70
3.1	Housfield machine . . . . .	74
3.2	Knots considered for attachment of samples . . . . .	75
3.3	Results comparing wet and dry tests . . . . .	80
3.4	Comparison of the steepest linear section of the load elongation curve for the dry pre-loaded sample with data from Davies et al. (2011) . . . . .	81
3.5	Final extension regime to be included in numerical analysis . . . . .	82
4.1	Herriot Watt wave basin . . . . .	86
4.2	Basin Wave Characteristics . . . . .	87
4.3	Comparison between calibration waves and target waves with wave tank limit curve superimposed . . . . .	89
4.4	Tank dimensions . . . . .	90
4.5	Pictures of tank setup . . . . .	91
4.6	Resistive type wave probe . . . . .	92
4.7	Coordinate system for installation . . . . .	93
4.8	Schematic of WEC device . . . . .	95
4.9	Calibration of the motion tracking system using a wand and calibration board . . . . .	96
4.10	Calibrated Qualysis system . . . . .	97

4.11	First mooring system for WEC device . . . . .	98
4.12	Light mooring arrangement . . . . .	98
4.13	Load cells . . . . .	99
4.14	Load cell positions for the WEC in the MarinTek centre basin . . . . .	100
4.15	WEC set-up in Heriot-Watt wave basin . . . . .	100
4.16	Time histories from Roll decay test . . . . .	103
4.17	Comparison between experimental surge data and re-sampled data . . . . .	104
4.18	Marker attachment method . . . . .	107
4.19	3 Dimensional representation of numerical models . . . . .	108
4.20	Comparison between wave profile data from experimentation at 80Hz and re-sampled data at 10Hz . . . . .	109
4.21	Comparison of tension in bow mooring line using different marker buoy approximation . . . . .	111
4.22	Numerical prediction of tension in mooring bow mooring line during test 3030 with different stiffness coefficients . . . . .	112
4.23	Comparison between simulation and experimentation of tension in mooring lines during test 3030 . . . . .	114
4.24	Error between simulation results and experimental results against experi- mental tension for tests 3030 position A . . . . .	115
4.25	Error between simulation results and experimental results against experi- mental tension for tests 3030 position B . . . . .	116
4.26	Difference between the numerical prediction and the experimental data for the tension in the bow mooring line during test 3030 at the different load cell positions . . . . .	116
4.27	Example of snatch load during test 3030 in bow line A . . . . .	117
4.28	Average proportional difference between the experimental data and the nu- merical simulations . . . . .	117
4.29	Comparison spectral density of the tension in the bow mooring line at po- sition A between experimental and numerical data . . . . .	120
4.30	Comparison spectral density of the tension in the bow mooring line at po- sition B between experimental and numerical data . . . . .	120
4.31	Comparison of cost of mooring line materials Harris et al. (2004) . . . . .	122
4.32	Nominal S-N fatigue curves for different mooring materials . . . . .	123

5.1	Applying a moving average and removing trend for time history data . . . .	127
5.2	Example of time history having been separated into individual waves . . . .	128
5.3	Comparison between frequency domain method and time domain method for WEC with light mooring and closed orifice . . . . .	128
5.4	Comparison between the RAO's for tests with the wave paddle gain set to 100% and 50% . . . . .	130
5.5	Comparison between tests with test moorings and soft moorings . . . . .	131
5.6	Comparison between tests with light moorings and open orifice and light moorings and closed orifice . . . . .	133
5.7	body geometry for Cylinder with damping plate . . . . .	135
5.8	Comparison of WAMIT calculated RAO's for a cylinder with damping plate using low, medium, high, very high and ultra-high resolution . . . . .	136
5.9	Error between the different resolution models against the highest resolution model . . . . .	136
5.10	Buoy geometry for Morrison spar buoy approximation . . . . .	137
5.11	Drag on a vertical cylinder source: DNV-RP-H103 (2011) . . . . .	138
5.12	Drag on a horizontal cylinder source: DNV-RP-H103 (2011) . . . . .	138
5.13	Comparison between experimental wave profile and numerical approximation	139
5.14	Comparison of Surge RAOs . . . . .	141
5.15	Comparison of Heave RAOs . . . . .	142
5.16	Comparison of Pitch RAOs . . . . .	142
5.17	Comparison between highest resolution geometry model with and without additional linear damping . . . . .	144
5.18	Comparison of Surge RAOs . . . . .	144
5.19	Comparison of Heave RAOs . . . . .	145
5.20	Comparison of Pitch RAOs . . . . .	145
5.21	Average difference between experimental data and numerical data of the motion and tension results for all tests . . . . .	147
5.22	Probability density estimate for the motion response of the WEC for test 3030 . . . . .	150
5.23	Probability density estimate for the Tension in the mooring line for test 3030151	
5.24	Comparison of spectral density of the wave field between the experimental and numerical data . . . . .	152

5.25	Spectral density of motion of the WEC body over resonant frequency range	153
5.26	Spectral density of motion of the WEC body over wave frequency range . . .	154
6.1	South West Mooring Test Facility . . . . .	165
6.2	SeaRaser device Ecotricity (2012) . . . . .	166
A.1	Translational motion mode decay time histories for the test carried out at Heriot-Watt . . . . .	168
A.2	Rotational motion mode decay time histories for the test carried out at Heriot-Watt . . . . .	169
A.3	Motion results for RAO tests . . . . .	170
A.4	Applying a moving average to the surge motion and subtracting from the data to remove drift motion . . . . .	171
B.1	Decay time histories for different motion modes for the test carried out at MarinTek . . . . .	173
B.2	Motion response for test 3000 . . . . .	174
B.3	Tension results for test 3000 . . . . .	175
B.4	Motion results for test 3010 . . . . .	176
B.5	Tension results for test 3010 . . . . .	177
B.6	Motion results for test 3030 . . . . .	178
B.7	Tension results for test 3030 . . . . .	179
B.8	Motion results for test 3041 . . . . .	180
B.9	Tension results for test 3041 . . . . .	181
C.1	RAO for WEC with moorings with wave paddle set to 100% gain . . . . .	183
C.2	RAO for WEC with moorings with wave paddle set to 50% gain . . . . .	183
C.3	RAO for WEC with soft mooring with wave paddle set to 50% gain . . . . .	184
C.4	RAO for WEC with soft mooring and closed orifice with wave paddle set to 50% gain . . . . .	184
E.1	Comparison of RAO results from WAMIT example 1 and Matlab generated geometry . . . . .	196
E.2	Wire frame models of the quadrant for simple cylinder geometry . . . . .	197
E.3	Full geometry for simple cylinder model . . . . .	198

E.4 Comparison of WAMIT calculated RAO's for a cylinder using low medium  
and high resolution . . . . . 199

E.5 Percentage error between simulations and the high resolution simulation . . 199

# LIST OF TABLES

1.1	Froude-Krylov formulations . . . . .	34
1.2	Numeric values of $C_1 - C_4$ . . . . .	35
2.1	IOPTN input . . . . .	69
3.1	Test schedule for preliminary load tests . . . . .	77
3.2	Schedule of test with used rope . . . . .	79
4.1	Waves used in test program . . . . .	88
4.2	Monochromatic wave properties . . . . .	92
4.3	Polychromatic wave properties . . . . .	93
4.4	Measured values for RMS derived wave amplitudes for monochromatic waves	94
4.5	Natural period ( $T$ ) and damping ratio ( $\zeta$ ) results for decay tests using test and horizontal moorings from the tests in the Heriott-Watt and MarinTek basin . . . . .	102
4.6	Line properties as input to numerical simulation . . . . .	105
4.7	Case 1 simulations . . . . .	109
4.8	Experimental data used in simulation comparison . . . . .	110
4.9	Maximum minimum and mean results from experimental data (exp) and numerical simulations (num) . . . . .	118

5.1 Mass properties for Morrison approximation . . . . . 137

5.2 Maximum, Minimum and Mean results for test 3030 . . . . . 146

5.3 Comparison of the natural periods of the system . . . . . 155

CHAPTER

1

INTRODUCTION TO MARINE  
ENERGY AND MOORINGS



## 1.1 Introduction

As renewable energy becomes a larger contributor to the global energy portfolio, more and more technologies are being developed that make use of different renewable energy sources. Converting ocean wave energy into other useful forms of energy has been of interest for centuries, with the first concepts being tracked back as far as 1799 Payne (2006). Since then, there has been evidence of navigation buoys using wave energy as a power source for lights after World War II where, 300 such devices were deployed around Japan (Payne (2006)). The oil crises of the 1970's kick started a serious interest in ocean wave energy to provide an alternative to fossil fuels and increase security of supply of energy. The wave resource (figure 1.1) in the UK has been estimated to provide a potential contribution of  $50TWh/y$  Thorpe (1999), which amounts to 10-15% of the UK's electricity demand. Research from the Department of Business Enterprise & Regulatory Reform MetOffice (2008) shows that in the UK, the largest resource is in the North Sea around a mile offshore where the resource is around  $70 - 80kW/m$  of wave crest. The general trend for the available resource at a site is an increase in wave power the further off shore the site is. From the current state of development of the marine energy sector, installation of WECs is expected in water depths of between 25-100m.

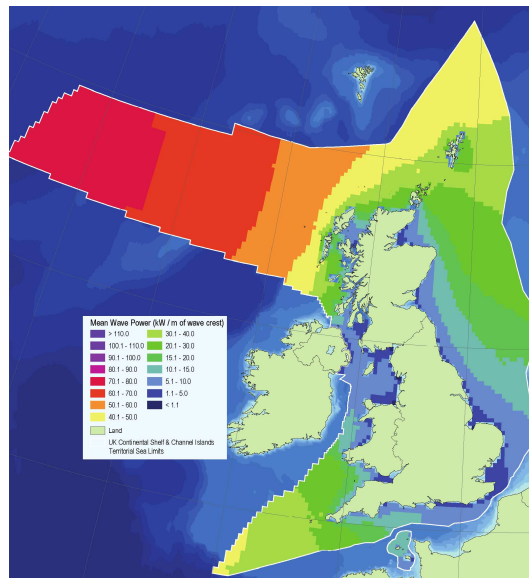


Figure 1.1: Annual mean wave power in the UK MetOffice (2008)

## 1.2 Wave Energy Converters

In recent years WEC devices have progressed through the early design and testing phases and are coming close to full scale operational prototypes (figure 1.2). Due to the infancy of the wave energy sector there has been little or no technology convergence. As such a number of device concepts are being developed simultaneously with many variations. The variation of the design of devices is mainly in the energy conversion method, known as the Power Take Off system or PTO. Several classifications have been made to group WEC devices. Harris et al. (2004) classified the different designs by the operating principal which puts the devices in to one of three categories:

- Oscillating water column (OWC) - Waves cause a water column enclosed by a hollow surface piercing structure, to rise and fall. This alternately compresses and depressurises an air column. The energy is extracted from the resulting oscillating air flow using a Well's turbine.
- Over topping device (OTD) - Ocean waves are elevated into a reservoir above the sea level, which stores the water. The energy is extracted using the difference in elevation between the sea surface and the reservoir using a low head Kaplan turbine.
- Wave activated body - Waves activate oscillatory motions of body parts of a device relative to each other, or of one body part relative to a fixed reference. Primary heave, pitch and roll motions can be identified as oscillating motions whereby the energy is extracted from the relative motion of the bodies or from the motion of one body relative to a fixed reference, typically using hydraulic systems or compressed oil which is then used to drive a generator.

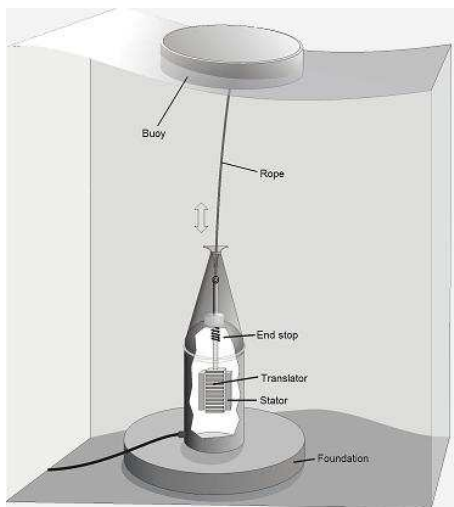
Further classifications were then made in the same work in terms of the installation location and the motion mode response of the devices. The operating location of the device can be either shoreline, near shore or offshore. Pointed out by Harris et.al there is a relation between the operating location and the operating principal of the WEC. The operating depth of 25-100m means that WECs can take the form of all three of the above classifications of WEC. Due to there being no examples of successfully deployed devices to date there is only speculation as to the form WEC installations will take offshore. From the success of the offshore oil and gas industry there is a wealth of knowledge on the design and installation for offshore floating platforms. Chakrabarti. (2001) gives a



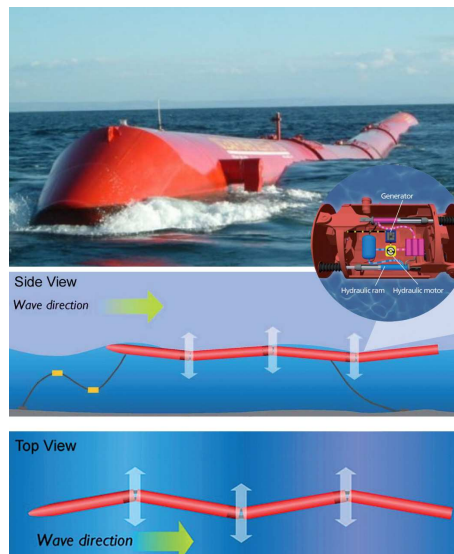
(a) Ocean Energy Buoy



(b) Wave Dragon



(c) Linear generator (Islandsberg project)



(d) Pelamis

Figure 1.2: Example of Wave Energy Devices

good overview of the history of offshore structures in the oil and gas industry. A key point from this shows that as oil and gas installations moved in to deeper water, seabed mounted structures became too expensive. Floating structures offered the solution to providing affordable stable working platforms in such depths. This gives a clue to the form that WEC installations could take, where devices will be floating to avoid costly infrastructure. To keep a floating structure on station in the open sea requires a mooring system, which can be defined as:

“A position mooring system is required to keep a marine structure on station, within an acceptable position envelope, in a specified marine environment and without compromising and preferably even enhancing, the operational function of that marine structure” Fitzgerald (2009).

### 1.3 Moorings

Experimental data regarding the motion response and mooring line tension of a floating moored structure available in literature is often focusing on the properties of the mooring system. The consideration of the requirements of WEC moorings has led for example to the work by Johanning and Wolfram (2005) and Fitzgerald (2009), where specific requirements pertinent to WEC moorings are outlined. The specific requirements for moored WECs come from the complication of allowing them to respond dynamically as required for energy conversion while, at the same time maintaining the device on station. Work by Parkin and Taylor (2005) and Rapaka et al. (2004) investigates the floating performance of a moored WEC and the implications on this caused by variation of moorings and wave parameters. More generic mooring experiments were conducted by Brown and Mavrakos (1999), Kitney and Brown (2001) and Huse and Matsumoto (1988) investigating mooring line loading and damping and comparison with numerical prediction methods. This work outlined methods for evaluating mooring line damping from and indicated the complexities and uncertainties of approximating this data in numerical models. Liu and Bergdahl (1999) compared experimental data to numerical predictions of the floating response as well as mooring line tension and details are given on the performance of the specific method used. Loukogeorgaki and Angelides (2005) provide the results of a parametric study of the effect of the mooring system (line stiffness and damping and mooring line configuration) on the floating response performance a breakwater.

The task of maintaining station even in the most energetic of sea states could be seen as the key requirement in the design of a mooring system. Directly implementing the experience of the offshore oil and gas industry could be seen as an appropriate first step. However due to the added complexity of the operation of WEC devices, the design approach for WEC moorings needs heavy consideration. The use of a mooring system for a wave energy converter where the design of the mooring system has not taken into account the full requirements of the WEC could result in a reduction in efficiency. For example, work undertaken by Parkin and Taylor (2005) where a floating body was placed in a tank and restrained using a rigid frame showed the negative affect of the moorings. The frame allowed the body to respond only in pitch and heave whilst subjected to a wave environment. The same device was then restrained using slack moorings and the same wave environment was used. The result was that the mooring line changed the motion characteristics of the body. By measuring the energy capture width ratio it was clear that

the moorings had a negative effect on the efficiency of the device (figure 1.3).

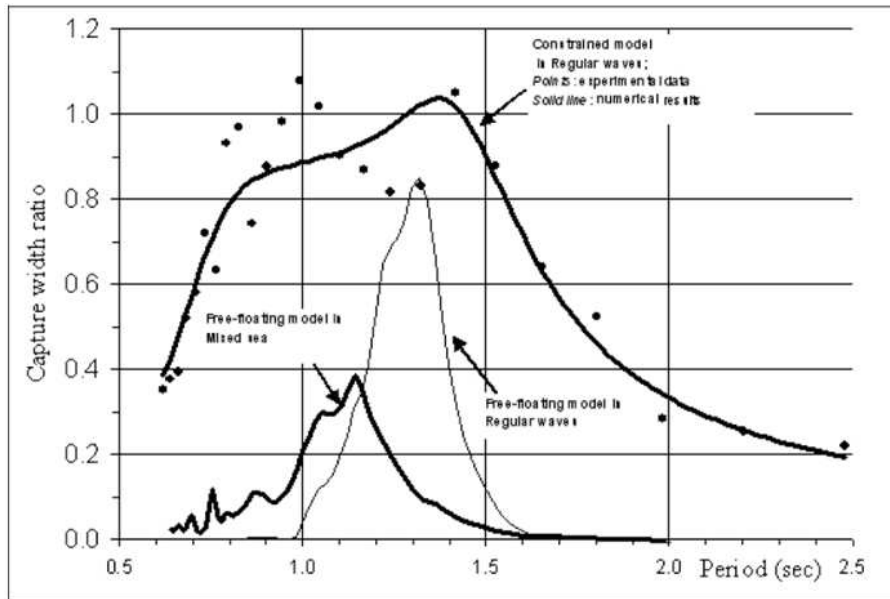


Figure 1.3: Tank power capture measurements on a free-floating slope IPS buoy (Parkin and Taylor (2005))

When looking at the operating conditions faced by offshore platforms and WECs there exists some clear differences. WECs will be designed to match their environment to promote large response characteristics. The WEC will be operating in resonant conditions to maximise its mode of motion required for energy conversion. Figure 1.4 shows the operating condition of larger structures. The largest natural period of the different structure does not coincide with the period of the excitation from the waves avoiding resonance conditions. When operating at resonance, the motion response of a system to excitation forces is large, putting complications on the operability problem for platforms that require a stable environment for their day to day operations. Figure 1.5 shows the response of a single degree of freedom damped mass spring system, which is a simplistic representation of a floating moored structure. It is clear that the response of the mass increases due to the excitation force at a frequency ratio (the ratio of the natural frequency  $\omega_n$  and the excitation frequency  $\omega$ ) of 1, represented by the large amplification factor of the response.

An adequate estimation of the resulting response modes of a moored WEC due to environmental loadings needs to be carried out in order to identify the coupled interaction between the floating body and its mooring. This response of a moored structure in its six degrees of freedom ( $DOF$ ) $\xi_j$  can be expressed in the form:

$$\sum_{j=1}^6 \begin{bmatrix} -\omega_i^2 (M_{ij}^{structure} + M_{ij}^{Mooring}) \\ +i\omega_i (B_{ij}^{structure} + B_{ij}^{Mooring}) \\ + (K_{ij}^{Structure} + K_{ij}^{Mooring}) \end{bmatrix} \xi = F_i \quad (1.1)$$

with  $i = 1, \dots, 6$  being the complex amplitudes of the exciting forces  $F_i$  with the related excitation frequencies  $\omega_i$ . The response is dependent on the environmental excitation forces, in form of primary (wind, wave and current) and secondary (earthquake and icing) sources, and on structural and mooring line inertia, damping and restoring properties. The inertia is dependent on relative acceleration and the total mass  $M_{ij}$  (sum of body and added mass). The damping  $B_{ij}$  coefficients can be considered to be proportional to the square of the relative velocity. The restoring forces are dependent on the stiffness  $K_{ij}$  within the mooring. For analysis purpose the response of the free floating structure is modelled in the first instance separately, using sophisticated models. Structural mass, damping and stiffness characteristics are taken into account and the response of a structure is represented in response amplitude operators ( $RAO_j$ ) that are then used in coupled mooring analysis models.

The damping in the system plays a more important role in the response of the device at resonance where a WEC would be operating, as opposed to the region where the offshore structures place themselves. This sheds some light on the result from the work by Parkin and Taylor, where the mooring had a large impact on the efficiency of the device. The importance the damping has on efficiency of a WEC is an important consideration when designing a WEC. One could say that it shows the importance of the station keeping system in the design of the WEC and making the mooring system an integral part of the design.

### 1.3.1 Motion independent device (MID) and Motion dependent device (MDD)

To design a mooring for different applications the requirements of such a system must first be outlined. For a floating platform the requirements of a mooring position system are:

- Maintain the installation on station
- Provide a stable working platform
- Survive environmental loading

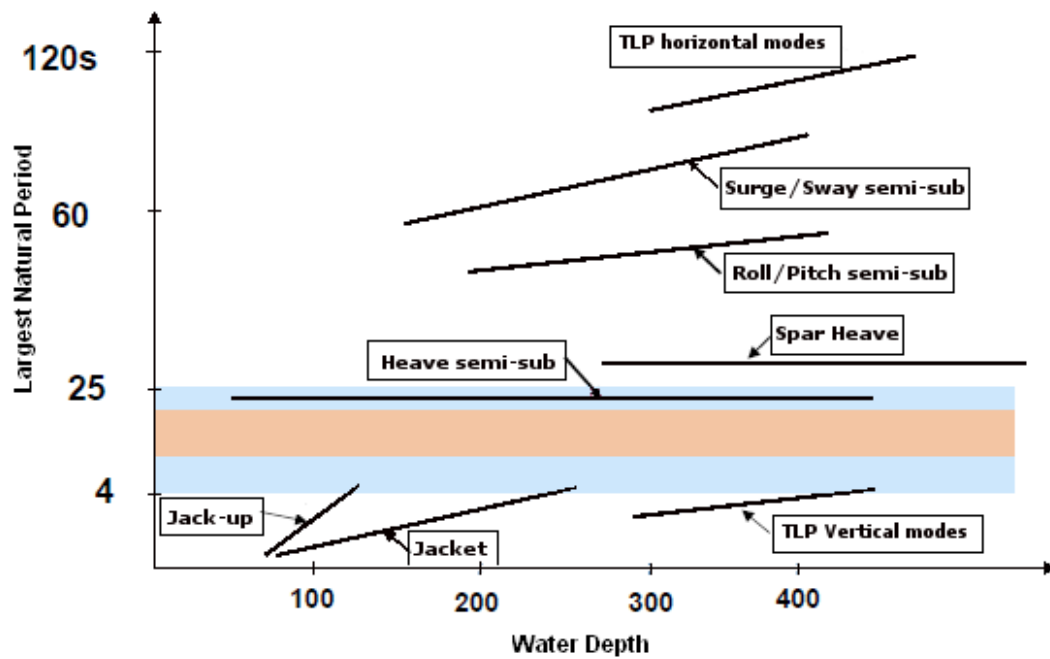


Figure 1.4: Illustrative figure of largest natural period against water depth (Haver (2010))

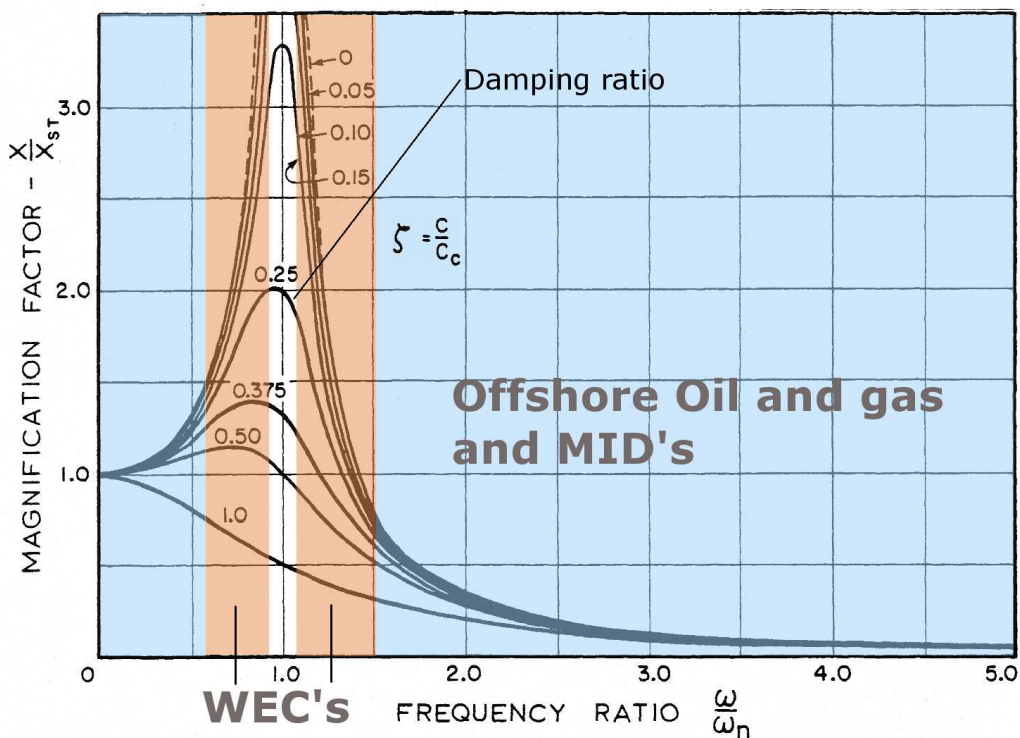


Figure 1.5: Magnification response with different damping ratios (Chakrabarti. (2001))

These criteria are designed for large structures such as oil platforms and FPSOs. WEC devices will be in general of a smaller size than oil and gas installations. Another clas-

sification that has an impact on the station keeping task is also made by Johanning and Wolfram (2005) where devices were separated in to “*motion dependent*” and “*motion independent*”. This is mirrored by Fitzgerald (2009) where reference is made to a similar distinction between “*self reacting*” and “*earth reacting*”. Both authors are classifying WECs by the PTO system.

A motion independent device is a device that is required to move very little in one or more degrees of freedom to maximize the relative motion of the water in the waves. Ocean Energy Buoy (figure 1.2(a)) from Ocean Energy Ltd is an example of a Floating Oscillating Water Column device. The principle of operation is for the water level in a chamber to rise and fall following the waves forcing air through a turbine. To get the maximum air flow, the structure should remain still. If the structure was to move with the waves then there would be no relative motion between the water surface and the turbine. Wave Dragon (figure 1.2(b)) from Wave Dragon ApS is an example of an over topping device and like Ocean Energy’s machine is a motion independent device. This device has a catchment area bound by two arms whose distance from each other decreases toward the structure. The device requires the wave to convert energy by raising the potential of the water up a ramp in to an elevated reservoir, before falling through a low-head turbine. Again this device requires the structure to remain still.

A motion dependent device is a device that is required to follow the surface of the sea to produce maximum relative motion between the floating structure and the stationary power take off system. Linear generator (Islandsberg project) figure 1.2(c) is an example of a heaving buoy. This device is designed to heave up and down with the water surface producing relative motion between the body itself and the power take off system. This device is mainly taking advantage of the heaving motion for the power take off. Rotational motions do not affect the devices ability to convert energy. Pelamis in figure 1.2(d) from Pelamis Wave Power is an example of a device that takes advantage of more than one mode of motion. This device generates power by creating relative motions between different sections of itself. This is done using hydraulic rams between articulated sections. This means the device can convert power from motions of sections in Pitch and Yaw where the axis of each motion is in the centre of that articulated section. The device is required to move about its mooring to align itself with the propagating waves.



This classification allows some criteria for WEC moorings to be established:

- MID's
  - Keep installation on station
  - **Create a stable platform**
  - Survive environmental loading
  - Be cost effective
  
- MDD's
  - Keep installation on station
  - **Allow the device to respond to the environmental loading in the required modes of motion**
  - Survive environmental loading
  - Be cost effective

The point in bold for both sets of basic criteria for the MDD's and MID's is the main difference in the mooring requirements for the different devices. This is an indication as to what degree the mooring will restrain the motion of the device when excited by the environmental loading. Generically this point can be grouped when comparing the mooring requirements for WEC's to offshore platforms as *“to not adversely affecting the primary operation of the device.”* This is more complicated for a MDD as pointed out by Fitzgerald (2009) where he commented that

“A well designed mooring system for wave energy applications will therefore:

a) React steady and slowly varying loads from wind, current and wave drift, without large offset of the device from its zero mean load position (e.g to avoid collisions with adjacent devices in an array)

b) comply with any additional wave induced offsets without inducing large loads in the mooring cables or anchor.

These are somewhat contradictory requirements because (a) requires a stiff response to steady and low frequency loads while (b) requires a compliant response to higher frequency wave loads. Frequency dependent stiffness is normally a function of mass in the system, so that heavier chain mooring

cables will in fact become stiffer at higher frequencies, the very opposite of what is desirable for this application. Therefore, to satisfy compliance to wave frequency loads the inertia and damping of the cable should be minimised. However, in a conventional catenary chain mooring, it is the weight of the chain that provides the static restoring forces. This is perhaps the first indication that the use of other elastic or hydrostatic characteristics of the cable might be better at resisting lower frequency loads while being more compliant to higher frequency wave loads.”Fitzgerald (2009)

## 1.4 Design Criteria for a floating moored system

To aid the design of systems used in the offshore industry such as floating drilling platforms there are a range of rules, guidelines and regulations for mooring systems published by various authorities (e.g. DNV 2001, API 1969, British Standard institution) around the world. These regulations and design criteria could be used for the wave energy industry, however as mentioned by Johanning and Smith (2005) the degree of applicability would be an issue due to the differences that exist in the mooring requirements for WECs and offshore platforms. For example, the level of safety applied to the design, analysis and maintenance of floating structures for the offshore oil and gas industry could be seen as excessive. A WEC, not being manned during operation would lead to a lower risk of loss of life in the event of failure, compared to a drilling platform. Also the environmental risk from harmful chemicals, if used at all, would be lower due to the lower quantities used compared to the oil and gas industry. WEC’s would still present a very real danger to other sea users and other devices due to collision as a result of mooring line failure. The Carbon Trust produced the “Guidelines on design and operation of wave energy converters” Trust (2005), which is designed “ to provide interpretation and guidance on the application of existing Codes and Standards (mainly from industries such as Offshore and Maritime) to wave energy conversion (WEC) devices”. This allows the guidelines and codes that already exist to be applied in a more appropriate way to WECs. However, it does not address the method involved in the derivation of the guidelines.

For all design guidelines for mooring structures the first step is to quantify the environmental loads from wind, wave and current. There is a clear distinction between the loads in terms of the way in which they are imparted to a system. The wind and current can be viewed as slow varying loads and for analysis purposes can be seen as constant.

Wave loads occur in an oscillatory fashion. Wave loads are separated into two categories:

- First order loads - These are loads that oscillate at the wave frequency and are proportional to the amplitude.
- Second order loads - These are slow varying drift loads primarily due to non-linear second order terms in the pressure field associated with the waves.

#### 1.4.1 First order oscillating forces on small structures

The method for the determination of the first order loads on a floating structure can be classified under three headings:

- Morrison equation
- Froude-Krylov force
- Diffraction theory

The size of the floating structure and the wave condition where the structure is placed determine which theory is used. This is because if the structure is small compared to the waves it will follow the surface of the water having very little effect of the wave field itself. However if the body is large compared to the wave field then waves could be reflected and diffracted away from the structure and there could exist a phase difference between the wave and the response. This means that for different sized structures, different effects dominate the response characteristic. To make an assessment of the response characteristic, the size of the structure and wave conditions are characterised using dimensionless quantities and compared against a diagram such as that in figure 1.6. There are two main divisions in the theories that are apparent in figure 1.6 when considering the axis. The x-axis is the dimensionless quantity known as the *Diffraction Parameter* and the y-axis is equivalent to the dimensionless quantity *Keulegan-Carpenter number or KC number*. The Diffraction Parameter (equation 1.2) indicates whether or not the scattering of waves at the water surface by the structure is important and the KC (equation 1.3) number determines the relative importance of inertia and drag forces. It is clear then that the division that can be made is, whether diffraction is important or not. If the structure is large enough with respect to the waves field (i.e  $ka > 0.5$ ) then diffraction and reflection of waves is the dominating characteristic of the response of the body. For situations involving smaller bodies where diffraction is less dominating (i.e  $ka < 0.5$ ) drag and inertia play a more

important role in the response of the body. In this region where the drag and inertia dominate, there is another division which determines the relative importance of the drag v.s the inertial effects. The y-axis in figure 1.6 can be said to be equivalent to the KC number. Starting from equation 1.3 if the flow is sinusoidal then the velocity is given by equation 1.4 which means the maximum velocity is given by equation 1.5 where  $a$  is the amplitude of the motion and  $\omega$  is the angular frequency. This means for a sinusoidal case, the KC number can be as shown in equation 1.6. At the point where the drag and inertia terms dominate, the loads on a submerged member are dependent on the flow regime around the member. Figure 1.7 shows how the flow changes with different KC numbers. Combining figures 1.6 and 1.7 one can deduce that as the flow velocity increases and the KC number increases, the drag becomes more dominant in place of the inertial properties. In this regime another important dimensionless quantity is the Reynolds number. The Reynolds number (equation 1.7) is a widely used and understood non-dimensional quantity when analysing fluid flow around a smooth cylinder in steady flow. The Reynolds number indicates what happens to the flow as it passes around a cylinder. As the Re number increases the flow regime changes from creeping flow to laminar flow and turbulent flow (figure 1.8).

$$ka = \pi \frac{D}{L} \quad (1.2)$$

$$K_C = \frac{U_m T_w}{D} \quad (1.3)$$

Where:

- $U_m$  is the maximum velocity of the flow.
- $T_w$  is the time period of the flow.

$$U = U_m \sin(\omega t) \quad (1.4)$$

$$U_m = a\omega = \frac{2\pi a}{T_w} \quad (1.5)$$

$$K_C = \frac{2\pi a}{D} \quad (1.6)$$

$$Re = \frac{DU}{\nu} \quad (1.7)$$

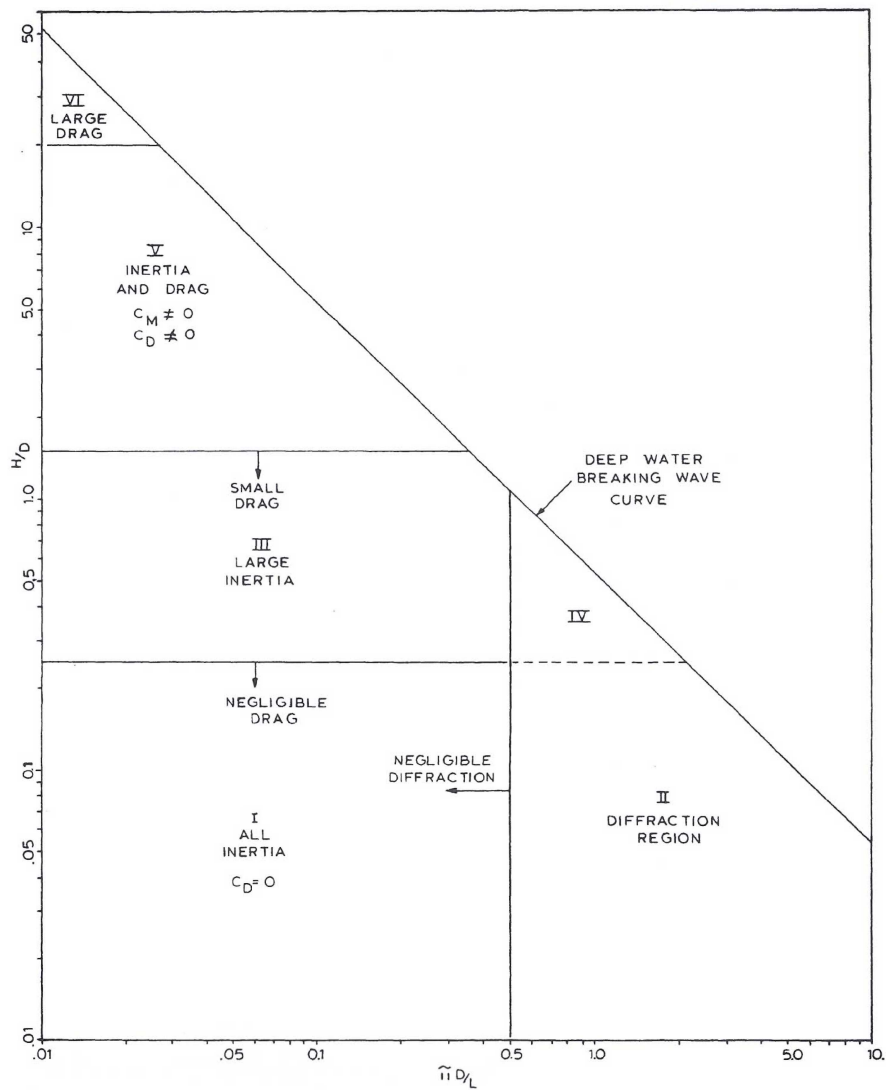


Figure 1.6: Selection criteria for load theories Chakrabarti. (2001)

### Morrison Equation

Whilst working to describe the forces on a pile that extends from the sea bed through the free surface, Morison, O'Brian, Johnson and Shaaf(1950) developed the Morison equation. The work by Morison et.al proposed that the force on the pile from unbroken surface waves consists of two components, inertia and drag. The inertia component of the force is explained by considering a moving water particle which carries momentum as it moves. If the moving particle encounters an obstruction it must pass around it. This requires the particle to accelerate changing its momentum and in turn requiring work to be done. The work done results in a force (1.8) on a small segment of the cylinder ( $dl$ ) that is proportional to the water particle acceleration at the centre of the cylinder (in the absence


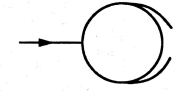
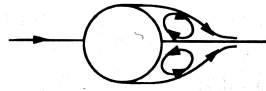
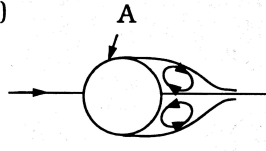
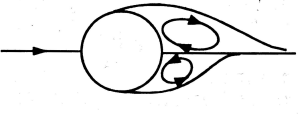
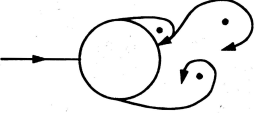
a)		No separation. Creeping (laminar) flow.	$KC < 1.1$
b)		Separation with Honji vortices. See Figs. 3.3 and 3.4	$1.1 < KC < 1.6$
c)		A pair of symmetric vortices	$1.6 < KC < 2.1$
d)		A pair of symmetric vortices. Turbulence over the cylinder surface (A).	$2.1 < KC < 4$
e)		A pair of asymmetric vortices	$4 < KC < 7$
f)		Vortex shedding	$7 < KC$  Shedding regimes

Figure 1.7: Regimes of flow around a smooth, circular cylinder in oscillatory flow.  $Re = 10^3$   
Sumer and Fredsøe (2006)

of the cylinder). The drag component comes from the wake region present downstream of the cylinder. The wake represents a region of low pressure which, coupled with the high pressure region on the upstream side of the cylinder causes a pressure differential. Because the water particle velocity in a wave is oscillatory an absolute velocity ( $|u|u$ ) term is inserted. This ensures that the drag force is in the same direction as the velocity (1.9).

$$df_I = C_m \rho \frac{\pi}{4} D^2 \frac{\partial u}{\partial t} ds \quad (1.8)$$

$$df_D = \frac{1}{2} C_D \rho D |u| u ds \quad (1.9)$$

Where:

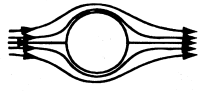
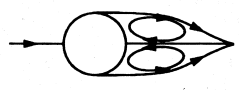
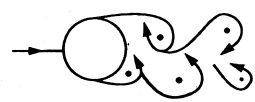
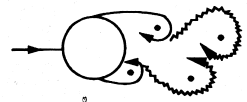
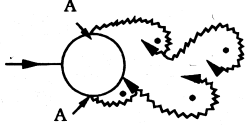
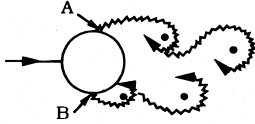
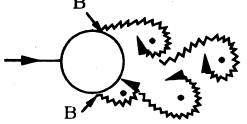
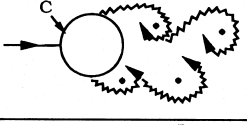
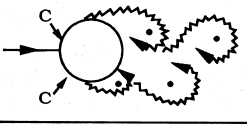
a) 	No separation. Creeping flow	$Re < 5$
b) 	A fixed pair of symmetric vortices	$5 < Re < 40$
c) 	Laminar vortex street	$40 < Re < 200$
d) 	Transition to turbulence in the wake	$200 < Re < 300$
e) 	Wake completely turbulent. A: Laminar boundary layer separation	$300 < Re < 3 \times 10^5$  Subcritical
f) 	A: Laminar boundary layer separation B: Turbulent boundary layer separation; but boundary layer laminar	$3 \times 10^5 < Re < 3.5 \times 10^5$ Critical (Lower transition)
g) 	B: Turbulent boundary layer separation; the boundary layer partly laminar partly turbulent	$3.5 \times 10^5 < Re < 1.5 \times 10^6$  Supercritical
h) 	C: Boundary layer comple- tely turbulent at one side	$1.5 \times 10^6 < Re < 4 \times 10^6$ Upper transition
i) 	C: Boundary layer comple- tely turbulent at two sides	$4 \times 10^6 < Re$ Transcritical

Figure 1.8: Regimes of flow around a smooth, circular cylinder in steady current. Sumer and Fredsøe (2006)

- $df_I$  is the inertia force on segment  $ds$  of a vertical cylinder
- $D$  is the diameter of the cylinder
- $\rho$  is the water density
- $\frac{\partial u}{\partial t}$  is the local water particle acceleration at the cylinder centre
- $C_m$  is the inertia coefficient

- $df_D$  is the drag force on segment  $ds$  of a vertical cylinder
- $C_D$  is the drag coefficient

Combining the inertia (equation 1.8) and drag (equation 1.9) components the Morison equation is written as shown in equation 1.10 in which  $f$  = the force per unit length of the vertical cylinder,  $A_I = \rho \frac{\pi}{4} D^2$  and  $A_D = \frac{1}{2} \rho D$ . The empirical nature of the origin of the Morison equation means that its application to non-streamlined flow problems can be questioned. Although Sarpkaya and Isaacson have described methods of improving Morison's equation the original two term Morison equation has proved reliable in producing accurate predictions of wave forces on small members. There now exists a large library of experimental data for the drag ( $C_D$ ) and inertia ( $C_m$ ) coefficients from numerous laboratory and field experiments. This data allows a designer to choose the appropriate values for  $C_m$  and  $C_D$  using KC number, Re number, roughness parameters and interaction parameters as selection criteria. Experiments by the likes of Sarpkaya and Chakrabarti have produced diagrams (figures 1.10 and 1.9) that allow the drag and inertia coefficients to be determined for specific shapes.

$$f = C_m A_I \frac{\partial u}{\partial t} + C_D A_D |u|u \quad (1.10)$$

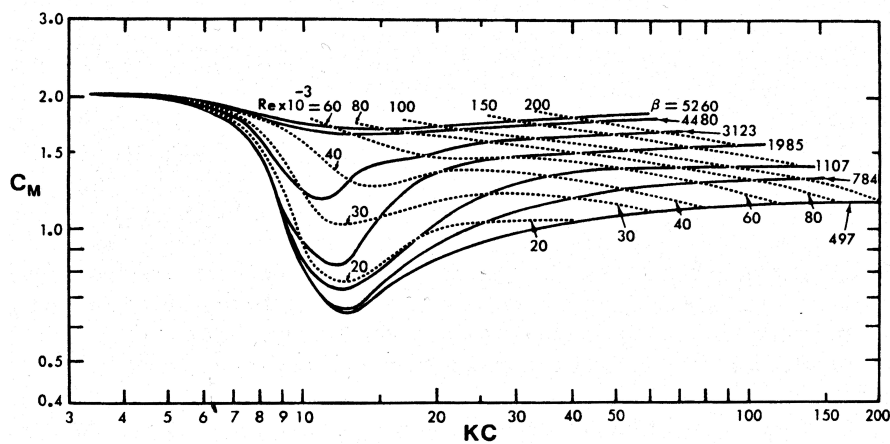


Figure 1.9: Inertia coefficient vs KC number for various Reynolds numbers Chakrabarti. (2001)



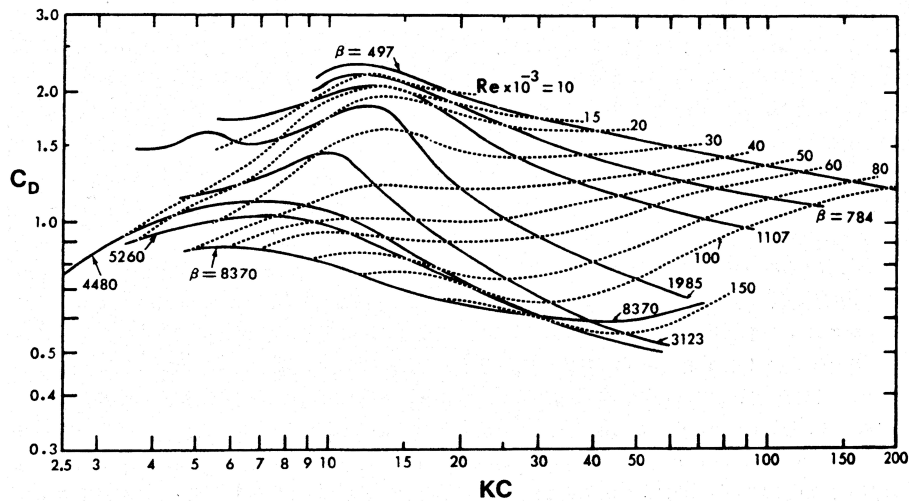


Figure 1.10: Drag coefficient vs KC number for various Reynolds numbers Chakrabarti. (2001)

### Froude-Krylov Theory

The use of the Morison empirical equation allows the computation of the force on a structure from waves to be calculated without the complication of taking into account the complex flow regimes around the structure. For a small body the flow around the wetted perimeter results in vortices. Since the force on the structure is a result of the pressure distribution on the surface, complex flow regimes and vortices make the force calculation complex and difficult. For larger structures the flow essentially remains attached to the surface of the structure. This makes it easier to calculate the force on the body that is due to the pressure distribution on the surface. An important consideration for larger structures is the effect the body has on the wave field itself. For structures where the size is large compared to the wave length a scattering type effect is observed. This scattering needs to be taken into account when calculating the pressure field. The Froude-Krylov force is the name given to the calculation of the force of the floating body when the scattering effect is waived and incorporated by a force coefficient, Chakrabarti (2005). This method has limited application in the offshore oil and gas industry as it is used mainly as a first approximation for large structures. It does however provide a good approximation for moderate sized simple geometry bodies.

The application of the Froude Krylov gives a reasonable approximation for shapes such as a horizontal or half cylinder, a vertical cylinder, a sphere or hemisphere and a rectangular barge. Table 1.1 shows the expression forces and force coefficients taken from

Table 1.1: Froude-Krylov formulations

Basic Shape	X-Force	$C_H$	Y-Force	$C_V$	$ka$ Range
Horizontal Cylinder	$C_H \rho V \dot{u}_0$	2.0	$C_V \rho V \dot{u}_0$	2.0	0-1.0
Horizontal Half Cylinder	$C_H \rho V [\dot{u}_0 + C_1 \omega \nu_0]$	2.0	$C_V \rho V [\dot{\nu}_0 + C_2 \omega u_0]$	1.1	0-1.0
Vertical Cylinder	$C_H \rho V \frac{2J_1(ka)}{ka} \frac{\sinh(kl/2)}{(kl/2)} \dot{u}_0$	2.0	-	-	-
Rectangular Block	$C_H \rho V \frac{\sinh(kl_3/2)}{(kl_3/2)} \frac{\sinh(kl_1/2)}{(kl_1/2)} \dot{u}_0$	1.5	$C_V \rho V \frac{\sinh(kl_3/2)}{(kl_3/2)} \frac{\sinh(kl_1/2)}{(kl_1/2)} \dot{\nu}_0$	6.0	0-5.0
Hemisphere	$C_H \rho V [\dot{u}_0 + C_3 \omega \nu_0]$	1.5	$C_V \rho V [\dot{\nu}_0 + C_4 \omega u_0]$	1.1	0-0.8
Sphere	$C_H \rho V \dot{u}_0$	1.5	$C_V \rho V \dot{\nu}_0$	1.1	0-1.75

Chakrabarti (2005) where:

- $C_H$  is the Horizontal force coefficient
- $C_V$  is the Vertical force coefficient
- $\dot{u}_0 \dot{\nu}_0$  is the horizontal and vertical water particle velocity at the central axis of the body
- $l_1 l_3$  are the length and underwater depth of the rectangular body
- Values  $C_1 - C_4$  depend on the diffraction parameter  $ka$  give in table 1.2

This table shows the X-Force and the Y-Force along with suitable values of the force coefficient. Also of importance is the “ $ka$ ” number known as the diffraction parameter ( $ka = \pi D/L$  where  $D$  is the diameter of the structure and  $L$  is the wave length of the waves).

### Diffraction Theory

When the structures are large enough compared to the wave length of the wave field, the structure itself alters the wave field. This is due to diffraction and reflection of the wave field depicted in figure 1.11, where the reflected waves move outward from the cylinder on the upstream side and the waves are bent (diffracted) round the cylinder on the sheltered or downstream side. Because the structure is large the flow around the structure again remains attached to the surface allowing the flow to be described well by the potential flow, Chakrabarti (2005). This allows the potential function generated in the vicinity of the structure from the known incident wave potential. Several methods have been established for the this, one of which is the Boundary Element Method (BEM). The BEM is the basis for a number of different commercially available computer programs. The technique for BEM is to discretise the geometry of the structure in to flat panels where the corners are identified to the program. This is known as “*Lower Order BEM*” (LOBEM).

Table 1.2: Numeric values of  $C_1 - C_4$ 

$ka$	$C_1$	$C_2$	$C_3$	$C_4$
0.1	0.037	15.09	0.042	12.754
0.2	0.075	7.537	0.085	6.409
0.3	0.112	5.056	0.127	4.308
0.4	0.140	3.825	0.169	3.268
0.5	0.186	3.093	0.210	2.652
0.6	0.223	2.612	0.252	2.249
0.7	0.259	2.273	0.292	1.966
0.8	0.295	3.024	0.332	1.760
0.9	0.330	1.834	0.372	1.603
1.0	0.365	1.385	0.411	1.482
2.0	0.673	1.105	0.745	1.034
2.5	0.792	1.031	0.876	0.989
3.0	0.955	0.989	1.015	0.978
4.0	1.000	0.087	1.945	0.985

This method requires a large number of panels to accurately describe complex or curved surfaces. Chakrabarti (2005) mentions the requirement of 2000-3000 panels for a structure such as a semi-sub or FPSO. This requirement of a large number of panels gives the pre-processor of the computer program, which is tasked with generating the panels, a lot to do, increasing the overall computation time. There is a more advanced panelling method developed which can incorporate curved panels. This is known as “Higher Order BEM” (HOBEM) and has the advantage of being able to better follow complex geometry due to the use of curved panels. Less discretisation is required, reducing the number of panels, decreasing the computation time. As mentioned by Chakrabarti (2005) the two methods provide similar results in predicting the response characteristics of a floating body.

#### 1.4.2 Radiation and added mass

The previous sections describe the loads on a floating rigid body due to wave excitation. If one considers a floating rigid body in calm water with no waves or current then the affect that the body has on the environment is considered. If the body is forced to oscillate at the wave frequency, the body will generate waves which will radiate away from the

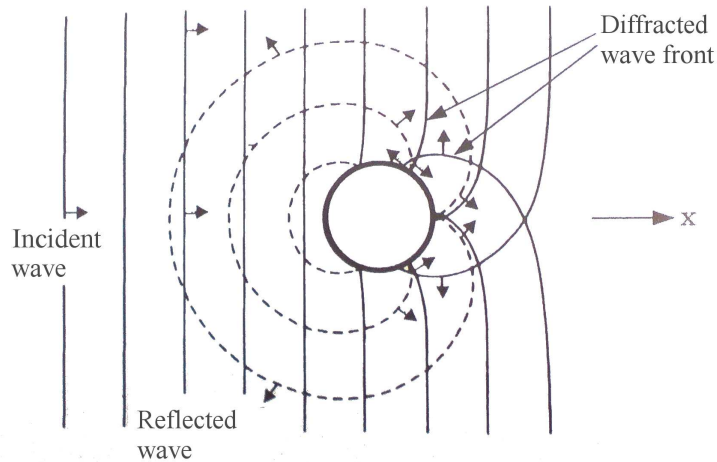


Figure 1.11: Sketch of the incident, diffracted and reflected wave fronts for a vertically placed cylinder Sumer and Fredsøe (2006)

body. Using the same principal as the diffraction calculation, the fluid pressure forces are integrated over the body surface giving the resulting in forces and moments on the body. The result of this allows the added mass and damping loads on the body to be written as equation 1.11 where  $F$  is the load or moment of the motion mode  $k$ ,  $\nu$  is the displacement in the motion mode  $j$  and  $A$  and  $B$  are the added mass and damping coefficients respectively. More detail on this can be found in Faltinsen (1990).

$$F_k = -A_{kj} \frac{d^2 \nu_j}{dt^2} - B_{kj} \frac{d\nu_j}{dt} \quad (1.11)$$

## 1.5 Theoretical Response Amplitude Operators (RAOs)

The inputs to the different methods depend on the assumptions that are to be made in the approximation. Chakrabarti. (2001) states “Generally inertial systems are linear and drag systems are non-linear”. An important point is that if a system is linear then the response of the system, when normalised to the wave amplitude, to regular waves will be invariant of the wave amplitude at a given frequency. If the normalised response of a given system is evaluated over a given range of frequencies, then this function is named a Response Amplitude Operator or RAO. The RAO is a transfer function that can transfer between the wave amplitude input and the motion response amplitude of the system, in the degree of freedom that the RAO has been calculated for. This means that the inertia part of Morison’s equation, Froud-Krylov force and the total force by diffraction theory

are linear with wave amplitude and can be written as in equation 1.12 where  $\eta$  is the wave profile as a function of time.

$$Response(t) = (RAO)\eta(t) \quad (1.12)$$

### 1.5.1 Mean drift forces on a small structure

The above calculations for the force on a floating body include only the first order forces. These are the linear forces that oscillate at the incident wave frequency. “Wave drift force” is the term given to the time independent portion of the second order forces on a floating structure. The introduction of non-linear forces on a floating structure arises from the motion of the floating body, the wave free surface and non-linear pressure terms. If these forces are considered up to the second order then the result would be steady and oscillating second order forces. The second order terms correspond to the second power of the wave amplitude. The steady drift forces are the forces over one cycle averaged in time. Four different effects contribute to the second order terms shown in figure 1.12 and detailed below:

- Free surface term - As the water level at the structure changes about the still water position level, the pressure distribution on the structure will change due to changes in the submerged portion of the body. A similar effect is observed due to angular motion of the body.
- Velocity-squared term - Second order forces can result from the inclusion of the velocity squared term in the Bernoulli’s equation, as opposed to only including the linear pressure term.
- Body motion term - The computation of the first order forces on a floating body considers the body to be in the still water position. If the floating body is displaced (as it would in a wave field) the pressure distribution would change. This means that first order pressure distribution along with the free body motion creates second order forces.
- Rotational term - Resolving the forces to the first order assumes that the forces act along the axes (in x,y and z) of the body. Rotational motions would change the direction of these forces in relation to the axis and require them to be resolved resulting in second order forces.

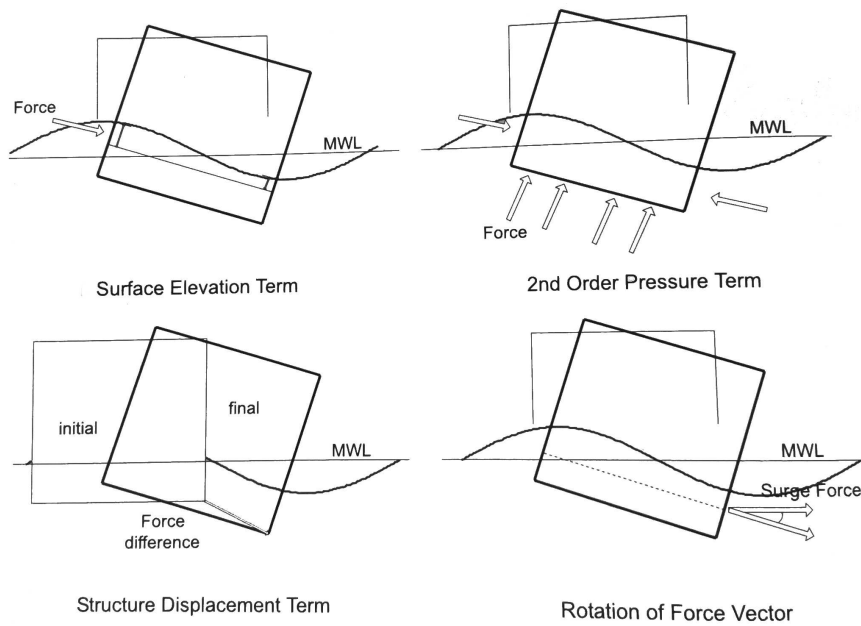


Figure 1.12: Definition of steady drift load contributions Chakrabarti (2005)

The above forces will be second order and higher and the magnitude of the forces will decrease as the order increases. As such, any force above the second order is neglected. The second order steady drift force is the time invariant of the four contributors mentioned above. Although the drift forces on the floating body are second order it is possible to compute them using only first order solution as described in Faltinsen (1990).

The magnitude of the steady drift force is generally 5% of the first order force which is often the order of the uncertainty in the computation of the forces. This could raise the question as to why it is included, Chakrabarti (2005) comments that the second order force is not important for an offshore structure unless it has soft mooring stiffness. This could be the case for renewable energy devices that are required to respond to the wave field.

## 1.6 Experimental Mooring line damping

Experimental data regarding the motion response and mooring line tension of a floating moored structure available in literature is often focusing on the properties of the mooring system. This is a result of the effect the mooring system has on the dynamic response of a floating body in terms of the stiffness of the system and in turn the natural period. This was indicated by the work by Parkin and Taylor (2005) and the example of a single

degree of freedom model. The results from this model (figure 1.5) suggested that the operating regime that WECs operate in causes them to be affected greatly by hydrodynamic parameters that contribute to system damping. There are different sources of damping for a floating moored structure as mentioned by Johanning et al. (2007b) and Bauduin and Naciri (2000). The sources for larger bodies are listed below:

- Viscous hull damping
- Radiation damping
- Wave drift damping
- Mooring line damping

The mooring line damping was, up until the work of Huse and Matsumoto (1988) thought to contribute little to the overall damping of a moored system due to the relatively small diameter of the lines. However as described by Huse and Matsumoto (1988) it has come to light that the motion amplitude of one point of the line can be many times larger than the drift amplitude of the floater bound fairlead. Also the drag force damping is proportional to the third power of the motion amplitude. Thus, in spite of their small drag area, the mooring lines may account for a large amount of the low frequency damping especially in deep water. Indications from Huse (1991b) show that mooring line damping can contribute as much as 80 % of the total damping, depending on the mooring configuration and ocean depth etc.

Physical model tests looking into the dynamics of mooring lines focus on the evaluation of damping of the system. This kind of research has been carried out more intensively by the offshore oil and gas industry but also more recently by researchers in the wave energy field. This lead to experimentation evaluating the motion

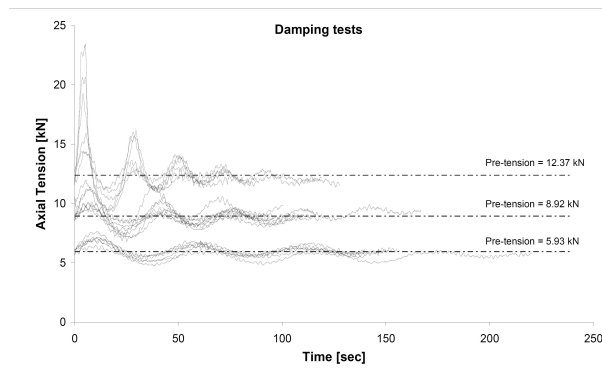
Experimental identification of damping can be done by applying the method of decaying motion (as done by Huse (1991a)) on an unforced oscillation. For this method the system of floating body and mooring is displaced to a known amplitude and then released. The system responds in a decaying motion where it oscillates about its equilibrium position with each oscillation having a smaller amplitude. The rate of this decay represents the damping attributed to the system. The amplitude of displacement is directly proportional to the energy and therefore the difference between one oscillation and the next is equal to the difference in energy between the two cycles. Since the amplitude is decreasing

the difference is proportional to the loss of energy attributed to damping. This method assumes that the floating moored system responds in the same way to a simple damped mass-spring system.

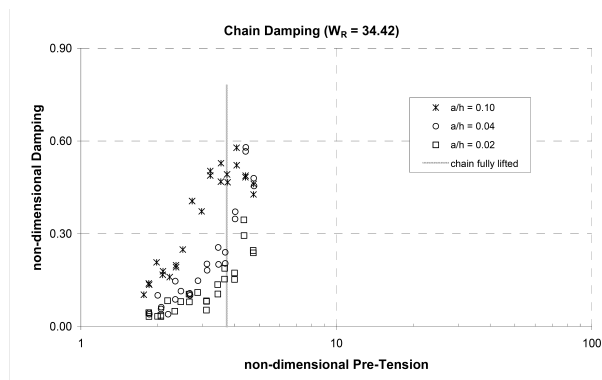
Another method for the evaluation of mooring line damping is using the Indicator diagram method. This method is discussed by Webster (1995) and Bauduin and Naciri (2000) and uses a forced sinusoidal motion. The top end tensions are measured along with the displacement of the fairlead. By plotting the load against displacement for the oscillations, a closed loop for each cycle is observed. The area within the closed loops is proportional to the energy dissipation caused by drag. Johanning et al. (2007b) conducted small scale experiments to evaluate the damping of a moored floating structure. In these tests a 500mm diameter buoy was used as the representation of a generic WEC. The test was done in 2.8m of water and the device was moored with a single catenary mooring line. This test adjusted the pre-tension of the line and evaluated the damping using both the decaying method and the indicator diagram method. The decaying test results are shown in figure 1.13(a). The damping results calculated using the decaying motion method are shown in figure 1.13(b). The sinusoidal forced oscillation is shown in figure 1.13(c) which produced damping results using the indicator diagram method shown in figure 1.13(d). The damping results from the decaying method have much larger spreading than those from the indicator diagram tests. This suggests better repeatability using the indicator diagram method. The increase in damping with pre-tension differs between the methods. The indicator diagram method results show a sharp increase in the damping as the pre-tension is increased to a point where the line becomes fully lifted. This happens when the maximum displacement is reached for each cycle, the damping and stiffness properties are dominated by the characteristics of a taut mooring system. This means that at the point of lift off the line damping is dominated by the elastic properties of the line. In the decay in tests this was not observed. The amplitude during the decay test reduces during the test, changing the lift off point of the line and so affecting the stiffness properties of the line. This means that the dominance of the line stretching on the overall damping reduces as the system response amplitude reduces.

$$\xi_0 + \xi_w + \xi_v = \ln \left( \frac{x(t)}{x(t + TN)} \right) / N \quad (1.13)$$

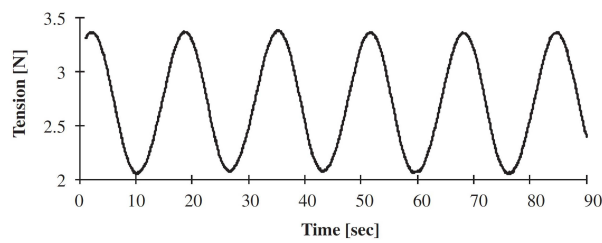




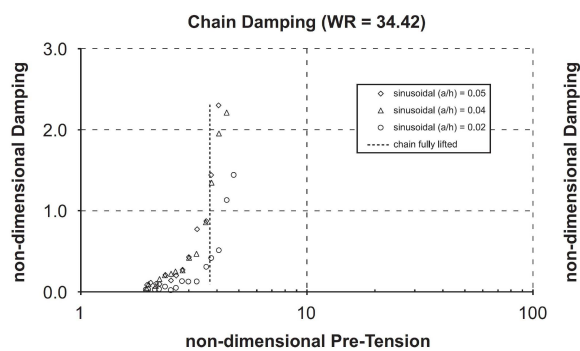
(a) Decaying motion Johanning et al. (2006a)



(b) Damping against Pre-tension from decaying method Johanning et al. (2006a)



(c) Sinusoidal motion Johanning et al. (2006a)

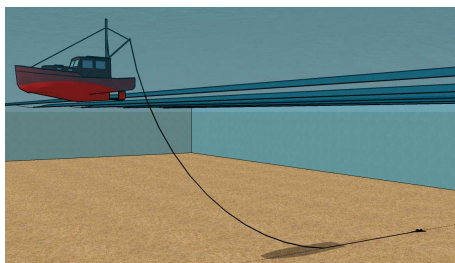


(d) Damping against Pre-tension from indicator diagram method Johanning et al. (2006a)

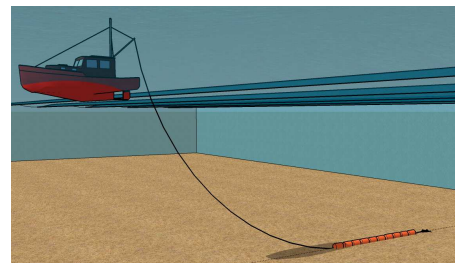
Figure 1.13: Small scale test results

In order to study the mooring conditions for the installation of wave energy converters, large scale experiments have been conducted by Johanning et al. (2007b) in the Scapa Flow in Orkney. In these tests a boat was used to represent the floating WEC. Three different mooring arrangements were investigated namely Catenary chain figure 1.14(a), Chain rope hybrid figure 1.14(b) and Floater sinker s-shape figure 1.14(c) mooring lines. The method for the test was to use the boats thruster to displace the mooring line to simulate the response of a WEC in a wave field. Different tests were performed which included decaying and sinusoidal tests. In the decaying tests the vessel was brought to an equilibrium position by maintaining the boats propulsion system at a constant level. The level of propulsion was increased and held constant, and the boat would surge forward. The boat would oscillate forward and backward with decreasing amplitude until the it came to a halt at the new equilibrium position (figure 1.15(a)).

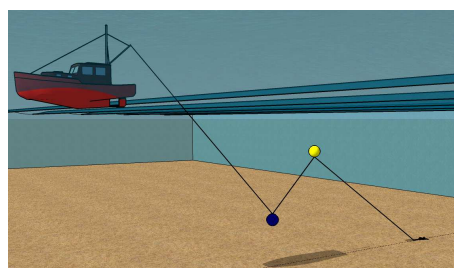
The oscillating tests had the boat surge forward, setting the propulsion system to an RPM setting of 600 (for example) and at the point where the boat had reached the peak excursion for that RPM setting, the revs were reduced to a lower setting of 500 (for example) allowing the vessel to surge backward until the boat had reached the maximum excursion in negative surge direction where the thrust was returned to the higher setting of 600. This produced a sinusoidal motion of the vessel (figure 1.15(b)).



(a) Catenary chain

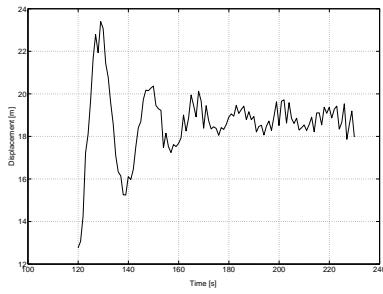


(b) Chain rope hybrid

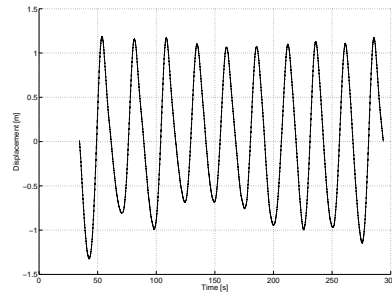


(c) Floater sinker s-shape

Figure 1.14: Experimental mooring arrangements



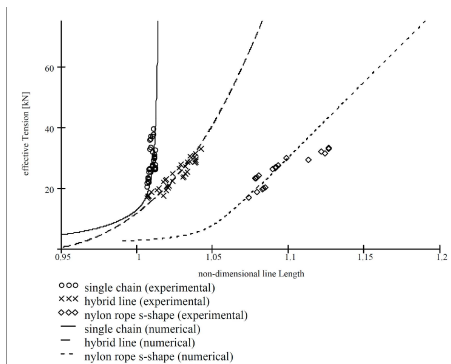
(a) Time history of displacement for decay-ing tests



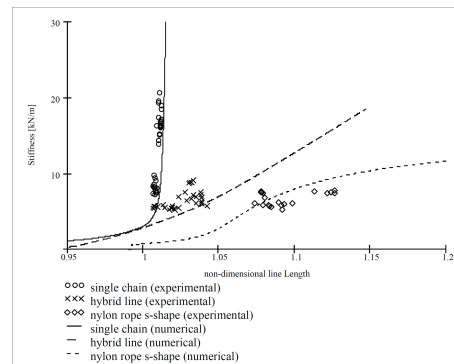
(b) Time history of displacement for sinu-soidal test

Figure 1.15: Time histories results for Orkney experiments

An initial analysis was done by Johanning and Smith (2008b) to identify the stiffness characteristics of the mooring lines. This was done by producing load extension diagrams for the mooring lines looking at the axial tension. The results of the analysis reveal the tension and stiffness characteristics as shown in 1.16(a) and figure 1.16(b) respectively. This information begins to paint the picture of the response characteristics that mooring lines have which is useful as a prediction tool used in the design of mooring systems.



(a) Numerical and experimental load extension for three mooring arrangements.



(b) Related stiffness characteristics towards measured tensions from 1.16(a)

Figure 1.16: Stiffness results Johanning and Smith (2008b)

### 1.6.1 HydraLab III

The Hydralab III project started in April 2006 as an Integrated Infrastructure Initiative (I3) providing translational access to 22 unique facilities. Consortium members from work stream 6 (Mooring and Positioning) of the Engineering and Physical Sciences Research Council (EPSRC) funded SuperGen Marine 2 program applied for additional funding

through this 6th EC frame work program Hydralab III to support their mooring research for multiple moored WECs Bryden and Linfoot (2010). Lead by the University of Edinburgh the consortium for this Hydralab bid also included members from Heriot-Watt University, Queens University Belfast and University of Exeter. The named academics for the University of Exeter were Dr Lars Johanning and Prof George Smith, supported by the author who was the named PhD student on the bid.

The HydraLab proposal was developed to gain access to the 50m by 80m Ocean Basin tank at the MarinTek centre. This facility allowed the measurement of the response of a moored array of floating WECs devices (figure 1.17). The WEC represented an OWC type device with an orifice plate at the top to represent the power take-off system. The tests were designed to measure the motion response of the WECs and the tension in the mooring lines in a range of sea states both regular and irregular as well as including current. Furthermore, the experiments were designed to investigate the behaviour of a single WEC device and the effect of WECs in an array formation of 3 and 5 devices. The scope of these tests was to provide data for the validation of numerical models of the device and mooring components and device motion and power interactions when moored in closely spaced arrays.

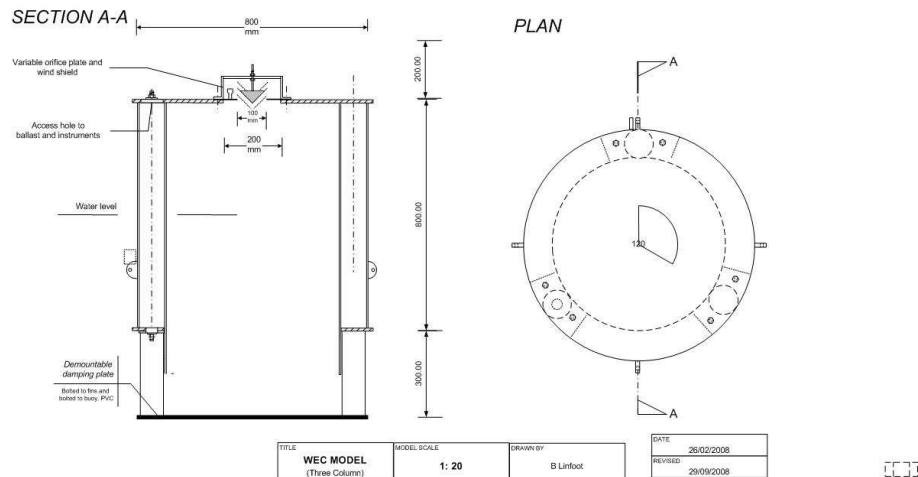


Figure 1.17: Schematic of WEC device

As the main design phase of the tests proceeded, the postgraduate study by the author commenced. The author's inclusion started near to the implementation of the test phase, with contribution to the final phase of preparation, execution of tests at the MarinTek Ocean basin and final analysis of data. Specific tests were identified by the author during the HydraLab investigation that would provide data to form part of the case study for this

project acting as a means for comparison to numerical models. To enhance the data set obtained from the HydraLab III tests further investigations were designed and conducted at the Heriot-Watt wave tank in Edinburgh using the same WEC device and mooring configuration.

CHAPTER

2

INTRODUCTION TO NUMERICAL  
MODEL

## 2.1 Introduction to Numerical model of a moored structure

The goal of a numerical study of a moored structure is to gain predictions of the magnitudes of the motion response of the structure and the forces on the station keeping system. This allows the propriety of the design to be assessed in terms of survivability and operational competence. This chapter introduces numerical models for moored floating structures and describes the inputs and outputs of the various parts of a coupled dynamic time domain model.

The first step is to establish the mooring design that is to be used and conduct an analysis on this design in a static fashion. A static analysis considers constant loads such as gravity, buoyancy and non-time varying current and wind. This allows an assessment of the ability of the design to fulfil the criteria on the mooring such as foot print area and response to mean environmental loading. If this is acceptable, the analysis of the design is taken further, to take into account both the steady forces on the system and the motion of the system. As outlined by the British-Standards (1989) there are three principal methods for the analysis of the response of a floating structure:

- Quasi-static analysis
- Frequency domain analysis
- Time domain analysis

According to the British-Standards (1989) “Quasi-static analysis is the most common form of analysis and is invariably sufficient for the design of most moorings”. The Quasi-static approach to a floating moored system assumes that the motion of the system between two static positions or time steps is uniform and linear. For example, the motion of a platform as it drifts due to tidal current loads from one position to another. If the total distance is broken in to small steps, the current load on the structure would be assumed to be constant between two steps and the motion response of all parts of the system from one static position to the other would happen at the same speed. This is a result of an analysis based on a static situation. For example Bauduin and Naciri (2000) states

A quasi-static approach is based on the following assumptions:

- Inertia effects in the line can be neglected compared to drag
- Line profile at any time during the surge is reasonably well described by the quasi-static catenary equations.

This was also explored by Johanning et al. (2006b) where it was concluded that for wave energy converters a quasi-static approach would only be appropriate as an initial design tool as modelling of a floating WEC system could include some coupling of the mooring controlled horizontal motions as well as the first order motions of roll, pitch and yaw.

The frequency domain analysis includes both first and second order motions of the system. This method requires linearisation of the load and deflection characteristics of the mooring system. The linearisation of the load and motion characteristics of the system may not always be appropriate. To take maximum advantage of a site for WECs, devices are envisaged to be placed in an array configuration. This means lots of devices in close proximity with small available seabed foot print and surface scope for moorings. This suggests the use of taut mooring arrangements. As argued by Johanning and Smith (2008a), in taut situations the tension characteristics of mooring lines become non-linear due to the domination of the elastic properties of the material.

Because WECs will be designed to respond at the wave frequency, the motion response of the system will involve fast responses. If there exists a faster response characteristic then the assumption of a uniform motion through the water of the line is no-longer valid especially for slack mooring arrangements. As mentioned by Barltrop (1998), if the top end structure responds quickly due to wave frequency motions, then a situation similar to that illustrated in figure 2.1 could occur. In this situation the top of the line follows the top end structure but further down the line there is a delayed response. This increases the tension in the mooring line as the line would be required to allow more material strain or resist the motion of the top end structure. This is backed up by the work by Brown and Mavrakos (1999) where different numerical modelling methods were tested and compared. The work revealed that frequency domain methods may not be suitable for systems where there is high frequency and high magnitude of motion in the cables.

The time domain analysis method takes in to account both first and second order wave forces and highly non-linear load deflection mooring characteristics, as well as coupling of the mooring line and the floating body. This method uses standard integral techniques and thus is demanding of computational resources. Often for time domain or dynamic simulation methods a finite element approach is adopted for the modelling of mooring lines. This allows the forces and the response of different parts of the mooring line to be individually calculated. A mooring design approach was suggested by Johanning and



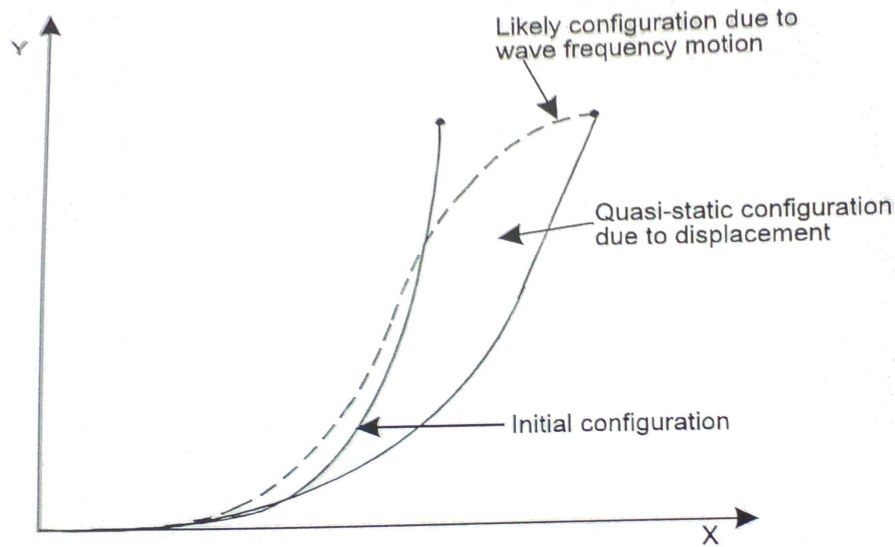


Figure 2.1: Difference in mooring line behaviour

Smith (2005)(figure 2.2) which included the use of both the quasi-static and dynamic methods depending on the type of device (MDD or MID).

From the work by Brown and Mavrakos (1999) time domain analysis methods were described as being “computationally highly intensive” based on finite element analysis. Brown goes on to comment that “time domain simulations appear at present to offer the only possibility for giving reliable results” when dealing with situations where the linearisation used in other numerical methods breaks down.

### 2.1.1 Simple Analytical Models

Simple analytical models have been used to predict mooring line response such as the work conducted by Huse, Lui and Bergdahl and discussed by Bauduin and Naciri (2000). The work by Bauduin and Naciri (2000) introduces the reader to the Quasi-static approach by first running through what governs the motion of a moored body. The motion in surge or sway of a moored body is governed by equation 2.1 where  $M$  and  $M_a$  are the structural mass and added mass respectively.  $K$  is the mooring stiffness, which plays an important part in the mooring task as discussed by Johanning and Smith (2008b). “The stiffness can affect the load extension characteristics of the mooring line causing the line to operate in the non-linear part of the curve”. The mass and restoring forces are such that the natural frequency ( $\omega_0$ ) is quite low, ie 50 to several hundred seconds Bauduin and Naciri (2000).

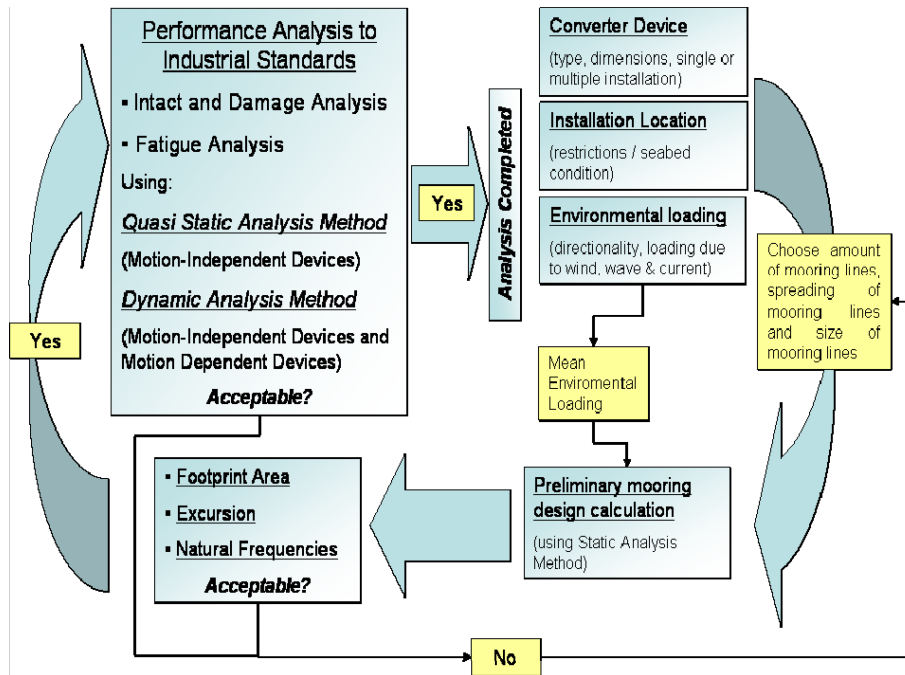


Figure 2.2: Flow chart for preliminary design approach(Johanning and Smith (2005))

$B$  is a *linear* damping coefficient that represents the system damping.

$$(M + M_a) \frac{d^2 X}{dt^2} + B \frac{dX}{dt} + KX = F \quad (2.1)$$

$\xi_d$  is the dissipated energy for one cycle at low frequency for period  $T_0$  and is related to  $B$  by the formula shown in equation 2.2, where  $X$  refers to the low frequency surge motion. If the energy dissipated from one cycle can be calculated then the linear damping coefficient can be calculated using equation 2.3, where  $X_0$  is the single amplitude of the surge oscillation.

$$\xi_d = \int_0^{T_0} B \left( \frac{dX}{dt} \right)^2 dt \quad (2.2)$$

$$B = \frac{\xi_d}{\pi X_0^2 \omega_0} \quad (2.3)$$

The damping may be obtained by integrating the work done by the top tension during one cycle. This would require the use of complex finite element analysis or physical tests. The alternative is to adopt a Quasi-static approach as in Bauduin and Naciri (2000) where the following assumptions are made:

- The mooring line damping is due to drag forces acting on the mooring line as friction effects from contact with the sea bed are not considered. Also only drag forces that

are perpendicular to the line are considered.

- The drag force  $dF$  on an element  $ds$  of the mooring line is described by the Morison equation, ignoring the dependency of the drag coefficient on the Reynolds and Keulegan-Carpenter numbers.

$$dF = \frac{1}{2}\rho_w DC_d |V| V_{ds} \quad (2.4)$$

where  $D$  and  $V$  refer to the drag diameter and the relative fluid velocity in the plane perpendicular to the mooring line element  $ds$

$$X(t) = X_0 \sin(\omega_0 t) \quad (2.5)$$

- Equation 2.5 is used to approximate the low frequency motion of the top end of the mooring line (known as the fairlead) where  $\omega_0$  is related to the un-damped natural period  $T_0$  by  $\omega_0 = 2\pi/T_0$

### 2.1.2 Dynamic analysis

Dynamic analysis carried out by the likes of Webster (1995) involved the modelling of a moored offshore platform. In this work the mooring line damping was estimated and presented using the indicator diagram method. The study presents the variation of mooring line damping from two sources, cross flow and internal damping and compares the magnitude of energy dissipation of the system when excited by different amplitudes and frequencies with different pre-tension in the mooring. Johanning and Smith (2008b) produced a fully dynamic time domain model for comparison with experimental work. The model was put together using the software package OrcaFlex from Orcina. The results showed close correlation between the experimental tension in the mooring lines and the numerical prediction. The Experimental data used in the comparison is from the large scale tests at Orkney described in the previous section 1.6, where a moored vessel was displaced using the vessel's engine. The size of the vessel and the frequency of the motion was such that the motion of the mooring lines could be explained with a quasi-static method.

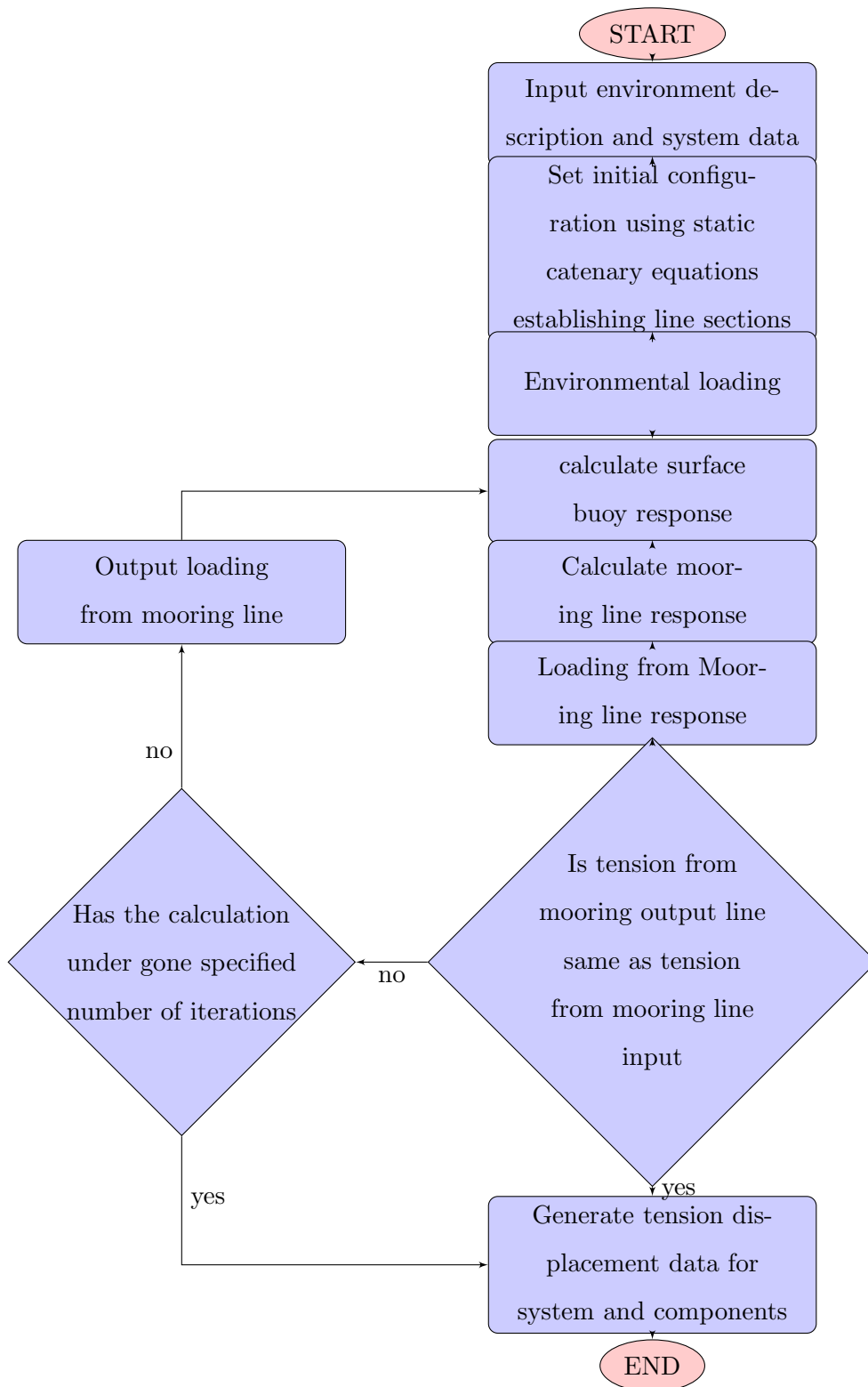


Figure 2.3: Example flow chart of a possible dynamic analysis

## 2.2 Dynamic time domain modelling

To dynamically analyse a physical system in the time domain is to describe how the properties of the system vary with time. To do this the total operating time of interest is broken down into increments. At each increment or time step, the input driving force that will affect change on the system is updated and the response of the system calculated. The simulation then advances to the next time step.

To model a floating structure's response to its environment there are two clear problems, one to model the environment and the other to model the response of the system to the environment. However when it comes to modelling a **moored** floating system, such as a floating MEC, there exists a coupled response of the floating top end structure and the mooring system. This means the mooring system is affected by the environment and the top end structure as well as the top end structure being affected by the environment and the mooring. This requires a dynamic analysis method that can iterate the solution for the floating structure and the mooring until they converge on a common solution. This means that the floating top end structure and the mooring system can be treated as two separate models each dependent on the other to achieve a solution. This is shown in figure 2.3 where the initial conditions of the model are defined. The next step is to define the dynamic driving parameters (in this case wind, waves and current) and then finally allow the model to run and solve for each time step.

The building blocks of such a model can be broken down in to two categories:

- Environment
- Floating moored structure

Due to the coupled interaction between the mooring and floating body, and the complication they independently bring to the modelling tasks it is appropriate to separate these two into their own sections making the problem a combination of the following problems:

- Environment
- Floating body
- Mooring

Each one of the above categories has its own inputs and variations of how the problem can be solved.

### 2.2.1 Environment

The definition of the environment must include all of the sources of environmental loading for the modelled floating system. For the case of a WEC the environment must include the following:

- Seabed
- Sea
- Current
- Wind
- Waves

The industrial standard by the DNV-RP-C205 (2010) outlines a list of environmental conditions to be included in the numerical simulation of floating installations. All of the above mentioned environmental conditions (except the seabed) are included in a list by the DNV as being “the most important to phenomena for marine structures”. The model environment can include a model of the seabed condition to allow the modelling of Catenary moorings that have a portion of the line resting on the seabed. This can be an important factor because the way the seabed will affect the movement of line resting on it will be different if the seabed is hard bedrock compared with soft sand.

#### Wind and Current

The inclusion of the wind and current are done in much the same way, with the difference being that one applies above the water surface and the other below. The wind and current are usually included by specifying the direction and the speed of the flow. The speed of the flow can of course change over elevation.

#### Waves

There are several different options when including the sea state in a model depending on the conditions being modelled:

- Regular waves

- Airy
- Dean
- Stokes'5th
- Cnoidal
  
- Irregular waves
  - Jonswap
  - ISSC
  - Ochi-Hubble
  - Torsethaugen
  - Gaussian Swell
  - User Defined Spectrum.

The selection of the wave theory used depends on the requirements of the simulation. It is possible to simulate regular and irregular waves. For regular there are, as shown above, different theories that can be used. Figure 2.4 shows the selection criteria for the different regular wave theories based on the water depth ( $h$ ), the wave height ( $H$ ) and the wave period ( $T$ ) ( $g$  is gravity).

The selection of the irregular wave spectrum depends on the conditions that the user is modelling. The different types of sea state and how the sea state was developed will change the shape of the spectra.

To aid the application of the hydrodynamic theory for the modelling of the forces and response of a floating system, software packages have been developed by the likes of Orcina and Wamit. While the aim of these packages is geared toward the oil and gas industries they can be applied to the problem of the design of a MEC. This level of applicability is dependent on the ability of the software to handle some of the more complicated issues surrounding the operation of an MEC as discussed in section 1.4.

### 2.2.2 The mooring system model

Programs such as OrcaFlex use a finite element model for the simulation of mooring lines. This means the line, although defined in total length by the user, will be divided in to small segments where each small segment is modelled as a strait rigid massless link in the

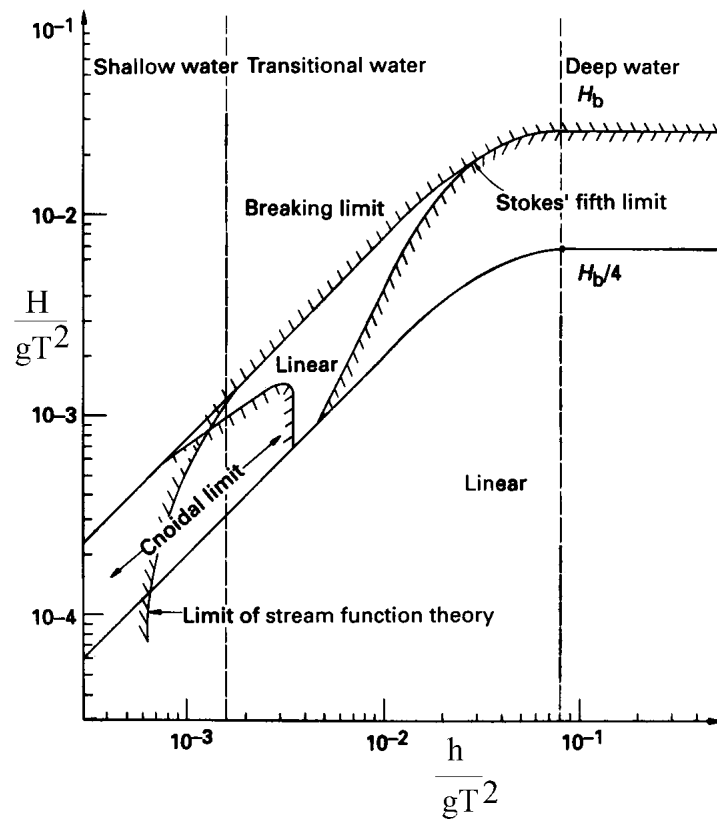


Figure 2.4: Diagram showing the regimes of applicability of the different regular wave theories(Chakrabarti. (2001))



line with a node at each end. The segments handle the modelling of the axial and torsional line properties only. The weight, mass and buoyancy effects are modelled at the nodes.

### **Mooring line mechanical properties**

The numerical approximation of the mooring line must take in to account the mechanical properties of a mooring line material. These are axial, torsional and bending properties. Outlined by Flory et al. (2004), the axial mechanical properties of fibre ropes can be characterised in a similar way to that shown in figure 2.5. Flory does state that “the spring-dashpot model is used here to describe the change-in-length properties of typical synthetic rope. It is over simplified. Simple springs and dashpots do not adequately represent the complicated non-linear and time dependent properties of a fibre rope”, however the model allows the methods of characterisation of the properties for use in time domain simulations to be explained.

The work by Flory characterises a fibre rope stretch characteristic as a spring (**A**), a dashpot **B**, a parallel combination of a spring (**C**) and dashpot (**D**) and a ratchet (**E**). The different components of the model characterise different effects that happen during load cycling of a fibre rope mooring line. The ratchet is designed to represent non-recoverable permanent strain due to a newly constructed rope being made under no-load conditions. This means the structure of a new rope will be relatively loose and uncompressed. An initial loading of the line with sufficient magnitude should allow the structure to “bed in” lengthening the rope permanently. The dashpot **B** represents permanent strain that is a function of applied load and the amount of time over which the load is applied. This strain will not recover over time and has a non-linear trend. The spring **A** and the parallel combination of spring **C** and dashpot **D** represent the elastic stretch of the mooring line. The elastic stretch of the line therefore has two components.

The first is a non-time dependent load extension characteristic which means the line will extend immediately when the load is applied and the magnitude of the stretch will be proportional to the magnitude of load. The second is a time dependent elastic property or delayed elastic stretch. This means that stretch will happen while and after a load is applied. If the load on a line is cycled quickly the time dependent portion of the stretch would not have time to take place. In this case the elastic stretch would be comprised of only the non-time dependent stiffness characterised by the spring **A**. Figure 2.6 shows how this theory would be applied to a finite element model of a mooring line. The following

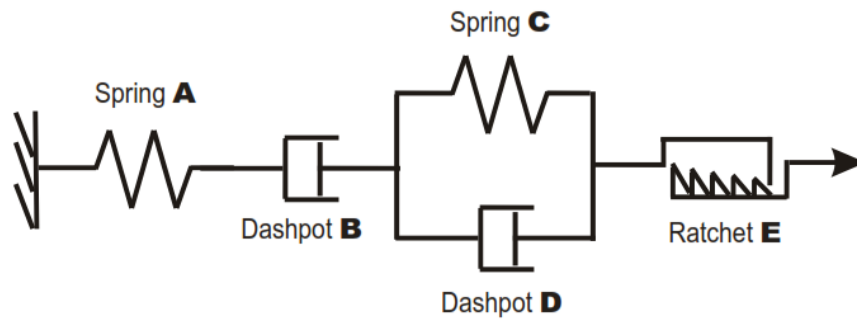


Figure 2.5: Analog model of Viscoelastic Synthetic Fibre Rope Flory et al. (2004)

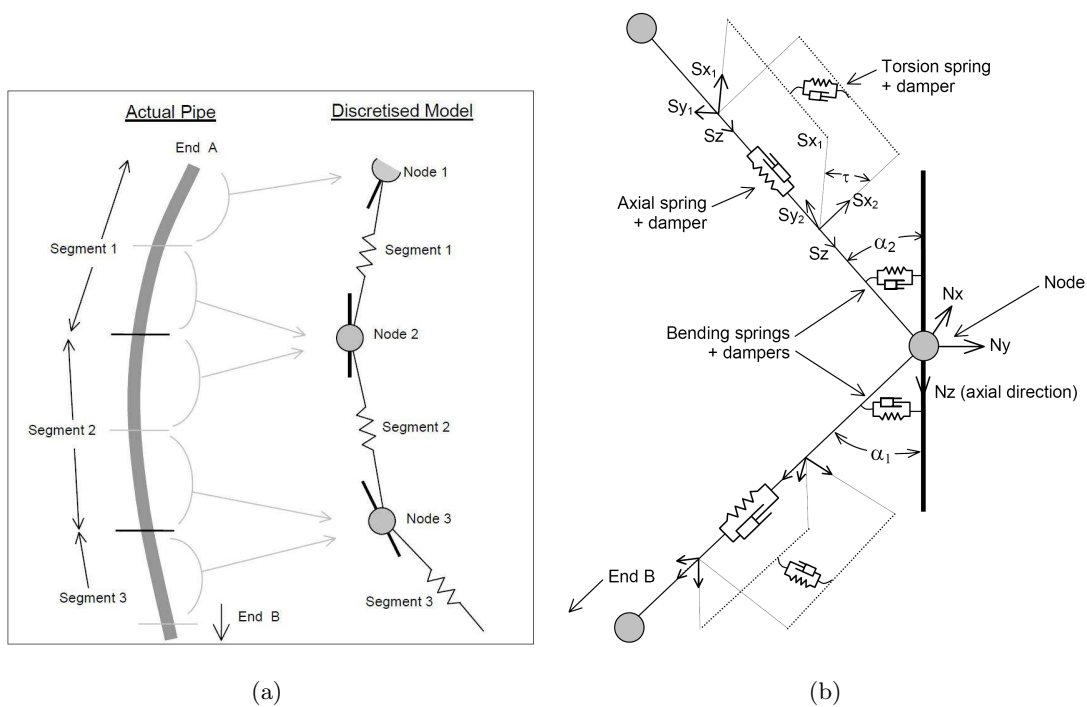


Figure 2.6: OrcaFlex model of mooring lines

definition of the inclusion of the different components of the mechanical stiffness properties use OrcaFlex as a case study.

For simple mooring structures the axial forces in the line would be a result of axial loading however for more complex situations such as hollow pipes the axial tension must be calculated to include the effects of pressure differentials between the internal and external structure of the line and the tension due to the rate of increase on strain (equation 2.6). The axial stiffness is the measure of how the mooring line will respond to axial strain in terms of the load per unit strain. For a non-linear load extension regime which would be a likely case for moorings of wave energy converters, the load extension properties can be defined by the user and replace the  $EA$  term in equation 2.6 as in equation 2.7.

$$T_e = EA\varepsilon + (1 - 2\nu)(P_0A_0 - P_iA_i) + EA.e(dL/dt)/L_0 \quad (2.6)$$

Where:

- $T_e$  =effective tension
- $EA$  = axial stiffness of the line
- $\varepsilon$  = total mean axial strain =  $(L - \lambda L_0)/(\lambda L_0)$
- $L$  =instantaneous length of segment
- $\lambda$  = expansion factor of segment
- $L_0$  = un-stretched length of segment
- $\nu$  = Poisson ratio
- $P_i, P_0$  = the internal and external pressure respectively
- $A_i, A_0$  = the internal and external cross sectional areas respectively
- $e$  =damping coefficient of the line, in seconds
- $dL/dt$  = rate of increase of length

$$T_e = VarT_w(\varepsilon) + (1 + 2\nu)(P_0A_0 - P_iA_i) + EA_{nom}.e(dl/dt)L_0 \quad (2.7)$$

Where:

- $T_w$  =the function relating wall tension to strain as specified by the variable data source defining axial stiffness.

This method for including the axial stiffness in the numerical simulation only takes in to account the non-time dependent stiffness of the mooring line. Experimentation for evaluating this property would be tensile testing where a sample of the mooring material would be axially loaded and measurements taken of the amount of extension. These values would then be normalised to the sample x-section and un-strained length giving the ratios of stress(equ:stress) and strain(2.9).

$$\sigma = \frac{F}{A} \quad (2.8)$$

$$\epsilon = \frac{L_{extended} - L_{original}}{L_{original}} \quad (2.9)$$

The bending moments are calculated by approximating the response to a bending spring damper at each side of the node (figure 2.6). The bending moment depends on the angle between the segment axial direction and the nodes axial direction. This option is suitable for analysing connections such as an umbilical where the stiffness of the umbilical to bending is great enough to have an effect. For rope and chain mooring lines the bend stiffness is assumed to be negligible. However the attachment points of the lines made from chains of rope may incorporate bend stiffeners. The Program can take in to account the following cases:

- Linear isotropic bend stiffness - This is where the stiffness is linear with curvature and the bending moment is the same in both the x and y direction.
- Non-linear isotropic bend stiffness - This is where the stiffness is not linear with the curvature and is the same in the x and y direction.
- Linear non-isotropic bend stiffness - This is where the stiffness is linear with the curvature of the line but differs in the x and y direction.
- Non-linear non-isotropic bend stiffness - This is where the stiffness is non-linear with the curvature and is not the same in the x and y direction.

In all cases the bending moment is based on equation 2.10 which is the linear isotropic case. For the non-isotropic case the curvature ( $C$ ), the bending stiffness ( $EI$ ) and the damping term ( $D$ ) are replaced for the components in the  $S_x$  and  $S_y$  direction ( $C_x, C_y, EI_x, EI_y, D_x, D_y$ ) and calculated separately. In the case of the non-linear bend stiffness.

$$M_2 = EI \cdot |C| + D \cdot d|C|/dt \quad (2.10)$$

where:

- $EI$  = bending stiffness
- $D = \left(\frac{\lambda}{100}\right) \cdot D_C$
- $D_C$  = The bending critical damping value for a segment  $L_0 = \sqrt{SegmentMass \cdot EI \cdot L_0}$
- $\lambda$  = Target bending damping

The shear force in a section is a constant vector as the segment is modelled as a stiff rod. The bending moment varies linearly from one end of a segment to another and so the shear force is equal to the rate of change in bending moment (equation 2.11).

$$ShearForceVector = (M_2 - M_1)/L \quad (2.11)$$

Where:

- $M_1, M_2$  = the bending moment at each end
- $L$  = Length of the segment

The torsion can, like the rest of the properties of the mooring line, be linear or non-linear. For the non-linear properties the stiffness  $K$  is replaced with a function of the twist. The torque is calculated using equation 2.12. The important thing to note is that the twist angle  $\tau$  is the angle between  $Sx_1$  and  $Sx_2$  where the suffix 1 and 2 indicates the different ends of the line.

$$Torque = \left( \frac{K \cdot \tau}{L_0} \right) + C \cdot \left( \frac{d\tau}{dt} \right) \quad (2.12)$$

where:

- $K$ =torsional stiffness
- $\tau$ = Segment twist angle in radians between  $Sx_1$  and  $Sx_2$
- $L_0$ = Un-stretched length of segment
- $\frac{d\tau}{dt}$  = rate of twist (radians per second)
- $C$  = torsional damping coefficient of the line

This method of the inclusion of the mooring line properties is limited to the definition of the non-time dependent, reversible load properties. This relates back to the work by Flory et al. (2004) for the axial properties, where a difference between the static and dynamic stiffness is described. This method of characterisation of the stiffness properties does not separate the static and dynamic stiffness of the mooring line. Instead it assumes there is no difference in the stiffness due to the rate at which load is applied. The work by Flory et al. (2004) shows that the dynamic stiffness of a fibre rope could be higher than the static stiffness. This could cause a model to under predict the load on a mooring.

Accumulated stretch is the property of the line which describes how quickly the mooring line can recover after loading. If the loading cyclic and of sufficient frequency the mooring may not have completely relaxed before the next cycle. This means that there will be residue stretch from the previous cycle. This would result in the mooring increasing in length reducing the stiffness of the mooring. This could lead to a numerical model over predicting the load on a mooring.

As for all of the mooring line properties stated here they assume there will be no damage or time dependent change in the properties due to the cyclic loading which during real conditions would result in fatigue.

### **Mooring line Hydrodynamic properties**

The total load on the line will be the combination of the loads mentioned above and the other non-structural loads such as weight, drag and added mass. Each node on the line will experience all five of the different loads mentioned above but from the segment each side of that node. A model can then calculate the translational and rotational acceleration of the node and integrate to calculate the velocity and position.

Both aerodynamic and hydrodynamic drag and lift are important during a simulation of a floating moored structure. In both cases, Morison's equation is used to implement the drag and lift. The drag formula uses drag coefficients specified by the user. The formula for drag (equation 2.13) uses the drag coefficient ( $C_{dx}$ ) and the relative velocity between the line and the water separated in to normal ( $V_n$ ) and axial ( $V_z$ ). The normal drag force is then a function of the relative normal velocity and the x-direction ( $V_x$ ) and y-direction ( $V_y$ ) components of the velocity. The drag force in the axial direction of the line is then a function of the vertical relative velocity ( $V_z$ ).

$$F_x = P\left(\frac{1}{2} \cdot \rho \cdot (D_n \cdot L) \cdot C_{dx} \cdot V_x \cdot |V_n|\right) \quad (2.13)$$

The selection criteria for the drag coefficient are the Reynolds number and the KC number as mentioned in chapter 1. The drag properties of the line are a contribution to the total damping of the mooring system which arise from the contact between the line and the sea bed (for catenary moorings) and friction within the mooring line itself. Experiments to evaluate the total damping of a mooring line have been undertaken by Johanning et al. (2007a) as mentioned in the chapter 1 where the indicator diagram method is used to evaluate the energy dissipated in a motion cycle of a moored body. Another method of

identifying the damping properties of a system is to perform a decay test on the system, again described in chapter 1.

### 2.2.3 Floating body response

Using industry standard software packages, a range of options are available for the modelling of a floating body in a dynamic analysis. An example package used in this project is OrcaFlex offered by Orcina, which allows the body to be represented as a 6D buoy or a Vessel. Within these options there are sub options as shown below:

#### 6D buoy

The “6D buoy” is a rigid object that has all six degrees of freedom (Surge, Sway, Heave, Roll, Pitch and Yaw). The geometry of the body can be represented in different ways to best approximate the actual case:

- Lumped buoy - A lumped buoy is an object defined by its mass, height and volume. The weight of the buoy is calculated in the same way as for all the different types of 6D buoy using  $F = mass \cdot gravity$ . The buoyancy force of the lumped buoy is dependent on the amount of the body that is submerged. The submerged portion of the buoy is determined by the depth of the centre of mass below the water surface. The precise geometry of the body is not defined and as such the stability of the body is not correctly modelled as variations to roll and pitch stiffness when the body pierces the surface are not included.
- Spar buoys - The Spar buoy model is designed for modelling axi-symmetric buoys where the axis is normally vertical. The spar buoy model is made up of co-axial cylinders mounted end to end. The surface piercing effects are much more sophisticated than the lumped buoy, as heave stiffness and righting moments are included. The intersection of the water surface for each of the cylinders used to make up the geometry is calculated allowing for instantaneous position and attitude.
- Towed Fish - The Towed Fish model is intended for modelling bodies such as towed fish, whose principal axis is normally horizontal. This would be useful for WECs such as the Pelamis device described earlier in the thesis. Towed Fish buoys are identical to Spar Buoys except that the stack of cylinders representing the buoy is

laid out along the x-axis of the buoy, rather than along the z-axis and as such are not suitable for this project.

For all 6D buoys the hydrodynamic loads are calculated using Morison's equation (equation 1.10). There are additional components to the hydrodynamic loading for specific cases. For the lumped buoy for example, the loading is calculated using fluid kinematics at the centre of the wetted portion of the buoy body. These loads are then scaled to represent the loads on the wetted portion only. For the spar buoy and the towed fish the hydrodynamic loading can be specified in different ways depending on the method of the definition of the damping and added mass. If the damping and added mass are defined as values for each cylinder then the all hydrodynamic loads are calculated and applied separately on each cylinder. The added mass and damping can be defined as RAO matrix which means the hydrodynamic wave loading, added mass and damping is applied for the whole buoy. The buoyancy and drag is calculated and applied for each cylinder with the only difference being that the software assumes that the effect of the buoyancy on the wave load is included in the RAO for the wave loads. This means that the buoyancy force is calculated using the mean water surface level across the buoy's structure rather than the instantaneous water surface level.

## Vessel

- **Time history**

An option for the motion of a floating body represented by a vessel is to use time history data. This allows the user to prescribe the motions of the body in 3 or all 6 degrees of freedom. This option can be used to recreate the motion of a vessel or body from data recorded in experiments or in real sea operations. This means there is no requirement to model the body geometry in detail except for visualization purposes or to aid in the spatial orientation of other objects in the model. This option allows measurements that were not taken to be calculated such as mooring line tensions or position and attitude of the mooring line.

- **Calculated (3 DOF)(6 DOF)**

The calculated 3 and 6 degree of freedom option uses user defined RAO(mentioned in chapter 1) to define the body motion in different waves. The 3 DOF option



would only define the translational motions of the body whereas the 6 DOF option would include the rotational motion modes with the translational modes. Using the 3 DOF model there is the option to include superimposed motion for the rotational degrees of freedom of the body using displacement RAOs for the harmonic motion or time histories. The RAOs can be specified to define the displacement of a body in a specific motion mode, normalised to the wave amplitude for a given set of wave periods. Alternatively, they can define the force in the direction of the specific motion mode over the given range of wave periods, again normalized to the wave amplitude.

#### **2.2.4 Experimental RAOs**

In the experimental derivation of the RAOs a regular wave of a known amplitude is generated in a wave tank and the motion response of a device measured. The amplitude of the response of the device is then normalised to the wave amplitude giving the response amplitude operator for the wave frequency used. The experimental derivation of RAOs is generally limited to motions of roll, pitch and heave of the floating body where the restoring force can be purely the buoyancy of the body. For the translational motion of surge and sway and the rotational motion of yaw are often affected by the station keeping system designed to keep the subject with the test window. This means that any response in those latter motions would be a coupled response. The normalised amplitude of the coupled response is not invariant of the wave amplitude due to the mooring system and as such cannot be applied in the method outlined in chapter 1 equation 1.12.

#### **2.2.5 Numerical RAOs and QTFs using diffraction theory**

Numerical derivation of RAOs and QTFs can be done using radiation/diffraction theory. WAMIT is an example of a radiation/ diffraction program developed for analysis of the interaction of surface waves with offshore structures. This means it calculates the core computation that can be used to describe the behaviour of a body in a wave climate. WAMIT is based on a 3D panel method. There are two sub-level programs to evaluate the velocity potentials and desired hydrodynamic parameters called POTEN and FORCE respectively. The environment includes the specification of water depth which can be infinite or a defined depth. The program can handle multiple bodies which can be free floating, restricted or fixed in position. Figure 2.7 shows the structure of WAMIT and the

sub-programs including all inputs and outputs where the input file extensions are shown in italics.

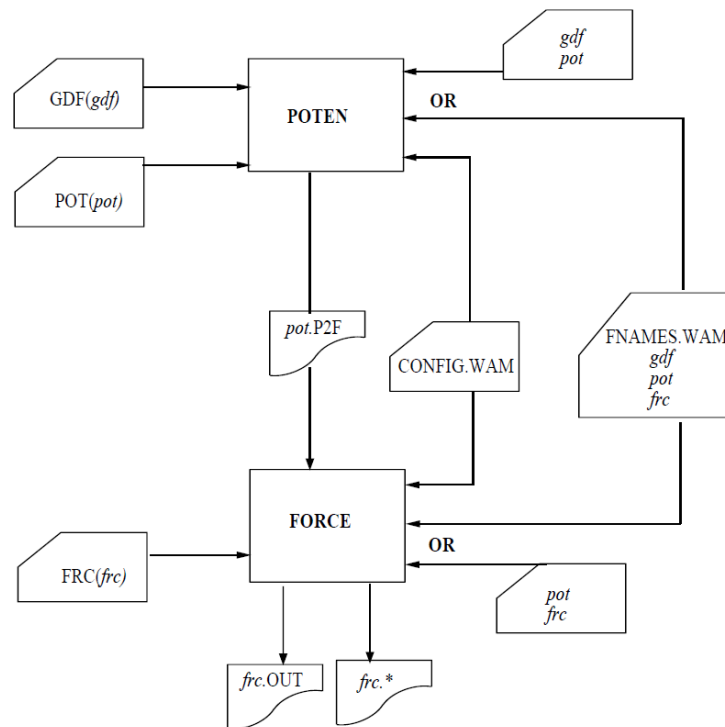


Figure 2.7: Flow chart of WAMIT showing the subprograms POTEN and FORCE with their associated input and output files

The complete range of inputs and outputs for diffraction theory models can be found in the WAMIT user manual C.H.Lee (1995). This section will look at the construction of the model for this project and include the description of the important inputs and results only. WAMIT can be viewed as a virtual water tank where the input files define the different components used in wave tank testing. The program can perform the static tests that are required for dynamic modelling of a device. The construction of the model can be divided in to four parts:

- Configuration
- Potential Control
- Force Control
- Geometric Data

### **The Configuration**

The configuration part of the model is used to define the settings of the algorithm. This includes information on the form of the input data for the other parts of the model. During the computation of the model the number of iterations before the model is classed as unstable will be defined here. This is also where the algorithm is informed as to the method for dealing with free surfaces and the method of discretisation of the body geometry in terms of higher or lower order. In summary this file deals with the computational requirements and matches the simulation to the required accuracy and the computational capabilities.

### **Potential Control**

Potential control allows the user to control the environment of the simulation. This defines information such as the position and orientation of the geometry with respect to a global axis. Also the modes of motion for which to evaluate the radiation, diffraction problem are specified. In WAMIT for example the value called MODE(I) represents the six degrees of freedom of the body, where I=1,2,3 represents surge, sway and heave (along the fixed body axis) respectively and I=4,5,6 represent the modes of roll, pitch and yaw respectively. As well as the body's orientation and position, the wave climate is specified. The wave climate will include the range of wave periods over which to evaluate the response amplitude and the heading in relation to the global axis of the wave field. The headings of the waves are defined by an angle between the positive x-axis of the global coordinate system and the wave direction as shown in figure 2.8.

### **Force Control**

The force control can be looked at as the part of the model that defines the physical properties of the floating. This allows the program to represent the weight and weight distribution of the body. The weight distribution is important to define the difference between a body made of a homogeneous material or one made from different components contributing different mass at different position on the floating body. The definition of the mass and inertia properties here are done using the radius of gyration or mass moments of inertia as well as the centre of gravity.

Also the required outputs are specified in this part of the model. The output options are as shown in table 2.1.

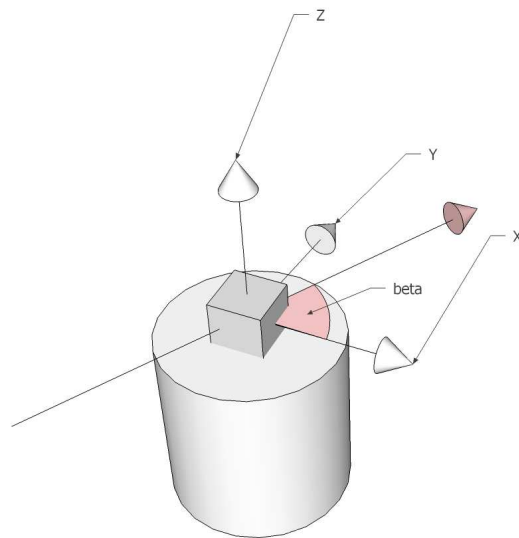


Figure 2.8: Definition of beta as the wave direction for Wamit simulations

### Geometric Data

The Geometric data defines the geometry of the body to be modelled. The input method of the geometry varies depending on the preference of the user as follows:

- The body can be defined using an input file that specifies the panels used to discretise the body geometry. (lower order method)
- Analytical representation
- B-spline representation
- Using Multisurf

In the lower order method the wetted surface of the body is represented by connected, four sided panels. These panels are defined by specifying the corners of each panel. Figure 2.9 shows a cylinder that has been divided into panel sections. The important thing to ensure when building the geometry is the directionality of the panels. Although there is no restriction to the order the panels are defined in, there is a condition on the order of the corners of the panels. As indicated in figure 2.9 the corners of the panels must be defined in a right hand Cartesian fashion. A panel constructed with the corners defined in an order such that the corners are listed in an anti-clockwise direction when looking from the wet side of the model will face the wet side of the model. Panels defined with

Table 2.1: IOPTN input

Option	Description
1	Added-mass and damping coefficients
2	Exciting forces from Haskind relations
3	Exciting forces from diffraction potential
4	Motions of body (Response Amplitude Operator (RAO))
5p	Hydrodynamic pressure on body surface
5v	Fluid velocity vector on body surface
6	Pressure/ free-surface elevation field points
7	Fluid velocity vector at field points
8	Mean drift force and moment from momentum
9	Mean drift force and moment from pressure

the order of the corners listed in a clockwise direction indicate the panel faces away from the wet side when looking from the wet side of the model.

### Model Outputs

The outputs of a model would depend on which options are selected in the input data. For the motion response of the floating body the displacement RAOs would be output. The Displacement RAOs, as mentioned in chapter 1 are the normalised response amplitude of the body in the different motion modes. This allows the response to be scaled to the amplitude of the input wave in a linear fashion. The phase angle between the response of the floating body and the incident wave is output for each wave period along with the RAO. This allows time domain models to take into account the phase lag of the response of the floating body.

The displacement RAOs are of limited use for the analysis of floating moored structures. This is because the assumption of linearisation of the response amplitude of the body is not appropriate when coupled a model is considered as the mooring system will affect the linearity of scaling of the response. A more useful output is the loads on the floating body due to the incident wave field which can again be normalised to the wave amplitude and can be scaled. The linearisation of scaling the load on a free floating body with no mooring system is more appropriate. This load data would allow a time domain simulation to couple the motion response loads with the load response characteristics of a

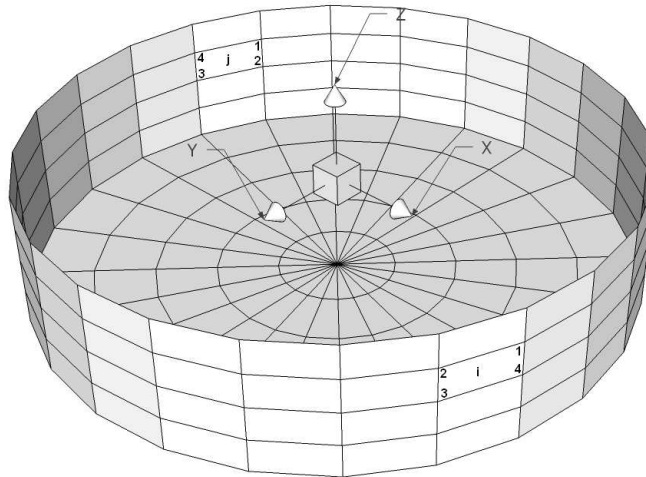


Figure 2.9: Panel definition of cylinder

mooring system. Coupling these two allow the overall response to be evaluated.

### 2.2.6 Numerical RAOs using 6D buoy approximation

The 6D buoy approximation uses Morison equation to solve the loads on the floating body as a result of the incident waves. This method of simulating a floating body in waves allows the problem to be solved in the time domain producing outputs of motion response. It is possible to calculate an RAO from this type of simulation which would allow comparison to experimental measurements of and unrestrained floating body and the frequency domain output from diffraction theory. This would be done by conditioning the numerical simulation to the same wave input regime as that explained in the Experimental RAO section. The analysis of the output of the model would then be identical to the method explained above.

### 2.2.7 Mean drift forces

The application of the wave drift force in the time domain simulation in the case of OrcaFlex mentioned in Chapter 1 depends on the method of representation of the floating body. In the case of the floating body being represented by a “vessel” and therefore using data from a radiation/diffraction package this can be done in much the same way as RAOs using QTFs. The difference between the two is that an RAO is a scaling factor applied to each wave component used to calculate the first order load or response. The drift load is quadratic with the wave amplitude and is applied to each pair of wave components in

the sea state using Quadratic Transfer Functions (QTF). Much like an RAO a QTF scales the amplitude and phase of the load or response. In the case of the floating body being represented by a 6D buoy the loads on the buoy will be calculated using Morison equation. The floating body in this case experience both drag and added mass loads. The wave drift arises naturally from these terms and does not need to be calculated explicitly, as is done for a floating body using diffraction theory data.

CHAPTER

3

CHARACTERISATION OF MOORING  
LINE STIFFNESS PROPERTIES



### 3.1 Introduction to mooring line property characterisation

As explained in chapter 2 the mechanical properties of the mooring are an important input to the numerical model. This chapter will describe experimental procedures and results for the characterisation of the mooring line material used later in numerical models

The mooring line material used in this investigation is a fibre rope supplied by Marlow ropes. The rope is a 1.5mm 3 Strand twisted Aramid Core which results in a very low stretch rope with abrasion resistant high tenacity 16 plait polyester jacket. This chapter will present the work performed to characterise the load extension properties of the mooring line to be used as an input to further numerical studies. To evaluate the load extension properties of the fibre rope a Hounsfeild H20WK tensile test machine (figure 3.1) is used. There are two attachment points at each end of the test area in the machine where a sample can be placed. This device uses an Archimedes screw thread to apply load to a specimen. The left hand attachment point of the machine is fixed in position and instrumented with a load cell. The right hand attachment point is attached to a moving cross beam that can traverse the length of the test area driven by the Archimedes screw thread on a shaft running the length of the test area. There is a dedicated data acquisition system that measures the extension and load simultaneously. The maximum displacement of the cross beam from one attachment point to the other is 820mm.

The specifications of the machine are as follows:-

- load measurement accuracy:  
+/- 1. 0% of applied load from 5% to 100% capacity
- Position measurement accuracy:  
+/- 0. 01% of reading or 0. 001 mm, whichever is greater
- Speed accuracy:  
+/- 1. 0% of full speed

### 3.2 Attachment method

To produce meaningful results it is important to develop a experimental method where the attachment method has a minimal influence on the tensile limit of the specimen. The method of installation was to tie knots at the attachment points of the machine. A problem with the use of knots is that any knot will reduce the tensile limit of the specimen



Figure 3.1: Housfield machine

to different degrees depending on the type knot used. This is because some knots cause “awkward” load paths where the rope bites in to is self.

Another issue is the knot affecting the test when the knot “beds in” or tightens. This will have the effect of allowing the specimen to extend whilst not taking the load as the tension is used to tighten the knot rather than strain the rope. Different knots (figure 3.2) were considered to find an attachment method that allows the maximum tensile limit with the steepest load extension curve. Table 3.1 shows how the different specimens are attached. The preferred outcome is to find an attachment method which produces the lowest percentage elongation before failure.



(a) Over hand stopper knot



(b) Round turn and two half hitches



(c) Bolin knot



(d) Figure of eight follow through



(e) Double fishermans bend

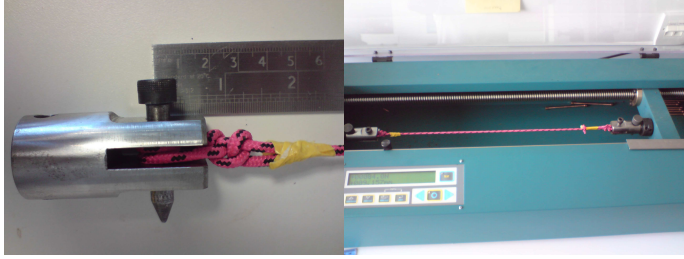
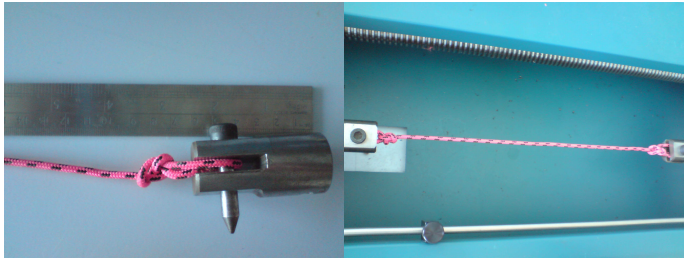
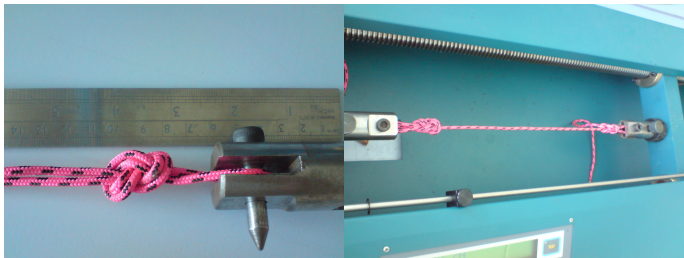
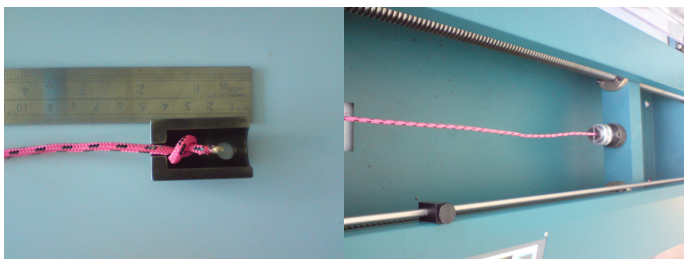
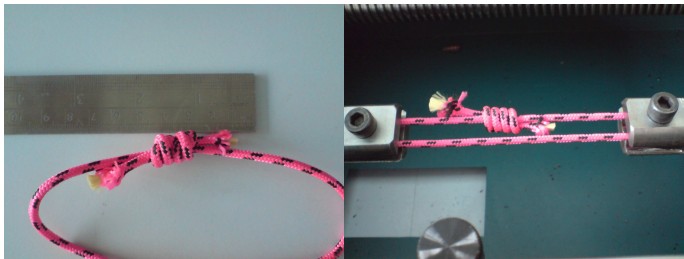
Figure 3.2: Knots considered for attachment of samples

### 3.3 Preliminary Tests

Preliminary tests were run on samples of the line that has not been previously loaded. Table 3.1 shows the attachment methods used and a description of the tests. The important outcome of these tests is to find an attachment method that does not weaken the rope to

such a degree that the load extension curve cannot be evaluated over the required range and also that the method does not result in too much “bedding in” or knot slippage.

Table 3.1: Test schedule for preliminary load tests

Test number	Details	Picture
1	Test 1 uses a round turn and two half hitches at each end	
2	Test 2 uses a boline knot at each end	
3	Test 3 uses a figure of eight follow through	
4	Test 4 uses a stopper knot in a different type of attachment as the other tests	
5	Test 5 uses a double fisherman's knot to form a continuous loop which means the load must be halved assuming the load is distributed evenly through the loop.	

### 3.3.1 Outcome of Preliminary tests

The results from the preliminary tests confirmed that the weakest part of the test sample was the attachment point. The only attachment that resulted in the line failing somewhere other than the knot was the double fisherman's bend. This sample failed at the pin because of the relatively small diameter turn the pin puts in the line. This weakens the line as, the fibres on the outside of the curved part of the line are required to strain more for a given load and there for fail. The mode of failure has two events:

- The fibres on the outer part of the line as it turns on the attachment pin fail first. This allows the line to extend reducing the tension on the line.
- The fibres in the inner part of the line as it turn on the pin take the load as the line extends failing at a similar load to the outer fibres.

The fisherman's bend attachment method allows for the highest load to be placed on the sample reaching a maximum load of 1.9kN. This exceeds the requirements as during the experiments in Norway with the generic WEC the maximum load was observed to be 1339 kN at full scale which would be 0.169kN at model scale. Although other attachment methods were able to exceed the required load, during the tests the knots appeared to slip and bed in. This has the effect of reducing the gradient of the curve causing an under prediction of the load. The double fisherman's bend had a curve that was the steepest that suggests that there was less bedding in of the knot.

## 3.4 Chosen load extension test method

Now that the methodology has been approved tests are run using this method on samples of the line that have been worked in mooring tests and samples that have not. This is to identify if there is any change in the stiffness characteristics due to the line being worked. As the line will be submerged in a mooring situation, samples will be tested both wet and dry to indicate if there is a change in the load extension properties when saturated with water.

### 3.4.1 Test schedule

The test to be done in this series will include testing pre-stretched (used and unused) and none pre-stretched (unused rope) ropes in wet and dry conditions. The pre-stretched rope will be loaded to 10% of its MBL before the main test. The pre-stretching aims to eliminate the bedding in of the knot. Used ropes were used during the Hydralab III tests and have seen various load cycles. All rope tests implemented here are summarised in table 3.2.

Table 3.2: Schedule of test with used rope

Test number	Description
1	Dry test on unused rope with no pre-loading
2	Dry test on unused rope with pre-loading
3	Dry test on used rope with no pre-loading
4	Wet test on unused rope with no pre-loading
5	Wet test on used rope with no pre-loading

### 3.4.2 Discussion of load extension results

Figure 3.3 shows the load against percentage elongation for all test identified in table 3.2. All curves derived from these tests show an initial failure of the ropes at a percentage elongation between 27 to 34. At this stage a breakage of some fibres bundles was observed resulting in a drop of load. A second uploading resulted in a total failure at a percentage elongation between 40 to 47. The findings do not agree with quoted strain data for Aramid, where the breaking strain is discussed to be around 3% (Davies et al. (2011)). It is argued that the results differ as a consequence of measuring a combination of material strain and mechanical elongation for the rope tests presented here. During the tests knot slipping was observed, as well as system slack during the initial phase of the tests. Furthermore, bedding-in on one pre-stretched rope was observed for both unused and used ropes (test 1 & 3 to 5) that resulted in shallower elongation curves up to 4% elongation in comparison to the pre-stretched rope (test 2).

Following the initial stages of loading where the slope is shallow (up to 10%MBL), the curve for test 2 between the range of 1.5% and 3.5% elongation, is significantly steeper in

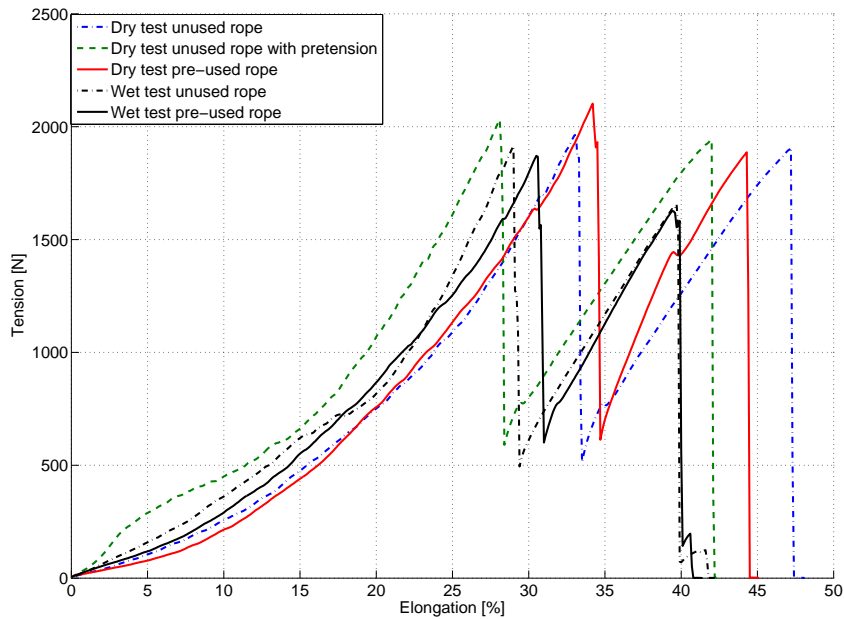


Figure 3.3: Results comparing wet and dry tests

comparison to test 1 (3.4), which provided same test conditions but no pre-stretching. The increase in steepness compared to test 1 is argued to be the contribution of the material strain of the rope. Ahead of the elongation range between 1.5% and 3.5% for test 2 system slack resulted in a shallower elongation curve; and knot slipping contributed to additional elongation after the discussed elongation range, resulting in significant elongation increase to final failure.

Figure 3.4 also shows the linear section of test 2 normalised to 0% elongation removing the system slack contribution. It is argued that making a linear approximation of the load elongation data within the initial shallower range the strain offset at 0% MBL can be removed. Furthermore, literature data have been used to generate a strain curve for an Aramid sample (Davies et al. (2011)) to allow a comparison between test performed here and existing results. Comparing the results from the correct test 2 and the findings from Davies et al. (2011) shows a closer correlation, however, a difference in slope can still be observed. It is argued that this is caused through knot slipping, which would have contributed to the elongation properties during the tests range between 1.5% and 3.5% elongation. Whilst the uncertainty surrounding the impact of the mechanical elongation cannot be quantified, the accuracy of the data acquisition system itself was identified to



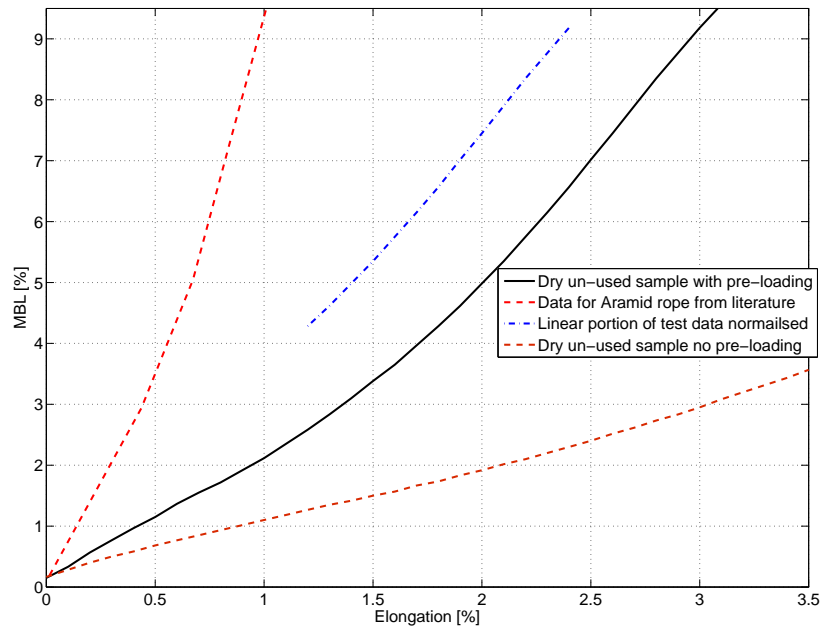


Figure 3.4: Comparison of the steepest linear section of the load elongation curve for the dry pre-loaded sample with data from Davies et al. (2011)

contribute to an experimental error at 5% strain and  $\pm 0.9\%$  in tension, cited earlier.

The characterisation of the elongation properties of the mooring line is required to inform the numerical models as to the stiffness of the mooring line and attachments. The information required can be implemented as a single coefficient or as an elongation curve. The rope tests conducted here were aimed to inform the numerical model with an appropriate elongation curve. Arguably, there still remains a large amount of uncertainty surrounding the stiffness properties of the mooring leg (including connection points, and mooring components) due to the knot slippage and contribution of other mooring components. As a consequence the Hydralab III tests were modelled using an elongation curve derived from test 5 (wet used rope not pre-stretched), arguably including additional elongation contributions. Figure 3.5 shows the graph used to inform the numerical model investigation. In addition some models were also performed with the corrected elongation properties from test 2, to identify the sensitivity contribution to the model. These sensitivity tests are described in a later section in chapter 4.

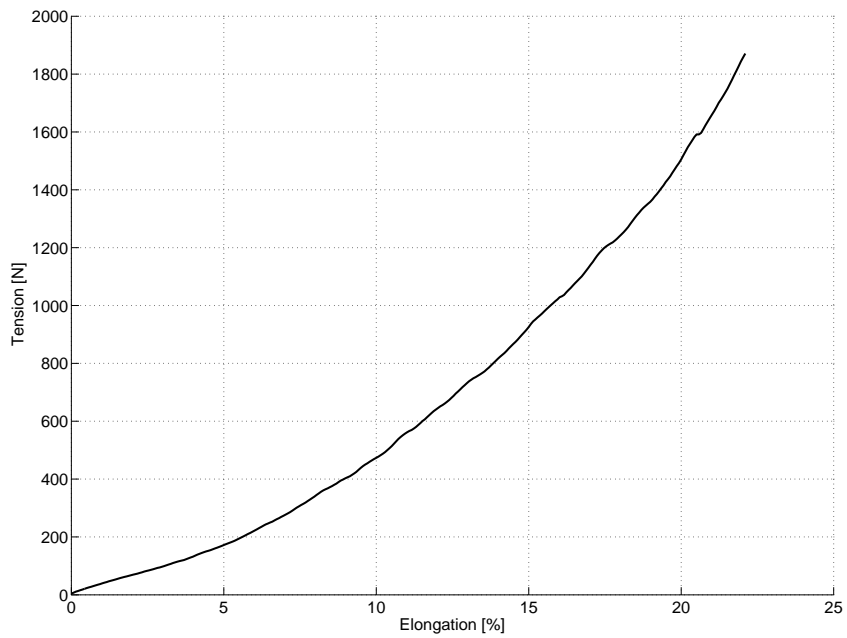


Figure 3.5: Final extension regime to be included in numerical analysis

CHAPTER

4

NUMERICAL PREDICTION OF  
MOORING LINE TENSION

## 4.1 Introduction to Mooring line tension prediction study

To create a case study with which to assess the performance of numerical prediction tools experimental work was designed to expose a WEC device to a controlled wave environment. These experiments were conducted by the members of the SuperGen consortium under work stream 6. These experiments included testing a single “generic WEC” as well as an array of 3 and 5 WECs in the Ocean basin and the Marintek centre in Trondheim. The experiments were a joint collaboration between some of the members of the SuperGen consortium, namely University of Edinburgh (as lead), University of Exeter, Queens University Belfast and Heriot-Watt University. This set of experiments was funded under the Hydralab III project.

Later experiments were designed and carried out by the author at the Heriot-Watt wave basin in Edinburgh in order to complete the data set for the “generic WECs”. These later tests include a single device only in the wave basin and would allow measurements to be taken for direct comparison to the output of numerical models. This chapter will describe the experimental set-up and procedures for the tests as well as the equipment used. This chapter will then go on to explain the construction of numerical models which calculate the tension response in the mooring lines due to top end motions measured during the scale model experiments.

The mooring configuration was designed with the aim of providing a small surface footprint area for the scope of motion of the WEC body due to array constraints, however, at the same time the mooring is designed to allow the WEC full heave motions. The Hydralab team decided on an taut Aramid mooring rope arrangement, where an anchored line would be connected to a surface float followed by a horizontal line from the float to the device. Three lines of this configuration were used equally spaced around the device. It was thought as a consequence of small elongation properties of the ropes that this configuration would provide the sort after motion properties. Effectively the taut moored surface floats would create a freedom envelope for the buoy allowing motion in the heave mode due to cantilever effect from the horizontal lines.

### 4.1.1 Wave Basins

In order to subject a floating body to a controlled and designed wave climate, wave basins will be used. Wave basins use mechanically driven paddles to generate waves across a tank of water. Wave basin sizes vary, and the details of the wave generation system can also vary depending on the facility. Two wave basins are available for use during the course of this project. The first basin is the wave basin in Edinburgh at Heriot-Watt University, and the second is the wave basin at the Norwegian Technology Resource Institute in Trondheim in Norway. The use of a wave basin allows the sea states to be designed and controlled and allow repetition of the same sea state. There are limitations to the quality of the results that can be gained by wave basins as, unlike the real sea environment, the effective test area in a wave basin is bound by the edges of the tank. This can cause waves to be reflected by the extents of the tank affecting the controllability of the sea state. For this reason wave basins often include “beaches” which are designed to absorb the energy from the waves reducing reflection from the downstream end of the tank. These beaches can range from a mesh type material to a gradual reduction in the depth of the water. The former uses fine mesh or foam to dissipate the energy in the water as the waves pass through it rather than reflecting the energy. The mesh material can be small irregular shapes or, blocks of foam with varying density and porosity. The mesh material is held in a cage, where the cage can take different shapes. The later beach method requires the bottom of the tank to slope upward until the depth of the water is very low. After this point the water drops into a channel. This is known as an over topping type beach where variations can be the shape of the slope, from a strait incline to a parabolic cross-section.

#### **Heriot-Watt wave basin**

The wave basin at Heriot-Watt University is a 12m by 9m tank with a 2.8m depth. There is a further 2m deep pit in the middle of the tank that allows a maximum optional test depth of 4.8m (figure 4.1). The basin is equipped with 24 wave flaps which are wedge shaped panels behind a flexible water tight membrane. Each wave flap has an independently-controlled electro-mechanical drive with force feedback to minimise standing waves. The wave paddles are controlled by Edinburgh Design Ltd “Waves” Software which allows the basin to produce regular waves and short or long crested irregular waves. There is a beach

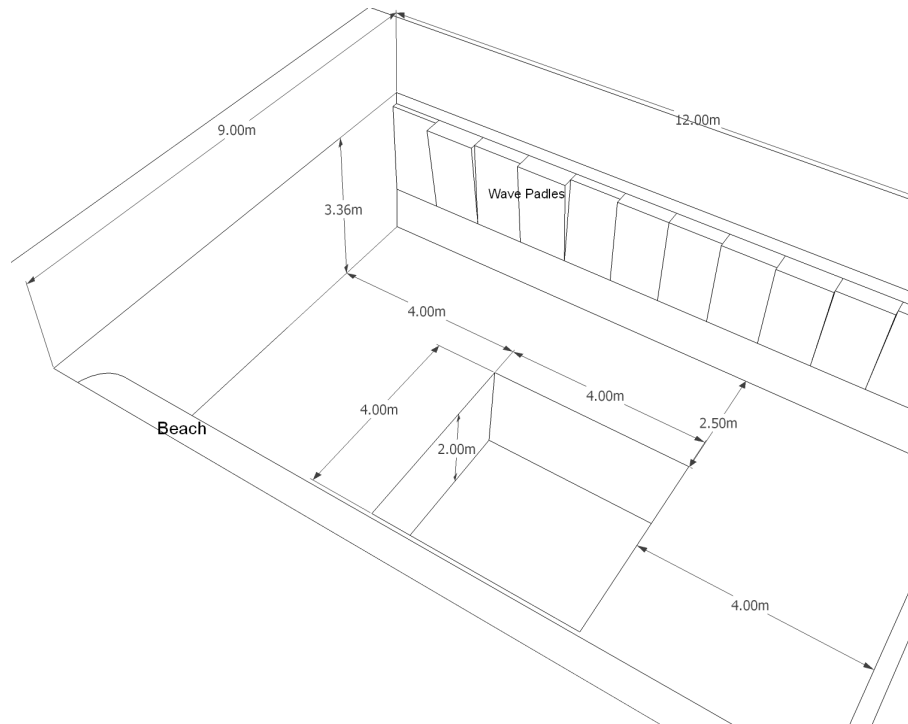


Figure 4.1: Herriot Watt wave basin

at the opposite end of the basin to the wave paddles consisting of a mesh cage with a parabolic cross-section filled with small plastic mesh shapes. The wave paddles can create long crested regular wave with heights up to 0.4m with a frequency range between 0.3 and 1.2 Hz. The wave height is restricted by the breaking limit of the wave between the frequencies of 0.7 and 1.2 (figure 4.2). Restriction on the wave heights for frequencies below 0.7 Hz are imposed by the power output of the wave generator amplifiers due to the risk of fatigue failure of the drive wires during continuous operation. The basin is equipped with a twin camera Qualisys motion tracking system capable of tracking 10 independent bodies simultaneously. The system works by tracking suitably arranged reflectors positioned in the view of the cameras. The system can output the motions in each of the six modes of motion of a body. The basin has a 16 bit, 32 channel data logger with Labview and Excel DAS Wizard software.

In order to produce meaningful results, the waves produced in the tank need to be controlled and follow a prescribed test series (table 4.1). For this reason the control of the wave paddles are calibrated and the program stored to be called during the tests. During the calibration of the wave paddles, the different sea states are generated in the tank and the water surface elevation at the test area of the tank is measured. This allows

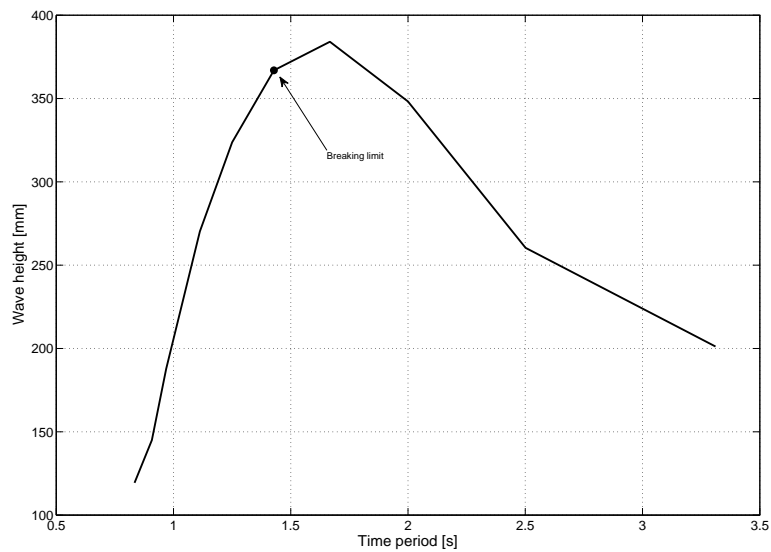


Figure 4.2: Basin Wave Characteristics

a comparison to be made between the intended and actual sea state. The direction of the seas with an angle other than zero will produce waves with an angle  $\alpha$  to the bow of a device in the test area when the device is facing the on-coming waves. In table 4.1 wave 1200 uses a Bret- Schneider long crested spectra. The calibration of the waves ensures that the wave generators are producing the waves specified in the program. This is done with the WEC removed from the tank to ensure that the radiated waves from the WEC in the basin do not affect the readings.

Table 4.1: Waves used in test program

Wave number	Time Period [s]	Wave height [m]	Angle [ <i>deg</i> ]( $\alpha$ )
101	1.12	0.05	0°
102	1.34	0.05	0°
103	1.57	0.05	0°
104	1.79	0.05	0°
105	2.01	0.05	0°
106	2.24	0.05	0°
107	2.46	0.05	0°
108	2.68	0.05	0°
109	2.91	0.05	0°
110	3.13	0.05	0°
111	3.35	0.05	0°
112	1.12	0.05	10°
113	1.34	0.05	10°
114	1.57	0.05	10°
115	1.79	0.05	10°
116	2.01	0.05	10°
117	2.27	0.05	10°
118	2.46	0.05	10°
119	2.68	0.05	10°
120	2.91	0.05	10°
121	3.13	0.05	10°
122	3.35	0.05	10°
123	1.12	0.05	20°
125	1.34	0.05	20°
126	1.57	0.05	20°
127	1.79	0.05	20°
128	2.01	0.05	20°
129	2.24	0.05	20°
130	2.46	0.05	20°
131	2.68	0.05	20°
132	2.91	0.05	20°
133	3.13	0.05	20°
134	3.35	0.05	20°
135	1.12	0.05	30°
136	1.34	0.05	30°
137	1.57	0.05	30°
138	1.79	0.05	30°
149	2.01	0.05	30°
140	2.24	0.05	30°
141	2.46	0.05	30°
142	2.68	0.05	30°
143	2.91	0.05	30°
144	3.13	0.05	30°
145	3.35	0.05	30°
146	1.79(Tp)	0.05 4	0°



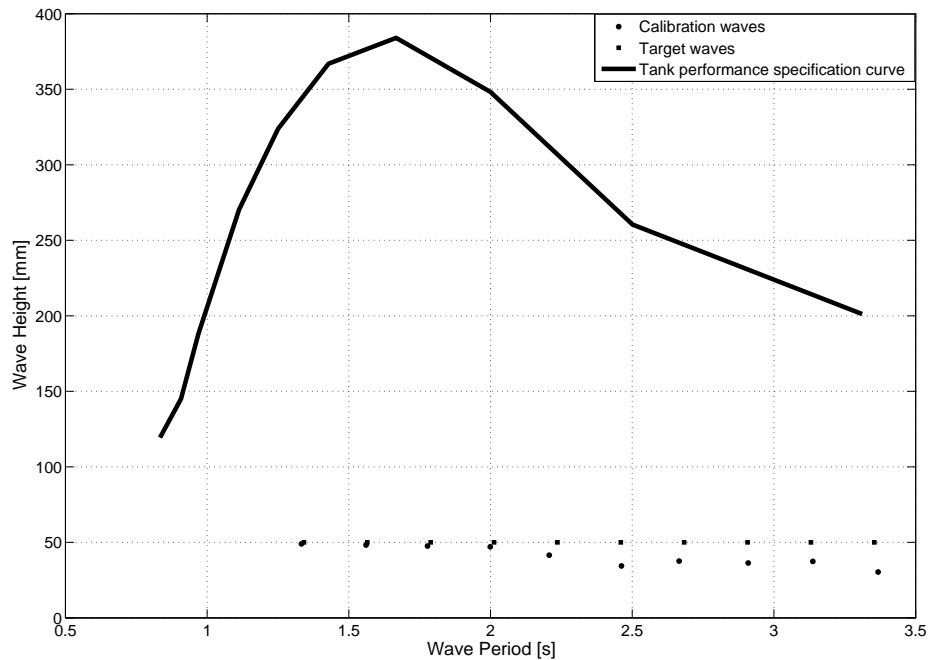


Figure 4.3: Comparison between calibration waves and target waves with wave tank limit curve superimposed

When comparing the calibration waves to the target series it can be observed that the calibrated waves in the tank are not exactly true to the target test series (figure 4.3). The wave amplitude reduces as the time period of the wave increases. The maximum error from the target is at a time period of 3.36 seconds where the difference is 20mm. 20mm represents a 40% error when compared to the target wave height. The time period of the waves also differs from the target waves where the maximum error is at a target wave period of 2.236 seconds, where the difference is 0.029 seconds which represents 13% of a time step of 0.2236seconds (1 second at full scale). The requirements for this test series are that the input waves and the motion of a device are recorded to be compared which means this variation is acceptable as long as the measured wave parameters are used.

### MarineTek Centre Wave basin

The wave basin at the MarineTek centre is a 50m by 80m basin with a variable depth between 0 and 10m (figure 4.4). The wave basin has two sets of wave makers, one on the long side which has multi flap wave makers and one on the short side which has double

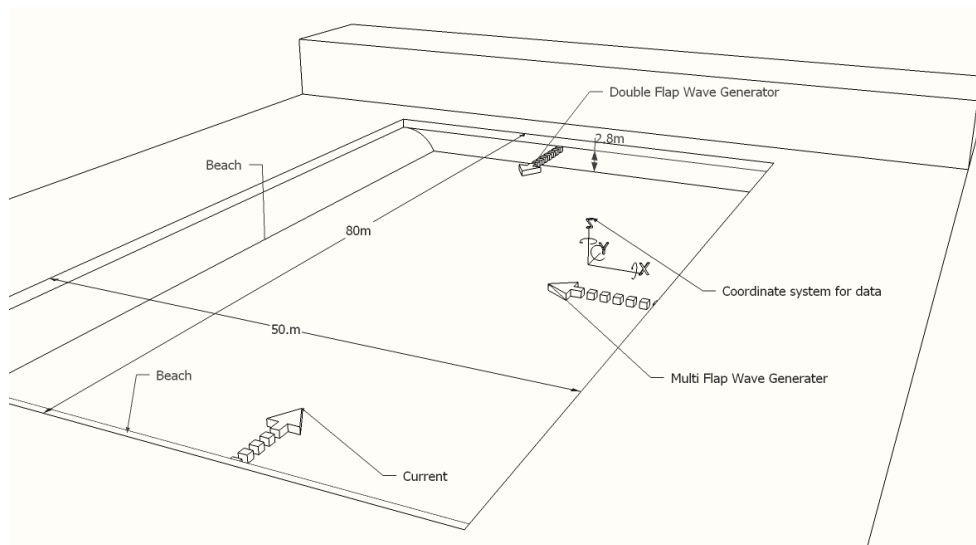


Figure 4.4: Tank dimensions

flap wave makers. The multi flap generator consists of 144 individually controlled flaps capable of creating waves with heights up to 0.4m and time periods of 0.6 seconds and above. The double flap wave maker can create waves with heights up to 0.9m and time periods of 6 seconds and above. The basin can also create water currents during a test with current speeds between 0.15m/s and 0.2m/s depending on the depth at which the current is generated. The floor of the tank makes it possible to install any equipment and devices in dry conditions by raising above the water level (figure 4.5). This allows the position of measuring equipment and anchor positions to be accurately placed on the tank floor and reduces installation time and cost as no divers are required.

### Calibration tests for MarineTek basin

Although the wave basins allow the generation and control of different sea states, to ensure the correct sea states are being generated, the surface elevation of the water in the basin must be measured. To measure the elevation of the water surface “wave probes” are used. The wave probes consist of two long stainless steel conductors positioned parallel to each other (figure4.6). The conductors are separated by an air gap using a terminal block at the top and bottom of the rods insulating them from one another. The lower portion of the wave probe is submerged to a depth defined by the possible range of the water surface during a test. A voltage is supplied across the conductors and due to the air/water gap between the conductors, there is a resistance to electrical current. The resistance between



(a) Welding anchor points to tank floor



(b) Welding anchor points to tank floor



(c) Welded anchor point

Figure 4.5: Pictures of tank setup

the conductors is proportional to the amount of the conductor submerged.

The calibration of the wave probes requires a controlled change of the submerged portion of the probes. This allows the change in voltage due to a known change in relative water level to be evaluated. The voltage change in the wave probe is directly proportional to the relative water level fluctuation. When this was done for the wave probe in the Heriot-Watt wave basin a wave probe in a fixed position on a gantry was displaced in the vertical axis. When the displacement of the probe is compared to the voltage difference a value of  $279 \frac{mm}{mV}$  is evaluated.

The test program shown in Table 4.2 and Table 4.3, show the range of waves to be used in the test program. The initial tests included wave sensors in positions shown in Figure 4.7 indicated as “WAVE”. The waves are divided into monochromatic waves and polychromatic waves as shown in the test program. Also shown is the current present in some of the tests. The tests for the monochromatic sea states were run for a duration of 6 minutes and the test for the polychromatic sea states ran for approximately 27 minutes. All tests required 10-15 minutes settling time to ensure calm conditions at the start of each subsequent tests. The longer run time for the polychromatic sea state was chosen

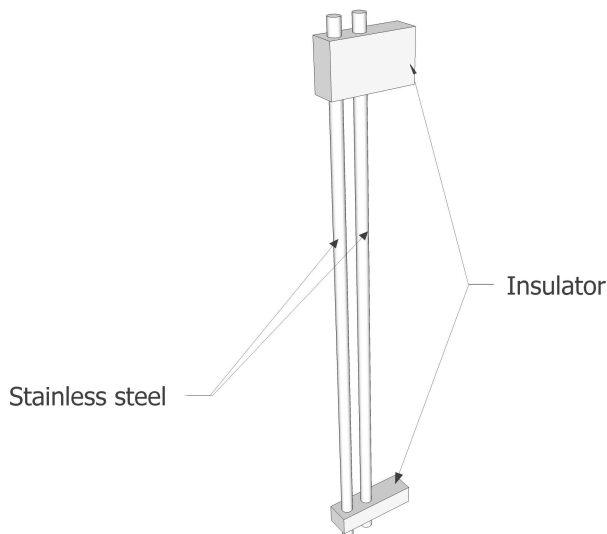


Figure 4.6: Resistive type wave probe

as this was the minimum repeat time to ensure enough data for analysis. The calibration tests defined the sea states that the WEC's would be tested in.

Table 4.2: Monochromatic wave properties

Wave calibration ref	Amplitude [m]	Period [s]	Current [ $\frac{m}{s}$ ]
8100	1	5	0
8110	1	7	0
81120	1	8	0
8130	1	9	0
8140	1	11	0
8150	1	13	0
8160	1.5	8	0
8170	2	8	0
8180	2.5	8	0
8370	2	8	0.44
8320	1	8	0.44
8340	1	11	0.44

During the calibration tests for the MarinTek wave basin a lot of reflected wave activity was observed. As pointed out by Ashton and Johanning (2009) the conditions in the tank are not consistent throughout the tank as would be expected for a regular wave test. Table 4.4 shows the wave heights recorded by different wave probes in different positions in the

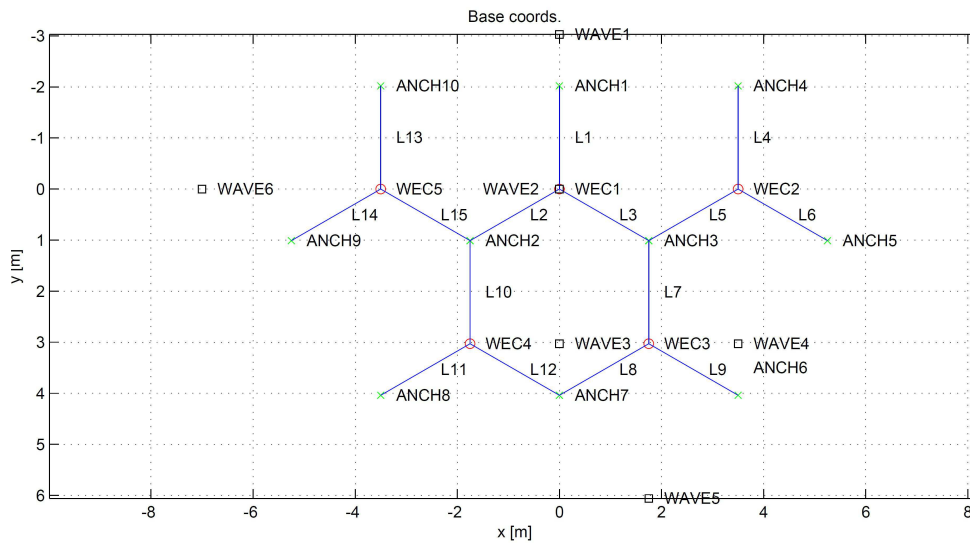


Figure 4.7: Coordinate system for installation

Wave calibration ref	Significant wave height[m]	Peak period[s]	Current[ $\frac{m}{s}$ ]	Spreading parameter	Direction[degrees]
8200	2.5	8	0	-	0
8210	3.5	8	0	-	0
8220	3.5	8	0	12	0
8240	3.5	8	0	-	-25
8415	3.5	8	0.44	-	0
8430	3.5	8	0.44	-	25
8440	3.5	8	0.44	-	-25

Table 4.3: Polychromatic wave properties

tank during the regular wave tests. This inconsistency is attributed to standing waves caused by reflections resulting in constructive and destructive interference. Due to the nature of the polychromatic sea states, the difference in the spectral energy density as a result of the reflected waves is less pronounced and the time histories appear to agree between runs of the same sea state.

#### 4.1.2 Generic WEC

A “generic” WEC designed to represent a wave energy converter has been designed and built (figure 4.8) and will be used as the case study for this project. The generic WEC is designed to represent an oscillating water column type wave energy converter device at 1:20th scale. The WEC has a tube like structure with a closed top or lid. The device sits in the water with a draft such that the open end of the tube is submerged. This produces

Table 4.4: Measured values for RMS derived wave amplitudes for monochromatic waves

Wave number	RMS wave height at probe:			
	1	3	5	6
8100	1.17	1.36	1.16	1.16
8110	1.03	1.20	1.09	1.11
8120	0.89	0.95	1.24	0.96
8130	1.19	1.35	1.09	1.42
8140	0.89	1.19	1.31	1.09
8150	0.45	0.91	0.96	0.91
8160	1.31	1.50	1.83	1.72
8170	1.95	1.99	2.25	2.12
8180	2.47	2.02	2.91	2.55
8190	2.90	2.51	3.54	3.09

an internal chamber bounded by the lid and sides of the cylinder and the water surface. In the lid of the device, an opening allows the air in the chamber to escape and enter when the water surface inside the chamber rises and falls in relation to the WEC. The motion of the air through the opening represents the energy that would be converted to electrical energy by a power take off system for an OWC. An attempt is made to maximise the relative motion of the water surface and the WEC by installing a damping plate at the keel of the device. This damping plate is a circular flat plate which increases the resistance to motion of the device in the heave direction. It is intended that this will allow the body of the WEC to remain relatively still as the water surface elevation varies.

### Variable orifice plate

For this project the electrical power is not required but the effect of a power take off system could be important to the response characteristics of the device. As previously mentioned the orifice plate in the lid of the device can increase or decrease the resistance offered to the air as it moves through the opening in the lid. An approximation to the power capture ( $\bar{P}$ ) of the device can be made measuring the pressure ( $p$ ) and volume change ( $\Delta V$ ) in the chamber during operation (equation 4.1 where  $n$  is the number of points in the record and  $\Delta t$  is the time step between data points). Calculating the power capture, one can

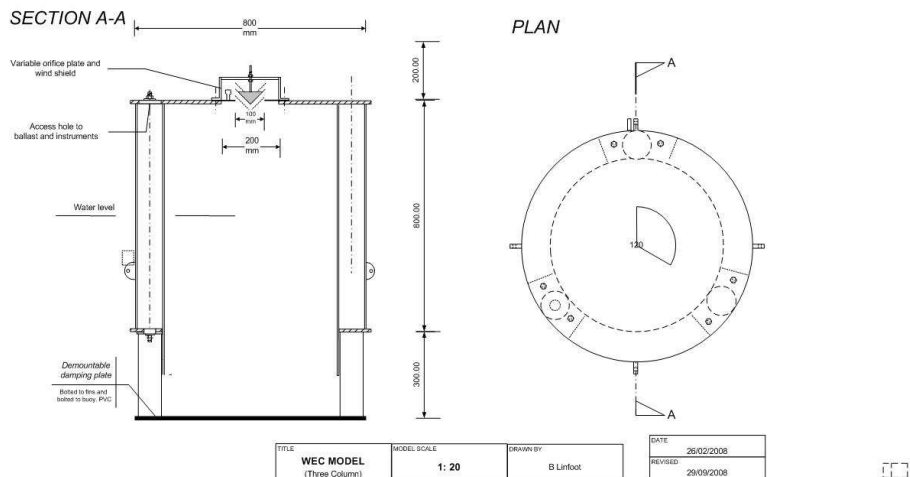


Figure 4.8: Schematic of WEC device

optimise the damping provided by the orifice plate by adjusting the area of the opening, changing the resistance offered to the air as it moves through it.

$$\bar{P} = \frac{1}{n\Delta t} \sum_{i=1}^{i=n+1} p(t_i)\Delta V(t_i) \quad (4.1)$$

### 4.1.3 Motion capture system

To capture the motion of the WEC device during experimentation the use of video non-contact motion sensing systems are employed. This section will explain the function and set up of the Qualysis system at the Heriot-Watt University. Heriot Watt University is equipped with a twin camera Qualisys motion tracking system capable of tracking 10 independent bodies simultaneously. The system works by tracking suitably arranged reflectors positioned in the view of the cameras. The system can output the motions in each of the six modes of motion of a body.

The setup of the Qualysis system required a calibration board with a 2D axis of reflectors and a wand which contained two reflectors. The calibration board is hung in view of the cameras and the wand is held between the board and cameras. The wand is then spun allowing the cameras to calibrate the rotation of the two wand reflectors that are separated by a known distance which move in front of a calibration board. The calibration board has three reflectors that are again at a known separation (figure 4.9).



Figure 4.9: Calibration of the motion tracking system using a wand and calibration board

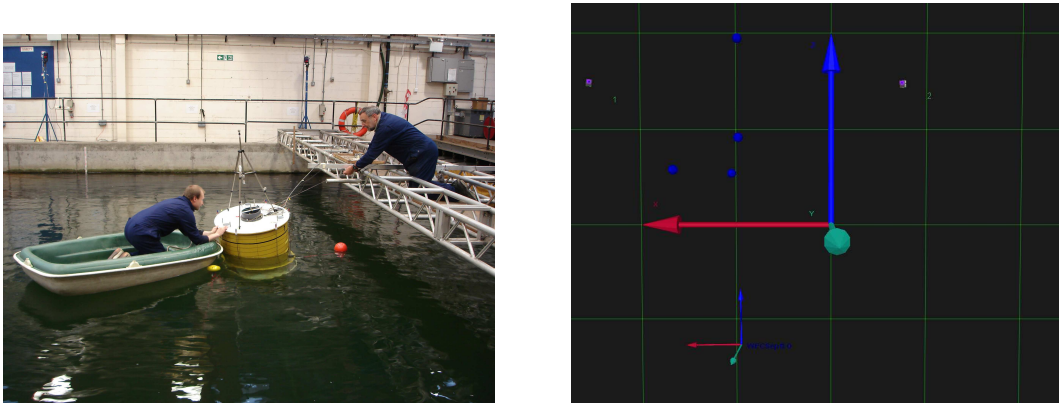
Once the system is calibrated the WEC could then be placed in the tank and a tripod of reflectors installed on it (figure 4.10). The Qualysis system was then given information as to the distance of the reflectors on the tripod to the centre of rotation of the WEC. This means that the Qualysis system can now track the motion of the WEC and distinguish between the 6 degrees of motion.

Once the Qualysis system has this information, a display on the screen graphically confirms the correct assimilation of the information (figure 4.10(b)). Two axes are displayed in the Qualysis screen, the smaller axis indicates the axis of rotation of the WEC body and the larger axis indicates the global axis. The WEC body with the small rotation axis at its centre can translate in motion modes of surge sway and heave in relation to the global axis. This system automatically separates the motions into the 6 individual modes of motion. The calibration is an important step to using this system as, if the calibration is done incorrectly, the system defines the model axis of rotation incorrectly which would result in incorrect rotation motion amplitudes as well as excess translation motions.

#### 4.1.4 Mooring systems

The “test” mooring system for the WEC represents a likely configuration of the mooring system for a full scale device. It is also desirable to evaluate the motion properties of





(a) Installing the reflectors on the WEC

(b) View from Qualysis system once calibrated

Figure 4.10: Calibrated Qualysis system

the WEC when unrestrained. Due to experimental constraints it is not possible to have the WEC completely unrestrained as it could collide with the sides of the tank causing damage, or could drift out of the capture window of motion recording instrumentation. For this reason two different mooring systems will be tested on the WEC device in the wave basins. The first mooring system is known as the test system designed to represent a typical mooring system that may be used by a WEC device at full scale. The second mooring system is a soft mooring allowing the WEC large freedom and compliance in the tank.

Each one of the mooring lines used in the test mooring will consist of two lengths of 3mm diameter fibre rope. The lower line of length 2.7m, is attached between the anchor point and a surface marker buoy. The surface marker buoy is 18mm in diameter. The second or upper section of fibre rope line will connect the marker buoy and the WEC. There are three mooring lines like this in the mooring system. The three mooring lines will be evenly distributed around the device as shown in Figure 4.11.

The soft mooring system (figure 4.12) uses four light lines attached to the WEC at the water line. Two lines are attached to the same point on the port side and two to the same point on the starboard side of the WEC. These lines were then attached to elastic sections or bungees, and the bungees are attached to the corners of the of the test area.

To measure the tension in the mooring lines during tests, load cells are attached at different positions. The load cells are made using a strain gauge attached to a metal ring and then water proofed (figure 4.13(a)). There are two load cell positions measuring the

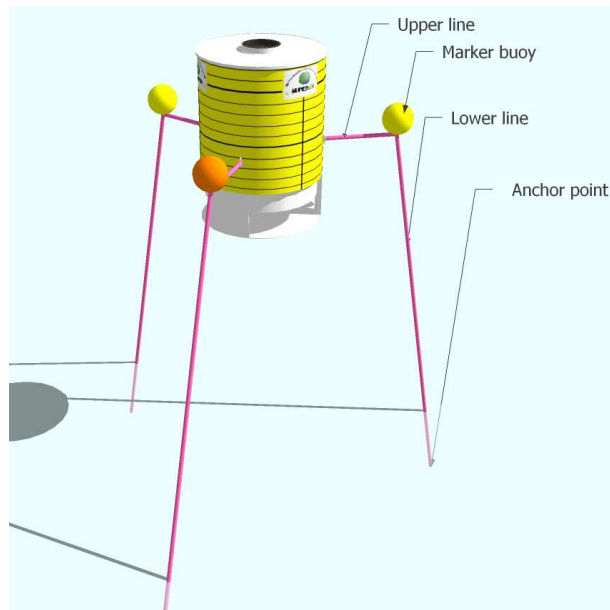
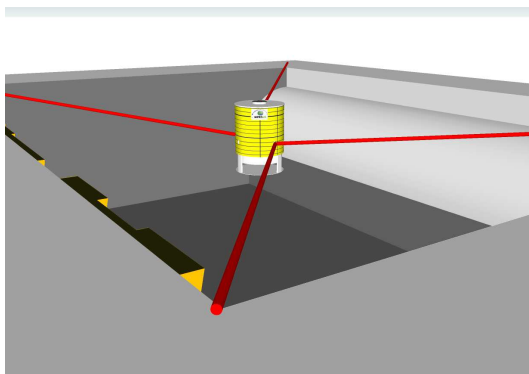


Figure 4.11: First mooring system for WEC device



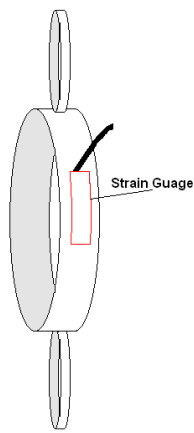
(a) Light mooring system



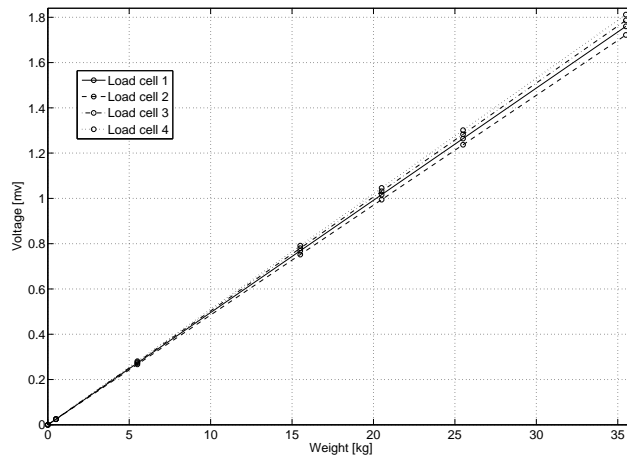
(b) Bungee section at tank attachment

Figure 4.12: Light mooring arrangement

tension in the two sections of fibre rope. Position A is at the top of the lower section of line and position B is between the upper section of line and the WEC (figure 4.14). The load cells are calibrated by loading them with known weights and reading the voltage change. In this case the calibration was done by connecting the load cells together in a chain and hanging them from a tripod. The weights were then added to the bottom load cell in the chain allowing the calibration of all the load cells to be done at once. Figure 4.13(b) shows the calibration curves where the accuracy of the load cell is  $\pm 0.03\text{N}$ .



(a) Load cell construction



(b) Load cell calibration curves

Figure 4.13: Load cells

#### 4.1.5 WEC Instrumentation setup

The instrumentation of the WEC is similar for the installation in both wave basins however due to the resources available the set up does differ slightly.

- Tests in the Heriot-Watt wave basin

For this set of tests the WEC will be installed with the two different mooring systems (test and soft). When moored with the test mooring system the lines will be instrumented with load cells on each line. The load cells are arranged with two cells on the bow line (mooring line 1) where one of the load cells is between the WEC and the marker buoy and one between the marker buoy and the anchor point. The other mooring lines (mooring lines 2 and 3) have one load cell each, between the WEC

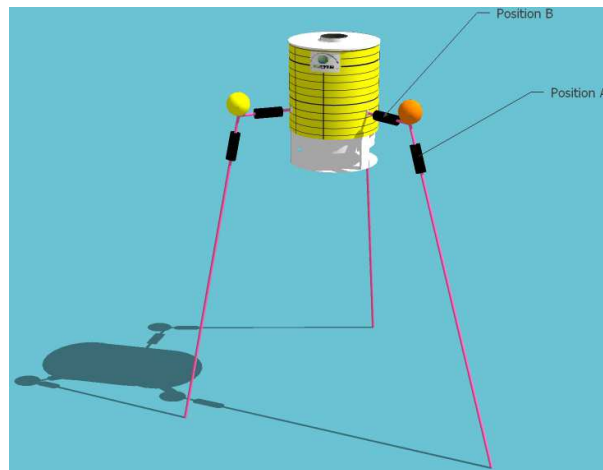
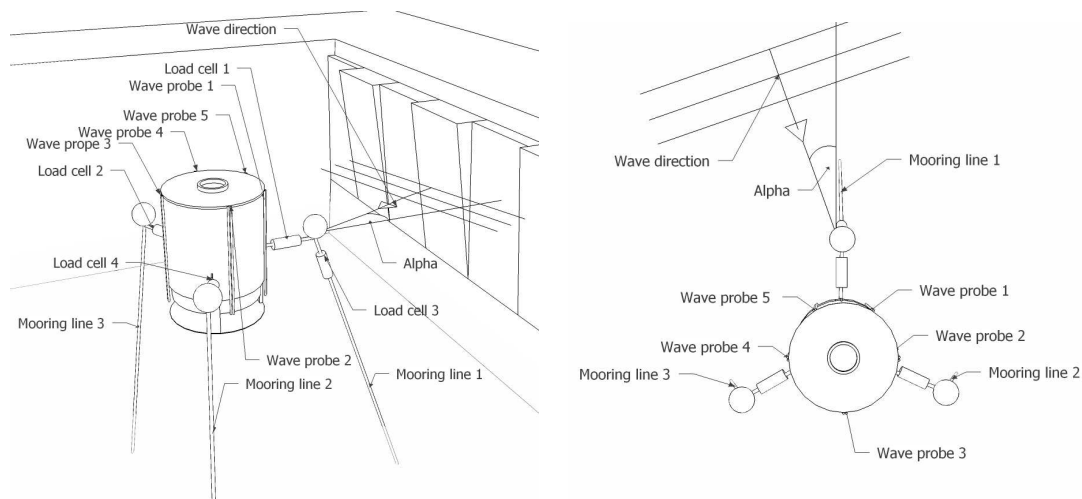


Figure 4.14: Load cell positions for the WEC in the MarinTek centre basin



(a) Aspect view of WEC in the Heriot-Watt wave basin (b) Plan view of WEC in Heriot-Watt wave basin

Figure 4.15: WEC set-up in Heriot-Watt wave basin

and the marker buoy (figure 4.15). The soft mooring system is not instrumented with load cells as only the motion of the device and the water surface variation is recorded.

- Tests in the MarinTek centre wave basin

For this set of tests the WEC is installed with only the test mooring arrangement. Similar to the set up for the Heriot-Watt basin, the WEC is installed with load cells on each line, however due to the availability of more channels the lines have load cells in the two positions on the mooring lines as shown in figure 4.14.

## 4.2 Test methodologies

To model the WEC and mooring system information must be gathered about its static and dynamic properties. As such different tests are used as follows:

- Decay tests
- Regular wave tests
- Irregular wave tests

### 4.2.1 Decay tests

The decay tests are used to evaluate the natural period and the damping ratio in the different motion modes of a system that could be approximated to a damped mass spring system such as a moored floating body. The methodology requires the system to be displaced from its equilibrium position in one motion mode, then released and allowed to return to rest as a result of the restoring forces of the system. For a moored WEC the restoring force will be the tension characteristic of the mooring arrangement and/or the buoyancy force of the WEC and mooring components that are submerged as a result of the initial displacement. The system will oscillate about the equilibrium point with a diminishing amplitude until it rests. The frequency of this oscillation is the natural frequency of the motion mode being tested for the system.

To calculate the damping ratio it is assumed that the amplitude of the motion of the device decays exponentially. As indicated in figure 4.16 the decay in amplitude follows the trend represented by equation 4.2 where  $\zeta$  is the damping ratio and  $\omega_n$  is the natural angular frequency in that mode of motion. Taking logs results in equation 4.3 which is in the form of a straight line (i.e  $y = ax + b$ ). This means that  $\zeta\omega_n$  is the gradient, also known as the logarithmic decrement. Differentiating equation 4.3 with respect to time and gives the equation for the logarithmic decrement (equation 4.4) between two peaks with  $N$  peaks between them. The damping ratio is then evaluated using equation 4.5. The natural frequency  $\omega_n$  is found using equation 4.6 where the damped natural frequency ( $\omega_d$ ) is  $2\pi/T$  where  $T$  is the damped natural period (the time between two successive peaks).

$$y(t) = X e^{\zeta \omega_n t} \quad (4.2)$$

$$\ln y(t) = \ln X - (\zeta \omega_n t) \quad (4.3)$$

$$\delta = \ln \left( \frac{y(t)}{y(t + TN)} \right) / N \quad (4.4)$$

$$\zeta = \frac{1}{\sqrt{1 + \left(\frac{2\pi}{\delta}\right)^2}} \quad (4.5)$$

$$\omega_n = \frac{\omega_d}{\sqrt{1 - \zeta^2}} \quad (4.6)$$

Figure 4.16 shows time histories of a decay test in the pitch motion mode. For this test the system is tilted in the pitch direction and then released. The time history shows the angle in pitch rapidly increasing due to the initial excitement. The trace then shows the pitch oscillating with decreasing amplitude about the equilibrium position. In the example shown by figure 4.16, two decay tests were done hence the second increase in pitch at around 75 seconds. Using the time history from this test and tests for the other degrees of motion the natural period of the device in all six motion modes and the damping ratio is calculated. Table 4.5 shows the natural period and damping ratio of the device with the two different mooring configurations at Heriot-Watt and Trondheim.

Table 4.5: Natural period ( $T$ ) and damping ratio ( $\zeta$ ) results for decay tests using test and horizontal moorings from the tests in the Heriott-Watt and MarinTek basin

Motion mode	Test mooring Heriot-Watt		Soft mooring Heriot-Watt		Test mooring Trondheim	
	$T$	$\zeta$	$T$	$\zeta$	$T$	$\zeta$
Surge	24.28	0.152	35.20	0.249	31.85	0.172
Sway	23.43	0.204	31.57	0.257	36.81	0.261
Heave	2.55	0.202	2.70	0.212	1.75	0.364
Roll	3.98	0.083	4.15	0.106	-	-
Pitch	4.12	0.089	4.26	0.106	4.42	0.071
Yaw	12.77	0.151	14.06	0.197	-	-

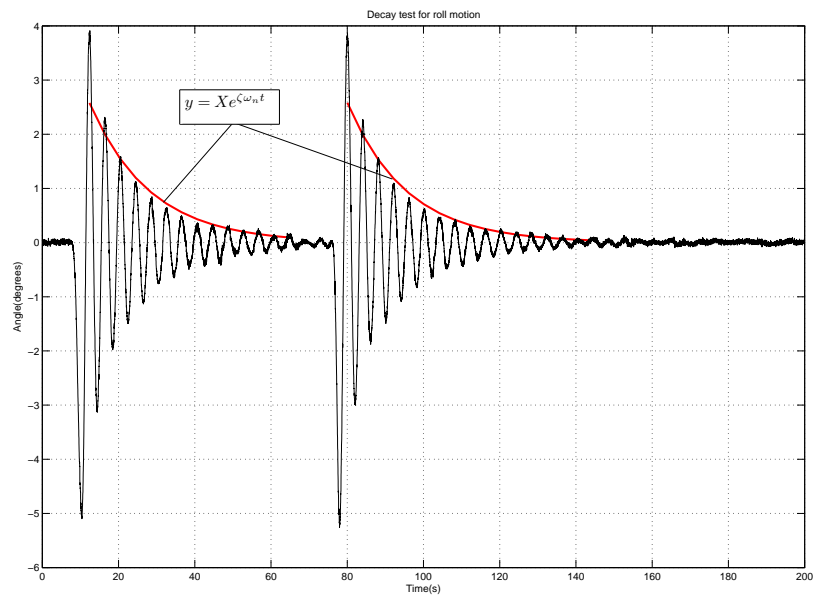


Figure 4.16: Time histories from Roll decay test

### 4.3 Time domain analysis of mooring system

This section will describe the construction of a numerical model to calculate the mooring line loads of the floating moored WEC. This model will only handle the calculation of the mooring response and the floating body response will be prescribed using the measure data. Below is a list of model inputs and outputs:

- Model inputs
  - WEC motions
  - Water surface elevation
  - mass properties for marker buoys
  - Stiffness and drag properties for the mooring material
- Outputs
  - Mooring line tension
  - Marker buoy motion response

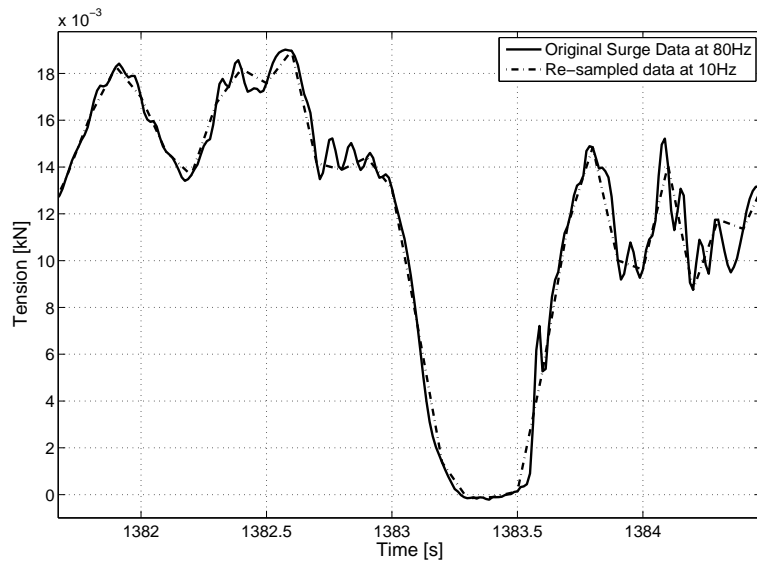


Figure 4.17: Comparison between experimental surge data and re-sampled data

### 4.3.1 Vessel representation of the floating body

For this model, a “vessel” is used to represent the floating body of the WEC. The geometry of the vessel is designed to represent the WEC body however, the definition of the geometry will have no effect its motion. The geometry is input as a visual aid to convenience the definition of the connection points of the moorings. The motions of the vessel will not be calculated by the simulation but prescribed from the experimental data. The experimental data from the Trondheim series has a sampling frequency of 80Hz which has a time difference between consecutive data points of 0.0125s. This would mean a large number of data points are to be processed during the numerical simulation. Therefore it is necessary to re-sample the data using a cubic spline to reduce the resolution. Figure 4.17 shows the comparison between experimental data of the surge of the WEC and the same data re-sampled at 10Hz. This indicates that very high frequency variations of the vessel (above 10Hz) will be excluded from the simulation. However the re-sampled data shows that the main important motions of the WEC will be included. This optimizes the calculation time of the simulation whilst still allowing it to represent the motion of the floating WEC.



Table 4.6: Line properties as input to numerical simulation

Property	Value
Line diameter	0.0035m
Mass per unit length	0.0095 <i>kg/m</i>
Drag coefficient normal	1.2
Drag coefficient axial	0.8
Added mass coefficient normal	1

### 4.3.2 Mooring approximation

The mooring limbs consist of the two sections of lines separated with a marker buoy. The lines are specified with finite lengths made up of segments of 20% of the total length. As in the experiments there are three mooring lines that are anchored to the seabed. The anchor points on the model have no properties of any real anchor as the anchor points in the tank tests were not tested for their holding capacity and did not fail or drag in any way during the experiments. These lines are defined with the properties shown in table 4.6.

The stiffness characteristics of the mooring line are defined using the data from the previous section (3.5). As mentioned in the chapter 3 the uncertainty surrounding the mooring stiffness will have to be investigated due to the apparent mechanical elongation affecting the stiffness of the line. For this reason different linear stiffness coefficients are used to define the stiffness of the mooring line to allow the sensitivity of the model to changes in mooring stiffness. The linear stiffness values range from a linear approximation to the data from the tests in chapter 3 to a linear approximation to maximum stiffness data from work found in literature for Aramid rope Davies et al. (2011). These stiffness coefficient values are input to OrcaFlex as the load required to double the length of the line.

### 4.3.3 Marker buoy approximation

The small marker buoys add a complication in the simulation of the system as the positions and motion of the marker buoys were not recorded during testing. This means in any simulation the marker buoys will have to be approximated. The definition for the

approximation of the marker buoys could be done in several ways:

- Attachments
- 3D buoys
- 6D buoys

Calculating the response of the marker buoys means that, in the mooring tension and response simulation where it is intended to evaluate the mooring line approximation, there lies an uncertainty in the models ability to truly represent the response. However the marker buoys are small and connected at a single point (figure 4.18). This means that the effect of the rotation of the marker buoys on the overall result can be assumed to be small. From the available options listed above it would not be possible to accurately represent the marker buoys by placing an “attachment” in the mooring line. This is because the method used to attach the marker buoy in the physical tests is a single point attachment. The “attachment” option in the numerical simulation would have a dimension of length where the line would feed through at each end. The 3 degree of freedom and 6 degree of freedom buoy approximations can be applied as it can facilitate a closer approximation to the definition of the actual attachment. To run simulations with both approximations will provide the basis for a comparison as to the importance of using a more sophisticated model (6 degree of freedom buoy theory) or using a simpler model to try to save on computation time.

#### 4.3.4 Simulation condition

Figure 4.19 shows representations of the model of the generic WEC. The shaded view is intended to aid in visual clarity in the absence of 3D display of the wire frame model.

#### 4.3.5 Wave field

To include the Waves in the model of the generic WEC for the model of the mooring tension and response, time history data sets from the wave probes are required. These must be re-sampled similar to the motion time history files to reduce the resolution of the



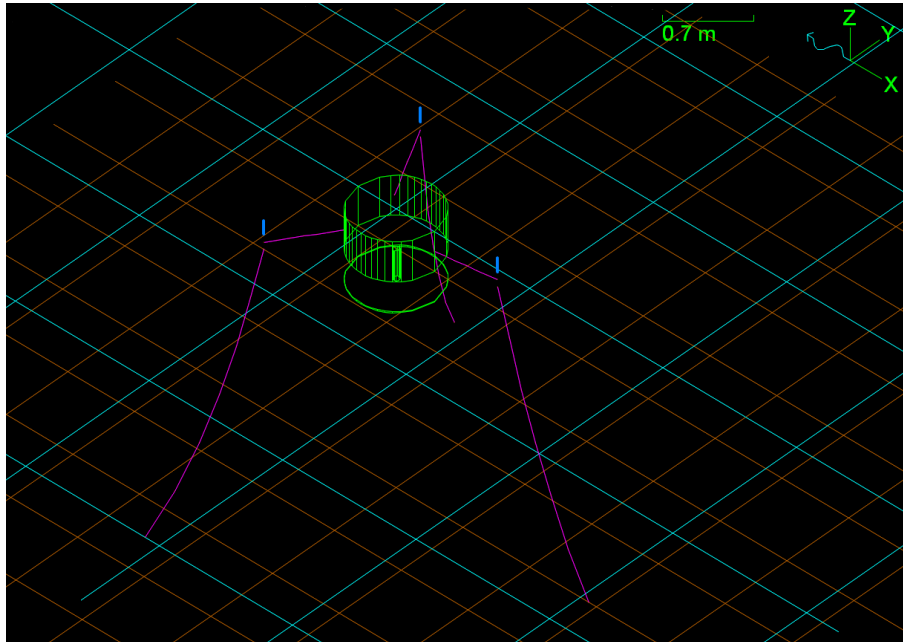
Figure 4.18: Marker attachment method

data and thus, reduce the calculation time of the simulation. Similar to the motion data, after re-sampling, high frequency variations will not be included. Also as shown in figure 4.20 there does exist the case where peaks on the wave field lie between the selected time intervals at 10Hz and therefore appear reduced in the re-sampled data set. however this is considered to be negligible and will not have a large effect on the result.

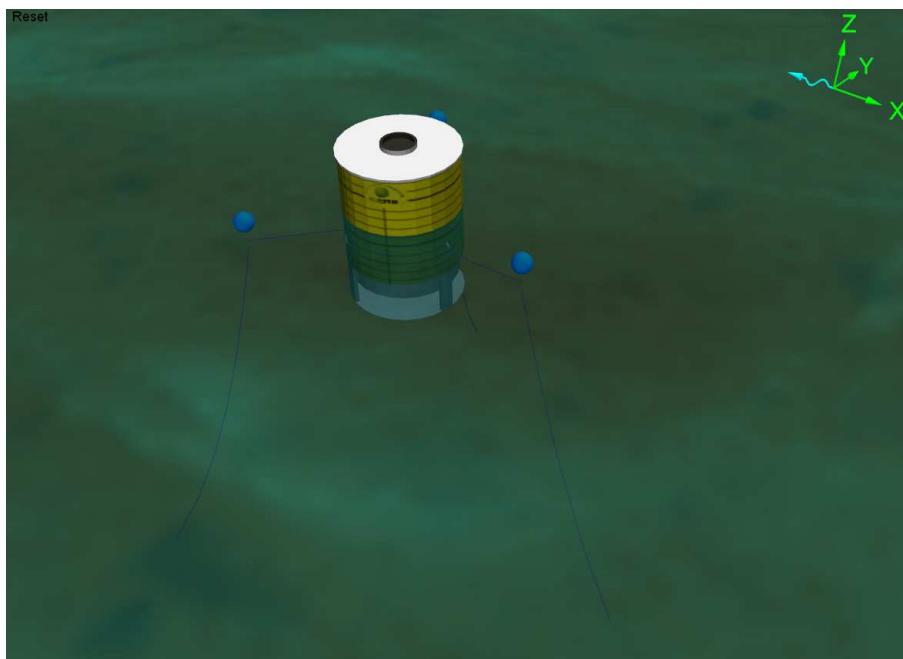
The position of the measurement of the wave profile during the tests is important for the simulation as this becomes the position of the wave source. For the Trondheim tests the probe was placed 3m upstream from the WEC. As such -3m is the origin of the wave field as defined in the numerical simulation.

#### 4.3.6 Simulation scheme

The build-up time for the simulation is 1s. This build up time allows the WEC body to arrive at the initial position at the start of the time history without too larger acceleration from its position after the static calculation. Simulations will be run in accordance to table 4.7 where the simulations differ in the method of modelling the marker buoys.



(a) Schematic representation of time domain model



(b) Shaded view of time domain model

Figure 4.19: 3 Dimensional representation of numerical models

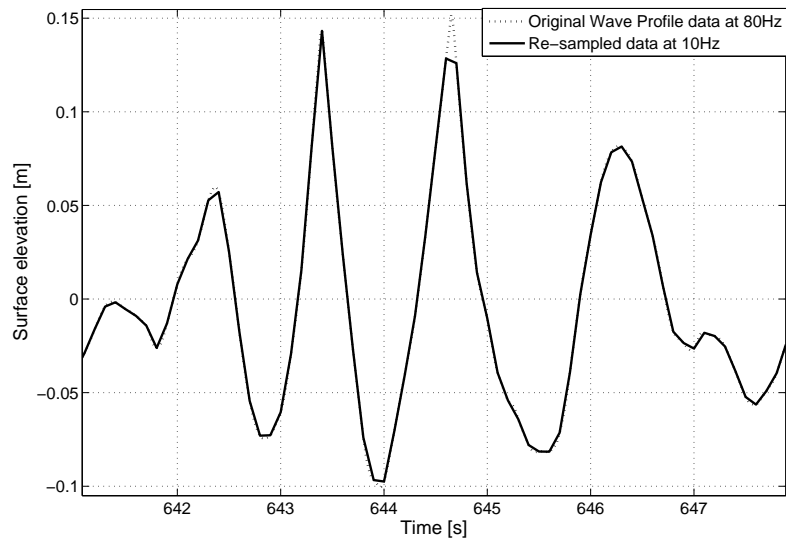


Figure 4.20: Comparison between wave profile data from experimentation at 80Hz and re-sampled data at 10Hz

Table 4.7: Case 1 simulations

Simulation n.o	Simulation Description
1	Simulation includes the WEC and moorings where the marker buoys are approximated using 3degree of freedom buoys. In the simulation the motion of the WEC and the wave field is considered. Motion of the WEC is prescribed using time history files for all six degrees of freedom from experimental data from test 3030 of the Trondheim test series
2	Simulation includes the WEC and moorings where the marker buoys are approximated using 6 degree of freedom buoys. In the simulation the motion of the WEC and the wave field is considered. Motion of the WEC is prescribed using time history files for all six degrees of freedom from experimental data from test 3030 of the Trondheim test series

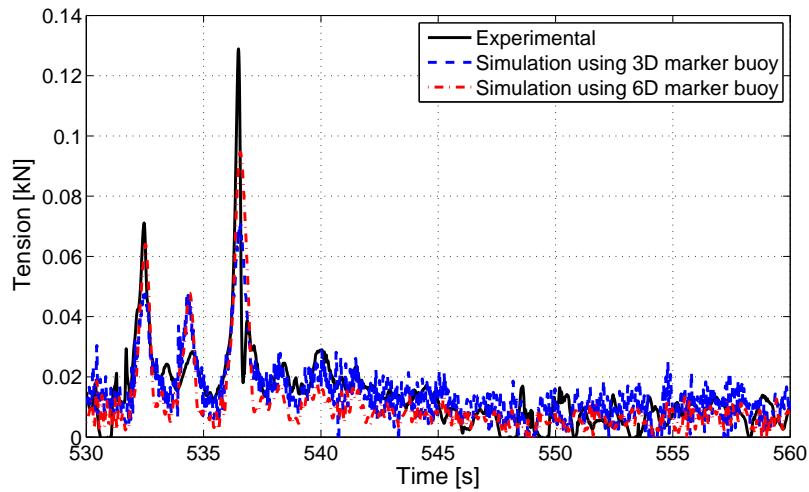
Table 4.8: Experimental data used in simulation comparison

Test number	Hs [m]	Tp [s]	Dir [deg]	additional text
3000	0.125	1.7	90	–
3010	0.175	1.7	90	–
3030	0.175	1.7	90	N=12
3041	0.175	1.7	90	AOA=-25

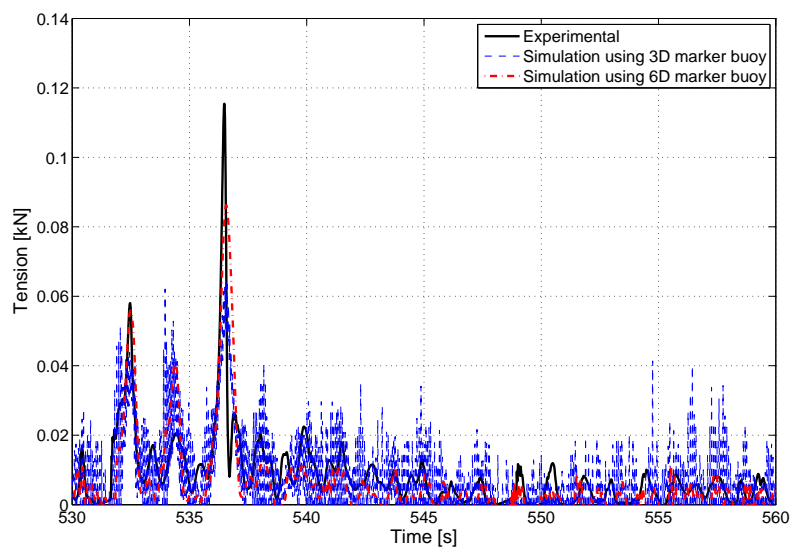
All of the simulations completed successfully, which is significant, as failing to converge on a solution for a given time step is a possibility for time domain simulations using iterative integration solvers. The simulations do need a small time step (0.001s) to allow the simulation to remain stable. This suggests that there are some high frequency response modes in the simulation that would not be catered for if using a larger time step. The output of interest from these simulations is the tensions in the mooring lines. The tension in the bow line mooring for all the simulations showed a similar trace to the experimental data where throughout all the simulations tension was within the same order of magnitude. Figure 4.21 shows the simulation results with the experimental results for the bow line tension. In these results there is a high frequency variation in the tension prediction from the model using the 3 degree of freedom marker buoy approximation. This high frequency variation comes from the approximation of the response of the marker buoy and makes the model susceptible to becoming unstable. The 6 degree of freedom marker buoy approximation model appears more robust and a better result in terms of the prediction of the tension. Further runs for different sea states are run using the wave conditions defined in table 4.8 and the model using the 6 degree of freedom marker buoy approximation are used.

#### 4.4 Discussion on comparison between experimental and numerically predicted mooring loads

The numerical models of the mooring line use experimental time history data to provide the motion response of the WEC in all 6 degrees of freedom. This means that the model is only required to calculate the response of the mooring system. This produces no coupling between the mooring response and the floating body as the effect of the mooring system



(a) Comparison between tension in bow line mooring line at position A during test 3030 and numerical simulation including water surface elevation variation



(b) Comparison between tension in bow line mooring line at position B during test 3030 and numerical simulation including water surface elevation variation

Figure 4.21: Comparison of tension in bow mooring line using different marker buoy approximation

on the response of the floating structure is included in the prescribed motions. The mooring system includes the marker buoy modelled using a 6 degree of freedom buoy where the hydrodynamic parameters are applied using the codes set out by the DNV-RP-C205 (2010). The mooring lines load extension characteristics are informed using tensile test results on the line material and the hydrodynamic properties of the line are again applied using the codes set out in the DNV.

Due to uncertainty surrounding the stiffness data collected a sensitivity study was performed. This required the stiffness to be varied to give an idea of the impact errors in the stiffness definition could have. Figure 4.22 shows the numerical prediction of the tension in the bow mooring limb where stiffness coefficient is varied. This result shows that the stiffness of the mooring line has little effect on the overall stiffness of the mooring limb. This is due to other factors such as the floating marker buoy and the mechanical construction of the mooring limb diluting the contribution of the mooring line axial stiffness.

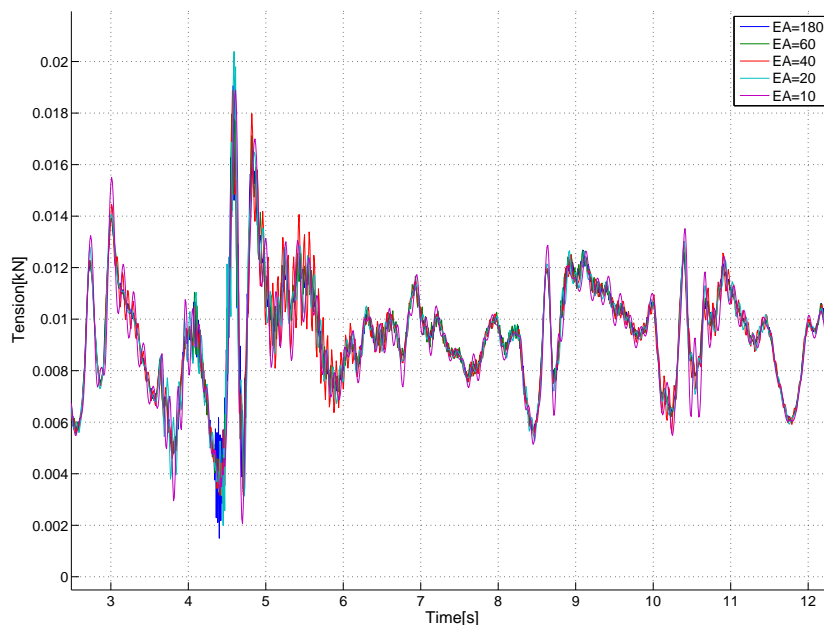


Figure 4.22: Numerical prediction of tension in mooring bow mooring line during test 3030 with different stiffness coefficients

Figure 4.23 shows a comparison of the tension in the mooring lines for test 3030 at the two positions in the mooring line between the numerical and experimental data. The numerical prediction of the mooring line tension appears to be fairly close to the



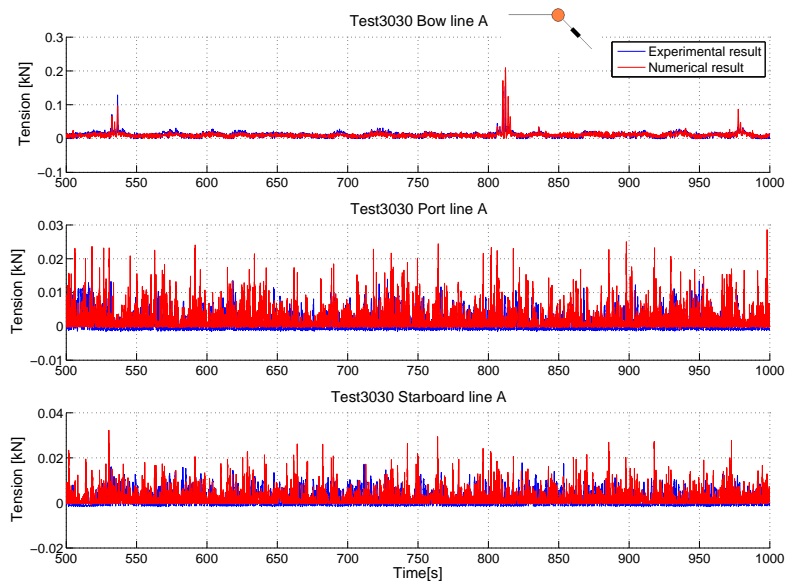
experimental results, especially for the more taut conditions which are present in the bow mooring line. During slacker conditions, that can be seen to be present on the lateral moorings, the numerical prediction agrees less with the experimental result.

Of all the wave tank tests conducted the results from test 3030 shows the most snatch loadings, where the tension in the mooring line increases dramatically over a very short space of time. These snatch loadings can be observed in figures 4.23(a) and 4.23(b) at 540 and 820 seconds. The numerical model predicts these peaks and follows the trend from the experimental data. The indications to this point are that the numerical model has made a good approximation to the mooring loads. To get a better picture of how well the numerical model is performing equation 4.7 is used to calculate the relative difference between the experimental data and the simulation result.

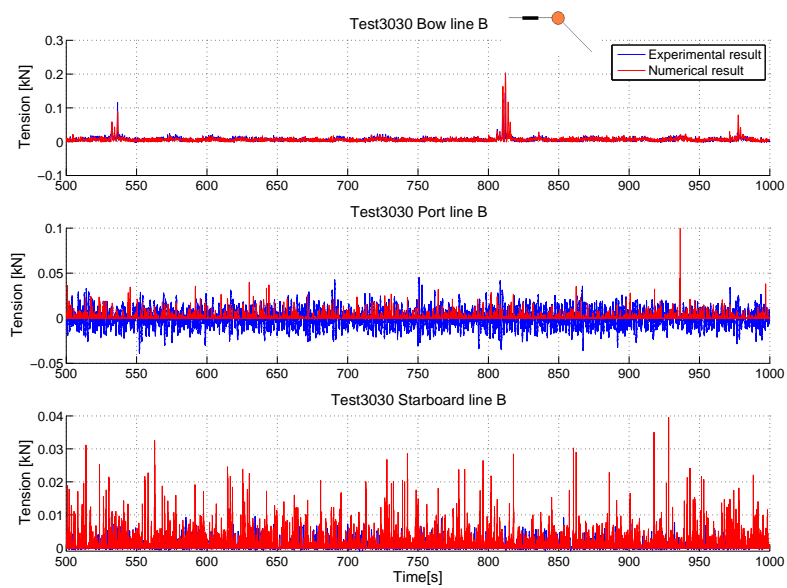
$$\epsilon = \left( \frac{T_{sim}}{T_{Exp}} \right) - 1 \quad (4.7)$$

Figure 4.24 and 4.25 shows the variation in the difference between tension in the mooring lines for the experimental data and numerical prediction at different loadings. The result shows that the numerical model's prediction becomes less reliable during slack conditions. The vertical red line in figures 4.24 and 4.25 represents the pre-tension in the mooring lines which is 0.002kN, below which the mooring line is considered to be in a slack condition. For tension situations experience below the pre-tension (slack conditions) in the mooring line the numerical result shows a large over prediction in the tension. As the tension regime increases the difference between the prediction and the experimental result reduces.

Although the numerical prediction of the tension can be as much as 100 times the actual tension during slack conditions the tension in this regime will be less likely to play an important role in weather a material can meet the mooring requirements. For example the survivability of a mooring line is not likely to be affected by tension ranges less than the pre-tension prescribed in the design of a mooring. The error in the prediction for tension above the pre-tension shows an under prediction from the model for a lot of the tension conditions (figure 4.26). The larger magnitude errors are over predictions which can be observed when the tension is below or close to the pre-tension or at the highest tension situations. The over prediction for the highest tensions can be observed in the

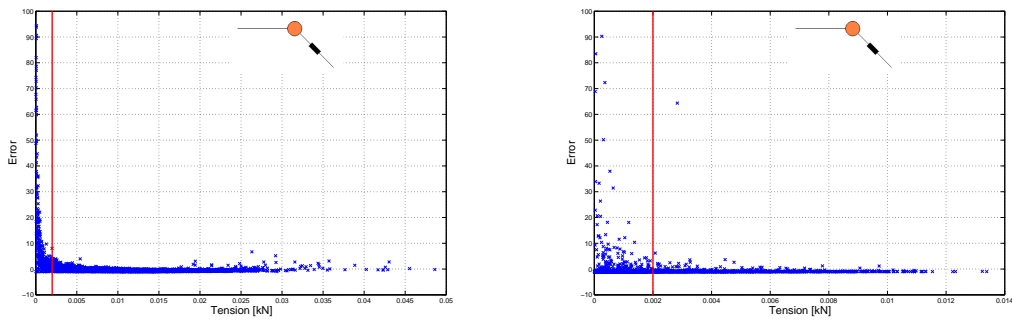


(a) Comparison between numerical simulation and experimental results of tension in line mooring line at position A during test 3030

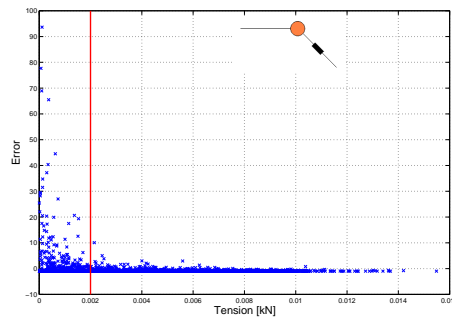


(b) Comparison between numerical simulation and experimental results of tension in line mooring line at position B during test 3030

Figure 4.23: Comparison between simulation and experimentation of tension in mooring lines during test 3030



(a) Error between simulation and experimentation against experimental tension in the bow line for test 3030 position A  
 (b) Error between simulation and experimentation against experimental tension in the port line for test 3030 position A



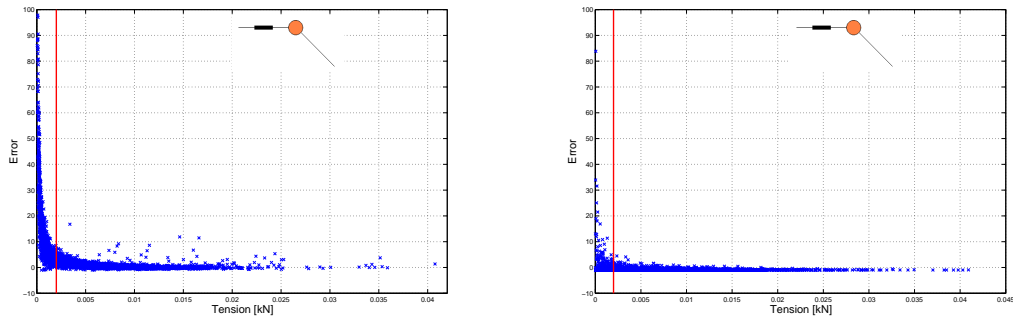
(c) Error between simulation and experimentation against experimental tension in the starboard line for test 3030 position A

Figure 4.24: Error between simulation results and experimental results against experimental tension for tests 3030 position A

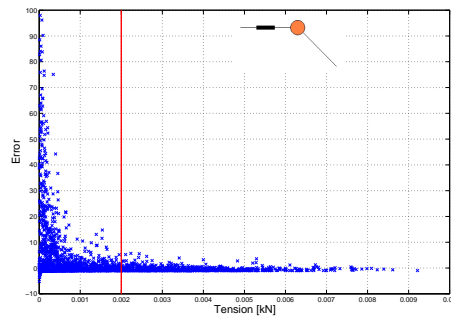
time history where snatch loading is present. The numerical model shows these events but the magnitude of the tension during the snatch loads is generally over predicted (figure 4.4).

From a design aspect the key data that would be taken from this result to make design choices for the mooring lines would be the maximum, minimum and the mean tension in the mooring lines (Table 4.9). An average of the proportional differences of the maximum, minimum and mean for the tension prediction over the different tests is shown in figure 4.28. This is calculated by dividing the numerical output for the maximum, minimum and mean by the experimental data and the averaging the results.

In an attempt to further represent this data in a more concise manor a spectral analysis of the time history of the tension in the mooring lines was performed. This is shown in

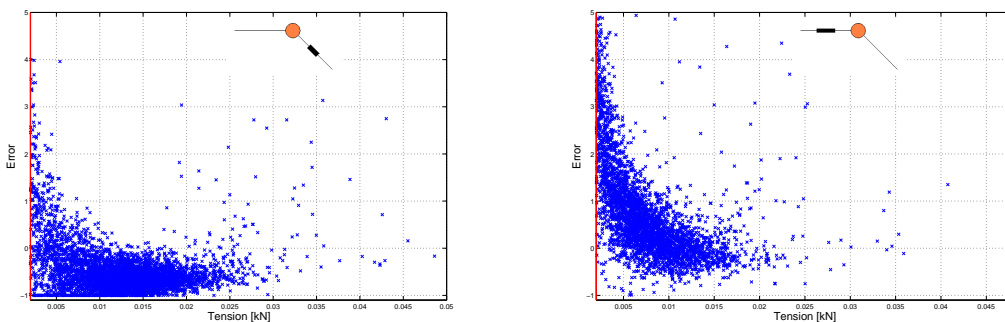


(a) Error between simulation and experimentation against experimental tension in the bow line for test 3030 position B  
 (b) Error between simulation and experimentation against experimental tension in the port line for test 3030 position B



(c) Error between simulation and experimentation against experimental tension in the starboard line for test 3030 position B

Figure 4.25: Error between simulation results and experimental results against experimental tension for tests 3030 position B



(a) Bow line A

(b) Bow line B

Figure 4.26: Difference between the numerical prediction and the experimental data for the tension in the bow mooring line during test 3030 at the different load cell positions

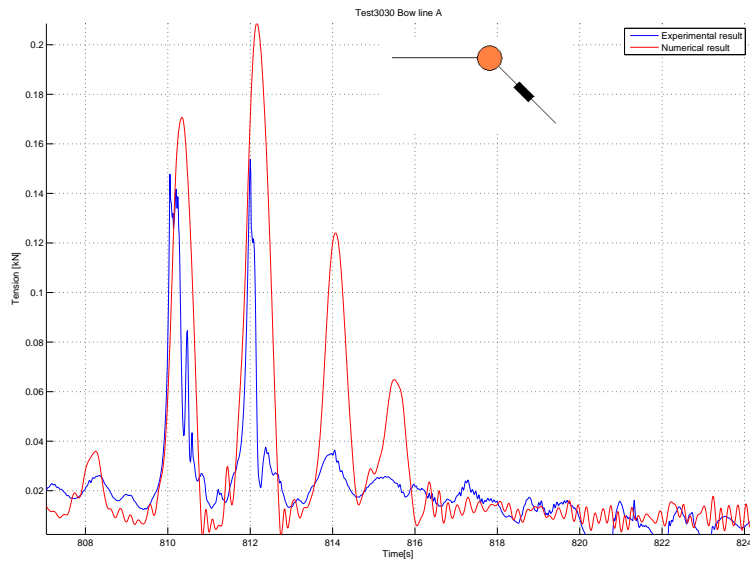


Figure 4.27: Example of snatch load during test 3030 in bow line A

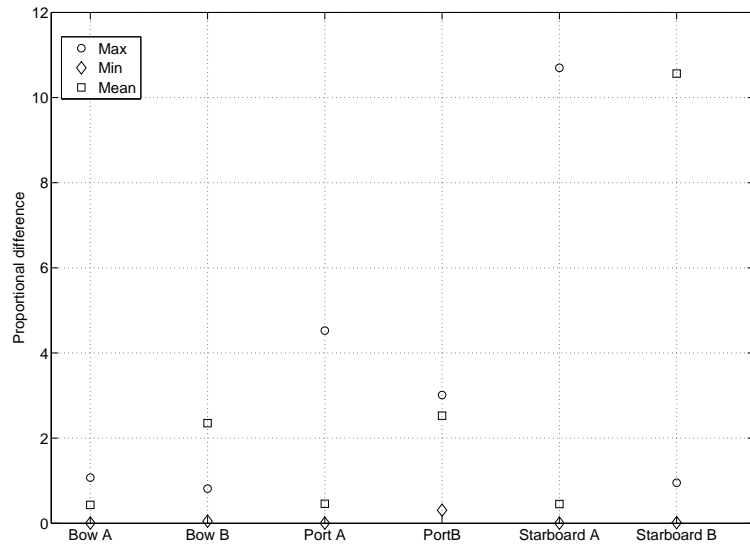


Figure 4.28: Average proportional difference between the experimental data and the numerical simulations

Table 4.9: Maximum minimum and mean results from experimental data (exp) and numerical simulations (num)

Load cell position	Parameter [kN]	Test 3000 Exp	Test 3000 num	Test3010 Exp	Test3010 num	Test3030 Exp	Test3030 num	Test3041 Exp	Test3041 num
Bow A	max	2.760E-02	3.896E-02	1.534E-01	9.386E-02	1.674E-01	2.031E-01	0.1528	1.607E-01
	min	-9.000E-04	-3.000E-06	-7.000E-04	-4.200E-06	-8.000E-04	-4.900E-06	-0.0034	-5.500E-06
	mean	7.100E-03	3.365E-03	1.090E-02	5.251E-03	1.120E-02	6.098E-03	0.0097	2.210E-03
Bow B	max	2.270E-02	2.267E-02	1.433E-01	1.021E-01	1.592E-01	2.088E-01	0.1426	3.414E-02
	min	-2.700E-03	-1.664E-04	-3.500E-03	-7.320E-05	-2.800E-03	-3.910E-05	-0.0027	-2.729E-04
	mean	2.100E-03	7.397E-03	3.600E-03	9.651E-03	5.500E-03	1.082E-02	0.0045	5.556E-03
Port A	max	1.590E-02	1.896E-01	1.980E-02	3.756E-02	1.790E-02	3.954E-02	0.0159	3.293E-02
	min	-1.600E-03	-3.300E-06	-1.600E-03	-6.200E-06	-1.800E-03	-4.900E-06	-0.0044	-2.100E-06
	mean	1.000E-03	4.820E-04	1.500E-03	6.317E-04	1.500E-03	7.116E-04	0.0032	1.450E-03
Port B	max	8.000E-03	1.937E-02	1.050E-02	2.502E-02	1.020E-02	3.229E-02	0.0089	3.629E-02
	min	-8.000E-04	-3.397E-04	-1.100E-03	-1.303E-04	-1.000E-03	-6.207E-04	-0.0016	-1.080E-04
	mean	4.000E-04	9.686E-04	5.000E-04	1.358E-03	6.000E-04	1.633E-03	0.0014	3.155E-03
Starboard A	max	1.450E-02	6.572E-02	1.780E-02	3.077E-01	1.390E-02	2.223E-01	0.0119	5.931E-02
	min	-1.300E-03	-3.300E-06	-1.500E-03	-6.200E-06	-1.600E-03	-4.600E-06	-0.0050	-6.500E-06
	mean	7.000E-04	3.949E-04	9.000E-04	5.748E-04	6.000E-04	6.144E-04	-0.0019	7.973E-04
Starboard B	max	3.140E-02	2.546E-02	4.190E-02	2.603E-02	4.540E-02	2.863E-02	0.0249	4.347E-02
	min	-2.710E-02	-3.273E-04	-3.640E-02	-4.026E-04	-3.880E-02	-8.656E-04	-0.0459	-4.306E-04
	mean	1.600E-03	6.899E-04	2.100E-03	1.054E-03	0.000E+00	1.342E-03	-0.0124	1.290E-03

figures 4.29 and 4.30 where the spectral density of the mooring line tension from the experimental data and numerical predictions are plotted together. The form of the spectral density plots for the experimental data and the numerical data agree closely. This shows that the source of tension variation in the mooring line comes only from the excitation of the WEC body and the marker buoy. If there were any other peaks in the numerical simulation this would indicate that the model was predicting some other source of excitation of the mooring line resulting in tension variations that were un-realistic. The comparison shows that the response of the tension of the mooring line happens at two main frequencies. This is at the wave frequency at 0.58Hz and at a lower frequency. The motion modes of the WEC body that have a dominant effect on the tension in the mooring lines is the surge, heave and pitch motions. The first order motion at the wave frequency clearly have an effect on the tension in the mooring line as can be seen from figures 4.29 and 4.30 by the peak at 0.58Hz. This shows that the motion of the WEC body and marker buoy are causing tension variations however the numerical prediction over predicts the contribution to the mooring line tension at the wave frequency. The second peak in figures 4.29 and 4.30 is at a much lower frequency of around 0.03Hz. This is at frequency in the range of the natural period on the surge motion of the moored system. This shows that the larger motions in surge from resonance in the system have a very large effect on the tension in the mooring line. At this frequency the numerical prediction under predicts the tension in the mooring line for the measurements at position A however the tension is under predicted for this frequency range for the measurement at position B in the mooring line. This has the effect of an under and over prediction in the mean tension in the mooring line for position A and B respectively. This is backed up by figure 4.28 and table 4.9.

This model only predicts the mooring line response and as such the cause of any disparity lies with the definition of the mooring line. One such source of error is the definition of the marker buoy as the motion of this was not measured during the experiments and the motion of which is not prescribed in the model definition. As such any excessive motion of the marker buoy from the still water position would cause over predictions of the mooring line tension. Due to the size of the marker buoy the motion response to the wave field would be close to the wave frequency.

The mooring line characterisation could also be a source for the error in the prediction. The error in the characterisation of the mooring line is known to be 0.9%. This kind of

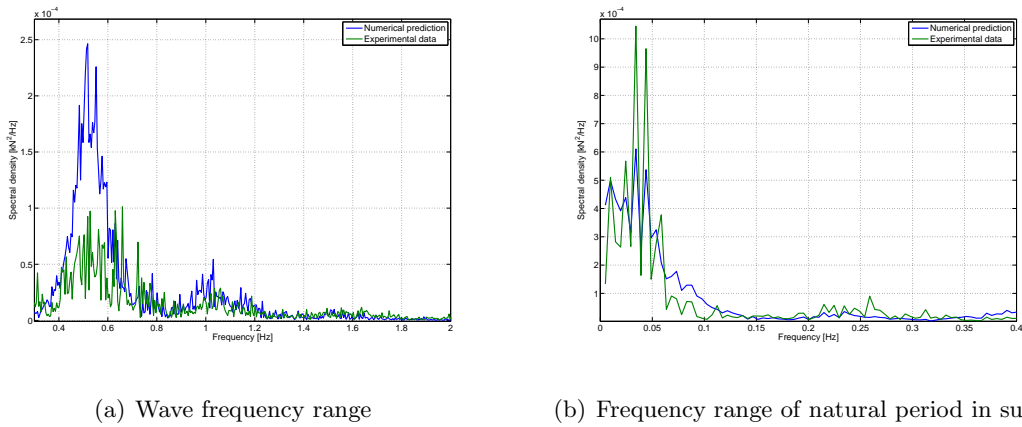


Figure 4.29: Comparison spectral density of the tension in the bow mooring line at position A between experimental and numerical data

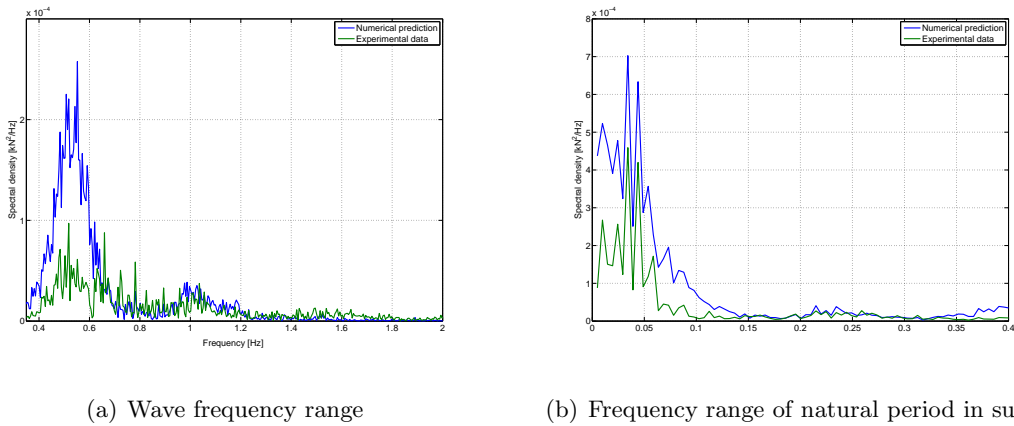


Figure 4.30: Comparison spectral density of the tension in the bow mooring line at position B between experimental and numerical data

error would count very little to the overall error in the simulation as the peak in numerical prediction of the spectral density indicates that the magnitude of the tension is 1.5 times the experimental data. The characterisation of the hydrodynamics of the mooring line would dictate the motion of the line through the water during top end displacements. As mentioned in chapter one due to the dynamic nature of the simulation the motion of the line during a displacement of the top end structure would not be uniform. This non-uniform motion can variations in the tension and any error in the definition of the drag parameters of the mooring line would lead errors in the overall prediction.

From the data presented in figure 4.28 the largest disparity between the prediction and the experimental data appears in the predictions for the tension in the lines at position B. This portion of the mooring line is more often in a slack condition during the tests than



the line in position A. As shown in figure 4.26 during slacker conditions the numerical predictions become less accurate and the predictions for position B contain more error than the predictions for position A. Due to the directionality of the waves the bow line tension prediction is of particular interest and as shown in figure 4.28 it is the predictions for this line that are the closest to the experimental results. Over the different test conducted in this test series the numerical models have been shown to under predict the mean tension in mooring line in position A and over predict the tension in the mooring line in position B. The under prediction of the mean tension in position A by the mooring lines means that the numerical model result is less than half the experimental result. This is the same for the starboard and port mooring lines in position A where the numerical models are under predicting the mean tension. For position B the mean tension for all the mooring lines is over predicted.

The largest difference between the maximum tension predicted by the simulations and the experimental result for tensions greater than the pre-tension has been evaluated here to be as much as 16 times the experimental result. This would clearly have an effect on the design of the mooring system in terms of the mooring component choices. The breaking load of the material is an important factor, as this is the first limit for the selection of mooring components. There is clearly a direct impact on the minimum breaking load required from a mooring due to any over prediction from numerical simulation. Harris et al. (2004) has shown how the cost per meter of mooring line material increases with the theoretical minimum breaking load of different materials including chains, wire ropes and synthetic ropes. The numerical prediction resulting in the maximum tension which is 16 times the experimental data can be seen in the tension in the starboard mooring line at position A during test 3010 of 0.01779 kN. This was predicted to be 0.30770 kN by the numerical model. At full scale the loading from this experimental data and the numerical prediction would be 14.5 tonnes and 250.9 tonnes respectively. According to the work by Harris et al. (2004) (figure 4.31) the breaking load of 14.5 tonnes would be a very small load and would not exceed any of the mooring line materials that were presented there, whereas the load of 250 tonnes would greatly increase this cost of the mooring line as the material choice would have to reflect this predicted maximum load.

This over prediction in the breaking load of the mooring line would force the designer to change the material used in the initial design of the moorings. The implementation of

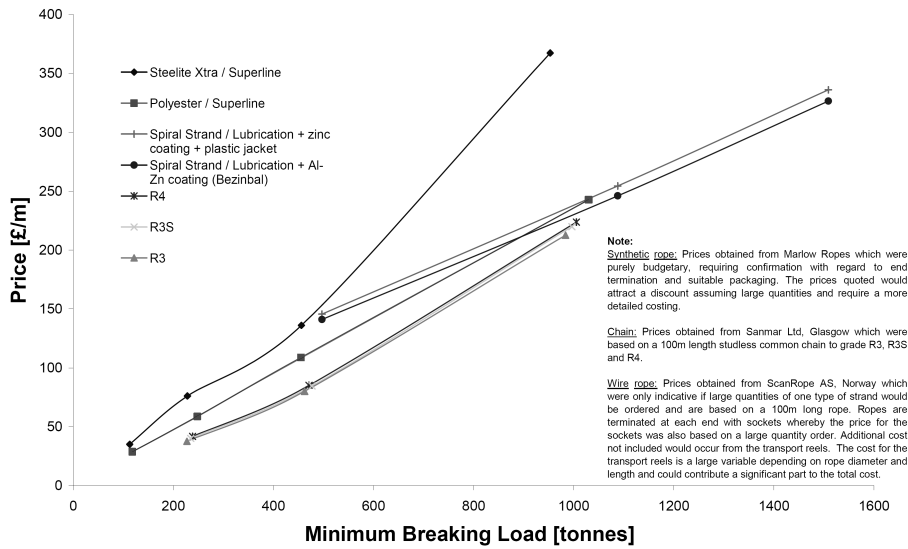


Figure 4.31: Comparison of cost of mooring line materials Harris et al. (2004)

this new mooring material could then change the hydrodynamic properties of the system in terms of the stiffness and damping in the system. As described throughout this project, WEC motion responses and power conversion efficiency are very sensitive to changes to these properties. As such the design task could become an iterative process where the motion characteristics, survivability and the practical application of the design could conflict.

Another aspect of the design process that is affected by the tension range of the mooring lines would be the component reliability. Thies et al. (2012) applied a life cycle analysis to the some of the data used in this project. This work used S-N curves taken from the DNV to calculate the fatigue damage and design years for different options of mooring line materials. The S-N curves are generated for different materials where  $S$  is the nominal stress to range and  $N$  is the number of cycles to failure. The S-N curve is based on equation 4.8 where  $N(S)$  is the number of cycles to failure at a certain stress,  $S$  is the constant amplitude cyclic stress,  $K$  is the intercept parameter and  $\beta$  describes the slope of the S-N curve. An example of S-N curves are shown in figure 4.32 taken from the OS-E301 (2001).

$$\log(N(S)) = \log(k) - \beta \log(S) \quad (4.8)$$

Using the rain flow cycle count method the number of cycles of the system the com-

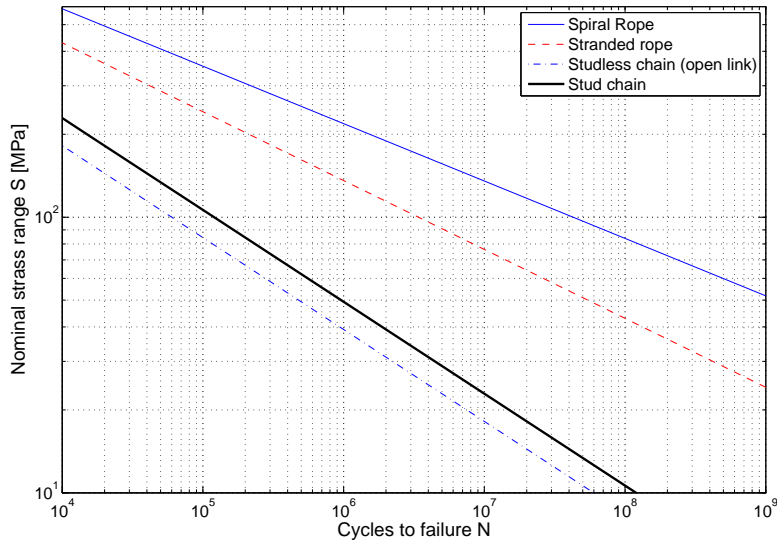


Figure 4.32: Nominal S-N fatigue curves for different mooring materials

ponents experience at different stress ranges was evaluated by Thies et al. (2012). The number of cycles at a given stress range is then compared to the number of cycles to failure at that stress range for different materials using the S-N curves. The percentages of the different numbers of cycles compared the number of cycles to failure are the added together using a linear cumulative fatigue rule. If the cumulative fatigue is above 100% then the system is classified as failed. The tension range predicted by the numerical analysis will clearly affect the life cycle analysis of the mooring line components where the range will be based on the tension during both taut and slack conditions. Clearly over prediction of the tension range due to over and under prediction of the absolute tension would lead to ill informed decisions being made by the engineer or designer as to the material selection for mooring components.

CHAPTER

5

COUPLED MODEL PREDICTION OF  
MOTION RESPONSE AND MOORING  
LINE TENSION

## 5.1 Introduction to coupled simulation study

To evaluate the capability of the numerical models in the prediction of the response of a floating moored WEC the calculation of the floating body will be included. This chapter explains how the motion response of the floating body can be represented in the numerical models and simulations are run of the coupled moored system. This chapter will also explain experiments to determine the motion response of the scale model and a comparison is made between the experimental data and the output of the numerical simulations.

- Model inputs
  - WEC response characteristics (RAOs and coefficients for Morison equation)
  - Statistical parameters for wave train using (Linear airy/JONSWAP spectrum)
  - mass properties for marker buoys
  - Stiffness and drag properties for the mooring material
- Outputs
  - WEC body motions
  - Mooring line tension
  - Marker buoy motion response

## 5.2 Experimental RAOs

Evaluating the amplitude response of the scale model system to a given wave frequency allows the RAO to be derived. In these tests a regular frequency oscillation is induced in the system. In the case of a moored WEC this requires regular waves to be produced in a wave basin. The device is allowed to respond in all degrees of freedom and the displacement is measured. The amplitude of the motion of the system at steady state (after any build up stage or transient) is compared to the amplitude of the water surface elevation. The amplitude of the motion response of the WEC body is then normalised to the wave amplitude for the frequency of the wave. A range of wave frequencies are used to produce an RAO curve across the frequency range of interest. The complication is

therefore to ensure that the system has reached a steady state of response to the regular waves for which to evaluate the response over.

There are two methods of evaluating the RAOs, a frequency domain and a time domain method:

- **Frequency domain** - This method requires the spectral density of the motion of the WEC be compared to the spectral density of the water surface elevation. The spectral density is calculated using a Fast Fourier Transform (FFT) routine. An FFT routine changes the signal of the data of the response of the body of the WEC from the time domain to the frequency domain. The FFT function (equation 5.1) breaks the time domain signal down in to a number of wave components which, when added together would produce the input signal. The spectral density can be calculated from this using equation 5.4 (more detail on these methods can be found in Tucker and Pitt (2001)).

$$\zeta(t) = \frac{1}{2}a_0 + \sum_{n=1}^{\infty} [a_n \cos(2\pi nt/D) + b_n \sin(2\pi nt/D)] \quad (5.1)$$

$$a_n = \frac{2}{D} \int_{-D/2}^{+D/2} \zeta(t) \cos(2\pi nt/D) dt \quad (5.2)$$

$$b_n = \frac{2}{D} \int_{-D/2}^{+D/2} \zeta(t) \sin(2\pi nt/D) dt \quad (5.3)$$

$$\widehat{S}(f)\Delta f = \frac{1}{2} \sum_{\Delta f} (a_n^2 + b_n^2) \quad (5.4)$$

- **Time domain** - This method requires the individual cycles of motion to be compared to the individual cycles of water surface elevation. This means that the moving average due to any second order drift motion must be removed from the data as shown in figure 5.1. This then allows the zero crossing points of the time history to be identified. The individual cycles can then be separated (figure 5.2) and the amplitude of the individual cycles can be identified. This is also done for the water surface elevation, again allowing the amplitude of the individual cycles to be identified. This then allows a direct comparison between each wave event and the motion response in all six degrees of freedom.

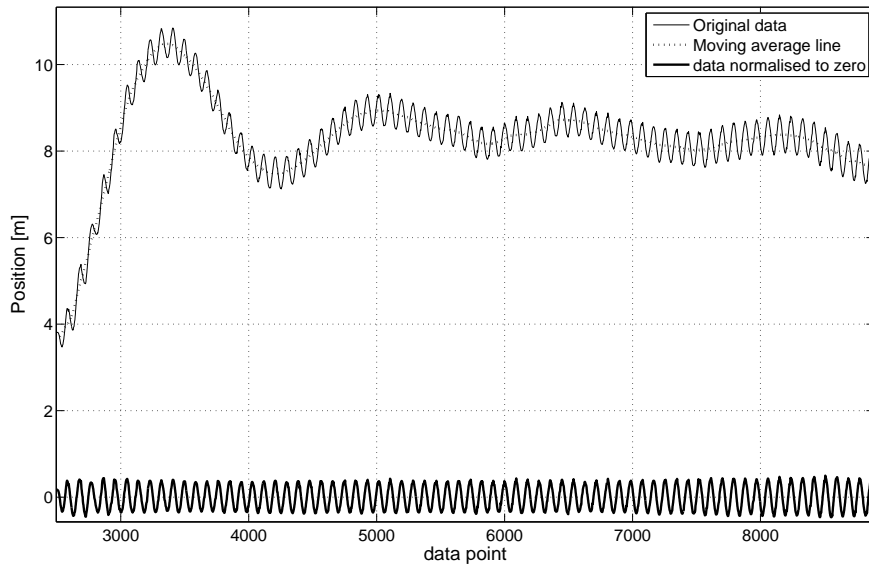


Figure 5.1: Applying a moving average and removing trend for time history data

The RAOs are evaluated for different cases within the regular wave test series in the Heriot-Watt wave basin:

- RAO tests at two different wave heights
- RAO tests with test mooring system and soft mooring system
- RAO tests with and without power take off system active

### 5.2.1 RAO tests with different amplitudes

Figure 5.3 shows the comparison between the two methods for deriving the RAO. A difference in the RAOs calculated by the different methods can be observed. This difference is due to the fact that the time domain analysis allows easier control over the data used. The analyst has the discretion to decide which wave peaks to omit or include depending on the signal. In some cases the waves are regular and the task of identifying the peaks of motion is simple. If the signal is noisy or the motion is high frequency and with lots of harmonics it can be difficult to identify the important peaks. In these cases it is better for the analyst to identify useful peaks in the time history rather than use a spectral result.

The RAO's calculated from the other tests are presented in appendix C. These include the tests with taut and light moorings where the experiments with light moorings include

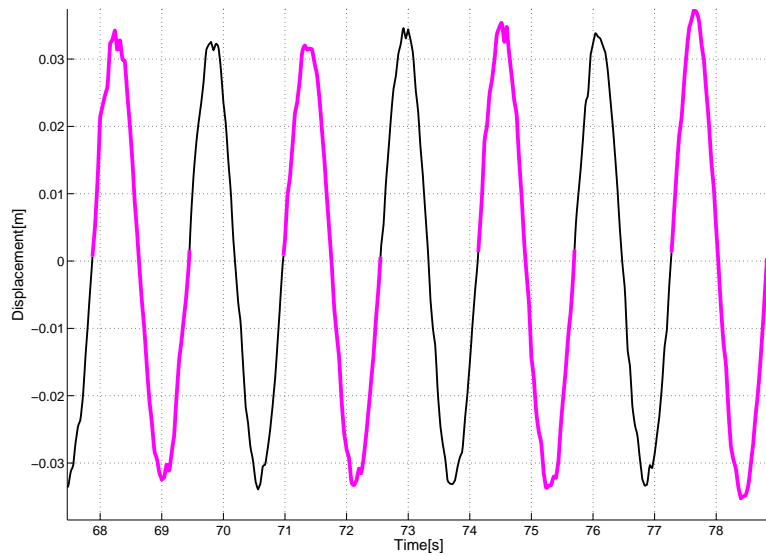


Figure 5.2: Example of time history having been separated into individual waves

tests with the orifice plate in the open and closed position. RAO's are also calculated for different angled seas which are important when taking into account the non-symmetry of the taut mooring system.

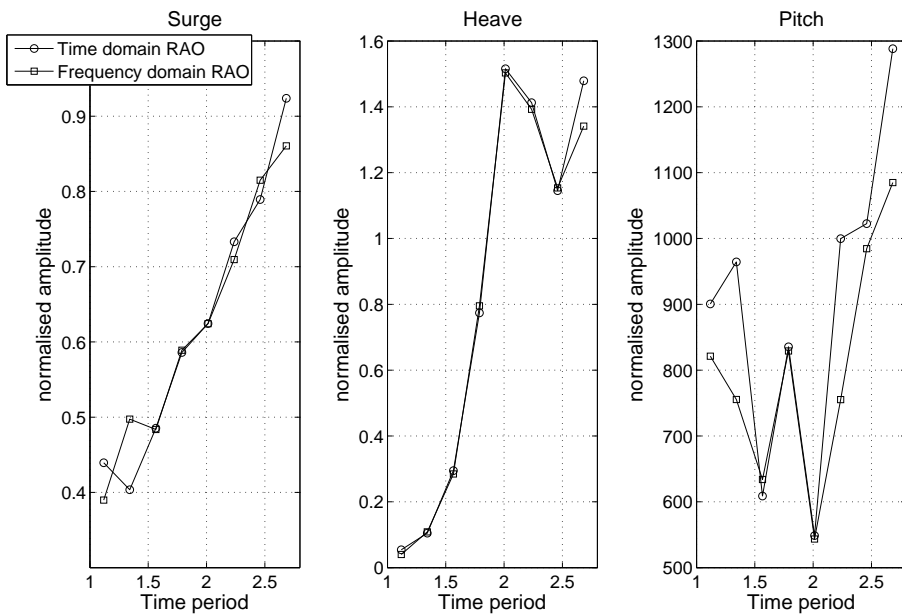


Figure 5.3: Comparison between frequency domain method and time domain method for WEC with light mooring and closed orifice



The RAO's produced represent the motion for the WEC under different configurations as well as different conditions. One of the RAO test had the settings on the wave paddles at 100% gain. This produced waves with an amplitude twice that of the amplitude required. From the theory regarding RAO's this should not produce a different RAO as the amplitude of the response is linear with wave height. When comparing the RAOs with the response normalised to the wave height from the test with the paddles set to 100% gain and 50% gain (figure 5.4) one can see a difference. The trend in the response is close for periods between 1 and 2 for all 6 degrees of freedom (although the modes of roll and pitch seem to differ more than the other modes).

From a time period of 2 to 3 the RAOs differ allot where the largest difference occurs at time period 2.9 seconds. The RAO for the test with the paddles set to 100% gain at 2.9 seconds wave period, the response appears to be reduced significantly for all degrees of motion. For the modes of motion of pitch and roll the trend between the two RAOs appears to diverge (more so for roll). For the motion of roll the shape of the RAO appears to be similar even though the magnitude of response is different. This suggests that the RAOs normalised response is not invariant with wave amplitude. This would be due to the mooring system as the assumption that the magnitude of response is linear with wave amplitude is for completely free RAOs where the floating body is not restrained. The RAOs for pitch have a similar shape but at the time periods of 3.1 and 3.4 seconds the RAO for the test with the paddle gain set to 100% indicated a response higher in magnitude than that of the RAO for the paddle gain set to 50%.

### **5.2.2 Different mooring arrangements**

The different moorings were designed to allow the response of the moored WEC to be evaluated as well as the response of an un-moored WEC. Due to experimental constraints it was not possible to run a test with the WEC completely un-restrained. For this reason the soft moorings were used to give an approximation to the response of a free floating device. The soft moorings used were designed to affect the first order motion of the WEC as little as possible. The mooring in this case was designed to reduce only the second order drift forces to ensure that the device remains in the capture window of the measuring equipment and does not collide with anything.

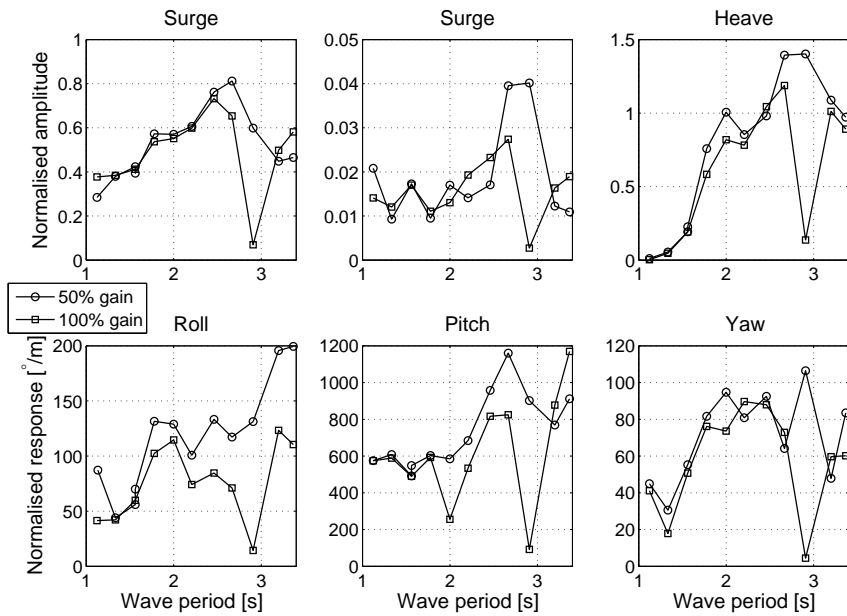


Figure 5.4: Comparison between the RAO's for tests with the wave paddle gain set to 100% and 50%

The comparison of the RAO's from the test with the different moorings (figure 5.5) show that the response of the WEC when moored with the soft moorings is larger than with the taut moorings. Due to the drift motions of the device it is difficult to get accurate first order response amplitude as using the moving average method can reduce the amplitude. For this reason the accuracy of the RAOs calculated could be questioned however due to the agreement between the different tests there is argument to suggest that the results are reliable.

The surge response of the two arrangements differ most at the lower wave periods and appear to agree at the higher periods. This could be explained when looking at the time periods, as the during the lower time period tests the second order drift motions are larger. This means that the WEC will be restrained in surge more by the moorings as the device surges away from the still water equilibrium position. A similar effect can be observed for the pitch where the difference in the response of the device is largest at the low time periods. Because the test mooring has a line connected to the bow of the device the pitch will be restrained at large excursions from the still water equilibrium point.

The heave motion of the device when moored using the test or soft mooring appear to be very similar in amplitude. This suggests that the heave motion is restricted in a similar

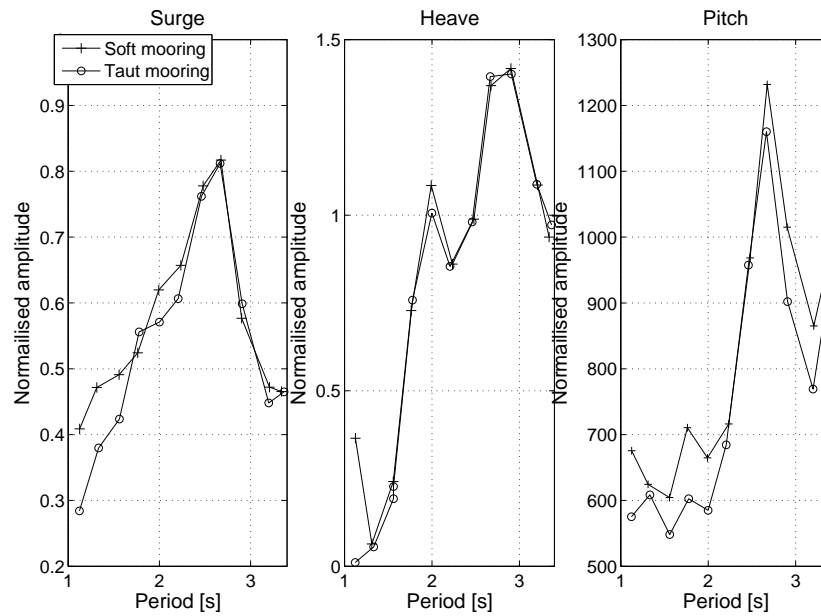


Figure 5.5: Comparison between tests with test moorings and soft moorings

way for both configurations. The presence of the damping plate could be providing a restraint effect greater than the mooring device and as such any difference in heave motion due mooring configuration could be being masked by the dominance of the drag from the damping plate.

### 5.2.3 Power take-off system

The effect of the power take off system (the orifice plate) adds a complication when trying to recreate the system in numerical models. To give some sort of validation to simpler models before adding the complication of the OWC, an RAO test was conducted with the orifice plate closed and blocked. This leaves the WEC resembling an upturned cylinder with one open end below the water and a damping plate at the keel. This set up was tested with the soft moorings in place. The first thing to notice from the comparison of the RAOs (figure 5.6) for the soft moored WEC with the orifice plate open and the soft moored WEC with the orifice plate closed is that the RAOs are of similar magnitudes.

Also the shape of the RAOs is similar although differing slightly and the data for the RAO for the light moored WEC with a closed orifice plate has a maximum time period of 2.68 whereas the test for the WEC with the open orifice continues to 3.35. The RAOs for

surge have very similar trends although the RAO for the WEC with a closed orifice has higher response than the WEC with the open orifice.

The RAOs for the heave motion again have very similar trends and in this case even at the higher time periods. The magnitude of response is higher for the higher periods (1.79 seconds +) for the RAO from the WEC with the closed orifice but has a peak at the same period (2 seconds). The response at 2.5 seconds for the RAO for the WEC with the closed orifice is the minima of a trough where as for the RAO for the WEC with the open orifice the response at 2.24 seconds is the turning point for the trough. Again because of the limited range of the data in terms of time period the second peak in the heave response for the closed orifice plate RAO could not be identified. The pitch RAO's differ allot where the response of the RAO for the WEC with the open orifice varies from 0.0018 to 0.018 whereas the RAO for the WEC with the close orifice varies between 0.009 and 0.019.

It could be interpreted from the comparison that the RAOs have similar shapes as there are two troughs for the RAOs within the range of the data from the test with the closed orifice. Although similar to the heave RAO the peaks do not necessarily happen at the same time period. An explanation for the increased in response amplitude that occurs when the orifice plate is closed is the movement of air in the internal chamber. The operating principal of the device is to allow the air in the chamber to pass though the turbine which, although offers a resistance reduces the pressure inside the chamber allowing the water to rise in the chamber reducing the upward force on the device. When the orifice plate is closed air inside the chamber has nowhere to go and the device must respond in heave to relieve the internal pressure. This means that the relative water height up in the chamber does not change as much as if the orifice plate were open. This means that that during the situation where a crest of a wave passes the device would not sit as low in the water if the orifice plate is closed and as such would reduce the stability of the device in the toppling motion mode of pitch.

### 5.3 Numerical RAOs

Using diffraction theory numerical predictions of the floating body response can be made in the form of RAOs. In the case of the “generic WEC” the application of diffraction theory will be done using WAMIT.

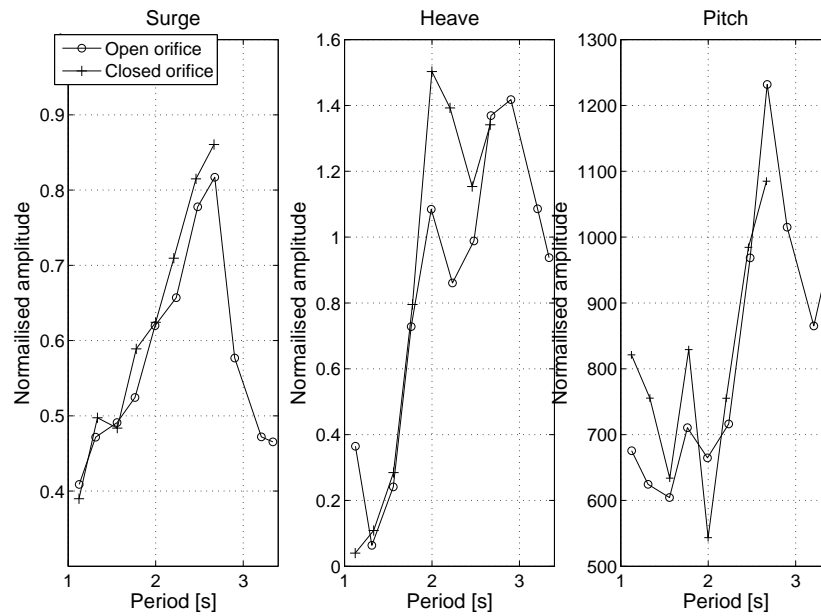


Figure 5.6: Comparison between tests with light moorings and open orifice and light moorings and closed orifice

The method for generating the body geometry will use Matlab routines (shown in appendix D.0.1) to define the different shapes that make up the WEC body. In order to validate the MatLab routines a simple cylinder model is created, the result from which is compared to a WAMIT example model of the same cylinder (appendix E) show the MatLab routines to produce the same result. The model is then refined to represent the mass properties and size of the scale model of the floating WEC (figure 4.8). To indicate whether the model is outputting sensible results convergence testing is conducted on the mesh resolution (Payne (2006), Lee et al. (Lee:1996)). These tests require the mesh resolution to be increased and the lower resolutions compared to the highest resolution model to indicate whether the difference between the models is reducing as the resolution is increased. The level of mesh resolution is a trade of between computation efficiency and accuracy of the result. The results of the simple cylinder model where the data reflects the size and mass of the scale model used in the experimentation show good convergence and can be found in appendix E.

The final model geometry is based on a simple cylinder with the addition of the damping plate at the keel. A simplification of the attachment of the damping plate is made by placing two thin attachments pieces rather than the three as on the actual WEC. The

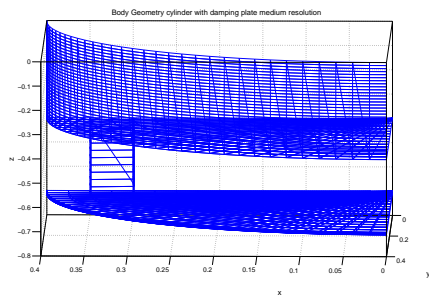
attachments on the WEC consist of a square loop of metal (figure 5.7(c)). The geometry, similar to the previous models in the appendices, is written as a quadrant of the final body (figure 5.7(a)). The geometry is reflected in the x and y axis creating the full model as shown in figure 5.7(b) where the blue colouration of the panels indicates the wetted face of the model.

Figure 5.8 show a difference in the response amplitude between the different model resolutions. This give some confidence that the model is producing sensible results as the difference reduces as the model mesh resolution increases. Figure 5.9 shows the error between the different models in the convergence test. The models show a convergence on the solution provided by the highest resolution. This gives confidence that a solution for the highest resolution model is an appropriate approximation to the response characteristic of the WEC body. Figure 5.8 shows the final RAO that will inform the time domain simulations. The RAO will however, be a load RAO as opposed to the displacement RAOs presented here.

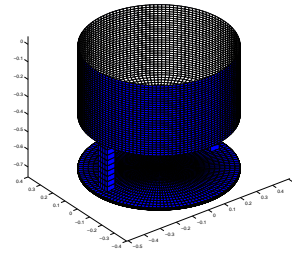
## 5.4 Time domain simulation of coupled system

For this simulation all three of the problems of solving the response of a floating WEC object will be included. This takes advantage of the ability of OrcaFlex to calculate the coupled response of the system using different methods. As such the breakdown of this section can be shown as follows:

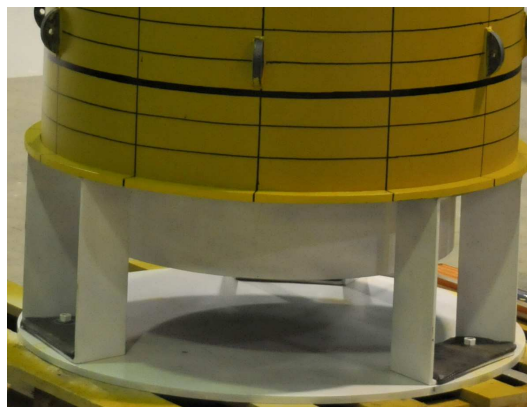
- Environment-wave data will be calculated using a JONSWAP spectrum for the irregular wave states and Linear theory for the regular wave states
- Mooring system - The model for the mooring system will be taken from the physical properties identified in the experimental section and the numerical study conducted in Chapter 4.
- Floating body - OrcaFlex has a number of options when modelling a floating body. This section will look in to modelling the body using two options; 6 degree of freedom buoy and using RAO's derived numerically from diffraction theory.



(a) Wire frame quadrant for the Cylinder with damping plate model medium resolution



(b) Full body Geometry for Cylinder with damping plate model medium resolution



(c) WEC attachment point

Figure 5.7: body geometry for Cylinder with damping plate

### 5.4.1 Floating body

Modelling the generic WEC using the 6 degree of freedom buoy option allows the user to define the geometry of the body using the “Spar Buoy” model. The spar buoy model takes advantage of the Generic WEC’s cylindrical structure. It requires the body be broken down in to cylinders specifying an inner and outer diameter and height. Figure 5.10 shows the geometric structure and Table 5.1 shows the mass properties for the model of the buoy. For this approximation the buoys response is controlled by added mass and drag parameters that must be defined in the model. The forces on the body are then calculated using the Morrison equation.

The drag parameters for the model are defined in this instance using the DNV codes as set out in DNV-RP-H103 (2011)(Figures 5.11, 5.12). The drag properties are calculated for each cylinder that makes up the geometry for the body. This allows the model to

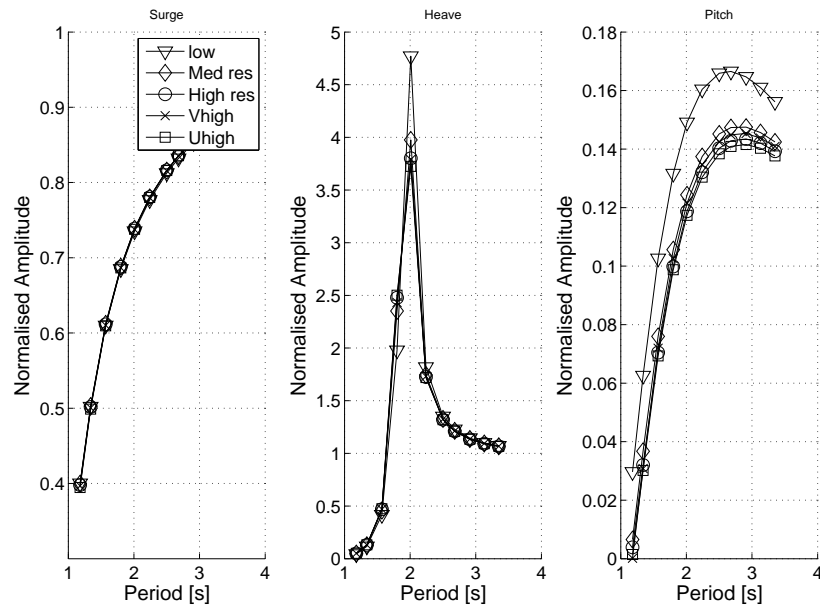


Figure 5.8: Comparison of WAMIT calculated RAO's for a cylinder with damping plate using low, medium, high, very high and ultra-high resolution

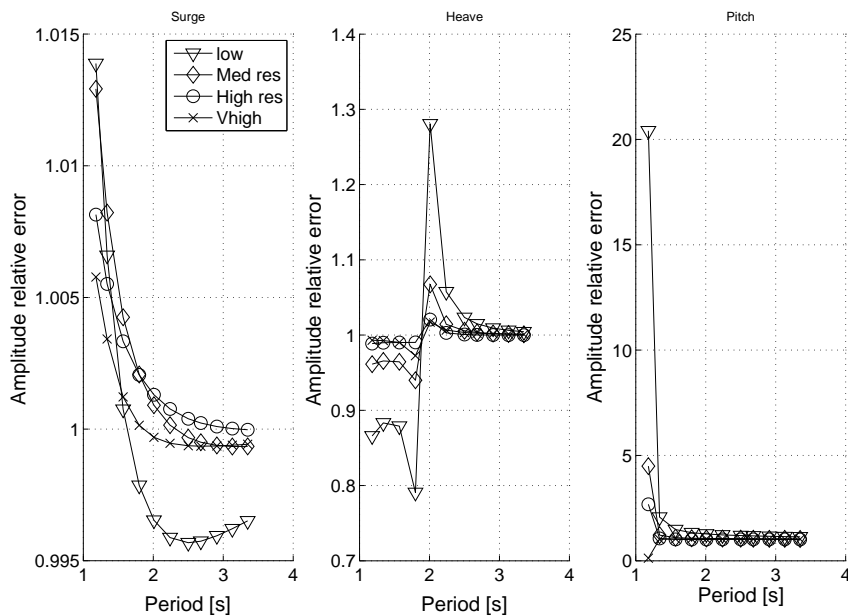


Figure 5.9: Error between the different resolution models against the highest resolution model



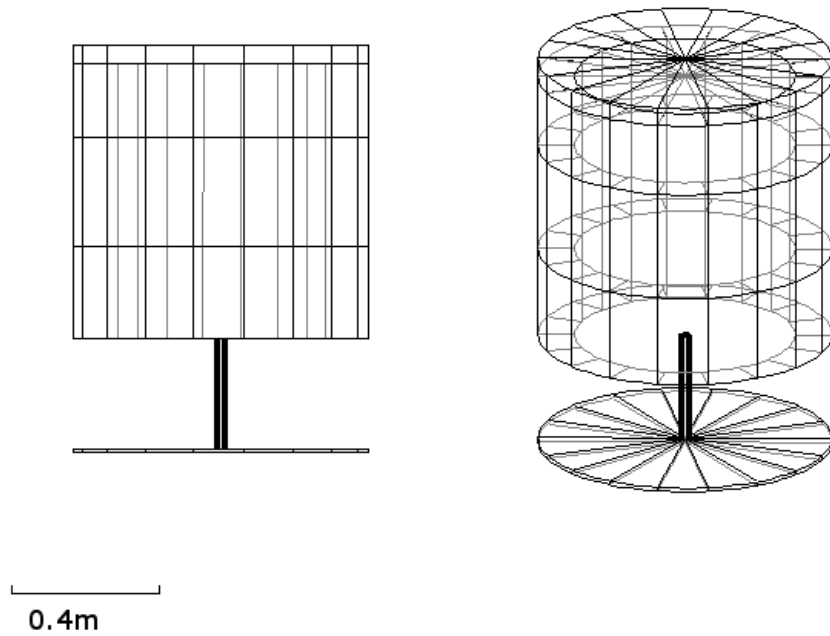


Figure 5.10: Buoy geometry for Morrison spar buoy approximation

Table 5.1: Mass properties for Morrison approximation

Mass	Mass Moments			Centre of mass		
	x	y	z	x	y	z
100	0.013	0.013	0.009	0	0	0.5

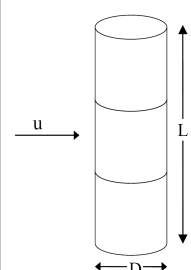
Circular cylinder normal to flow.	L/D	Sub critical flow	Supercritical flow
		$Re < 10^5$	$Re > 5 \cdot 10^5$
	2	$\kappa$ 0.58	$\kappa$ 0.80
	5	0.62	0.80
	10	0.68	0.82
	20	0.74	0.90
	40	0.82	0.98
	50	0.87	0.99
	100	0.98	1.00
$C_{DS} = \kappa C_{DS}^\infty$			
$\kappa$ is the reduction factor due to finite length. $C_{DS}^\infty$ is the 2D steady drag coefficient.			

Figure 5.11: Drag on a vertical cylinder source: DNV-RP-H103 (2011)

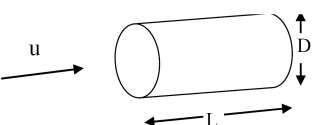
Circular cylinder. Axis parallel to flow.	L/D	
	0	1.12
	1	0.91
	2	0.85
	4	0.87
	7	0.99

Figure 5.12: Drag on a horizontal cylinder source: DNV-RP-H103 (2011)

handle the drag moments, as couples can be generated by a different loads being applied to different sub-cylinders. The added mass properties are set in a similar way with one difference. The added mass properties for a vertical cylinder have the coefficients set to 1 as is suggested by Orcina for this shape. The vertical added mass properties are again set using the DNV codes found in DNV-RP-H103 (2011). For this model the drift force on the buoy will arise naturally from the Morison approximation of the loads on the buoy and as such the drift force does not need to be explicitly calculated.

To model the WEC body using the numerically derived RAOs from diffraction theory the output from the WAMIT model from section 5.3 is imported directly in to OrcaFlex. The RAOs used will be the load RAOs where the load on the floating body in a specific motion mode is defined normalised to the wave amplitude. This allows the loads from the wave excitation to be calculated for the different regular wave components. The output from WAMIT includes the stiffness, added mass and damping properties for the body. The drift force will be evaluated using QTFs which, similar to RAOs normalise the drift force on the body to the square of the wave amplitude.

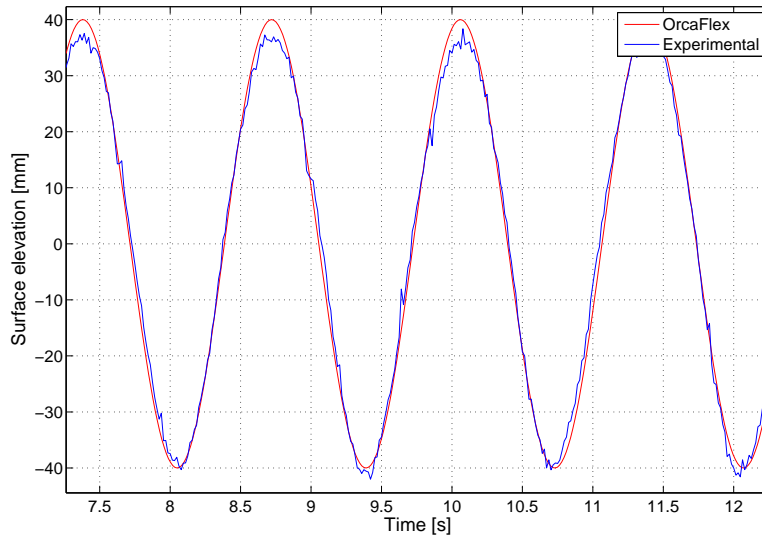


Figure 5.13: Comparison between experimental wave profile and numerical approximation

#### 5.4.2 Wave environment

This set of numerical simulations will use both irregular and regular waves. For the regular waves the wave height and period will match the regular wave set used in the experimental section. To create the waves in the numerical environment the selection of the appropriate theory is required. This is done referring to figure 2.4 where the linear theory is selected. The depth of the water in the numerical simulation is set to the depth of the wave basins (2.8m). Using the Linear theory and the environment set up to conform to the tank conditions, a simulation is run which includes only the water surface elevation. This allows a comparison can be drawn between the experimental wave form and the output from OrcaFlex. Figure 5.13 shows a comparison between the experimental wave form and the numerical approximation using linear wave theory. The wave example used for figure 5.13 is a calibration test with a wave height of 0.05m and a wave period of 1.34s. The tank produced a wave with a height of 0.04m, which is lower than specified and the correct wave period. Because the tank did not produce the correct wave height the actual height was used as the input to the Linear theory along with the appropriate wave period. It is clear there is close correlation between the two wave traces.

The results from this show that the linear approximation of the wave environment for the regular waves is appropriate. This theory can be in simulations with wave periods

1.12s to 3.35s, which provides a complete set of tests from the experimental work done at Heriott-Watt. The simulations are run for 100 seconds which allows the system to settle in to a working equilibrium.

For the irregular waves the sea state will be statistically similar to the experimental conditions. Table 4.8 shows the irregular wave parameters used to generate the wave field using a JONSWAP spectrum.

## **5.5 Discussion on comparison between experimental and numerically predicted tension and response of coupled system**

This section will review the output from the numerical models for the fully dynamic coupled models. These models are built from the perspective of a WEC device developer prior to any wave tank experimentation. The only inputs from experimentation are the material properties of the mooring lines. The motion response of the WEC body is calculated using two different methods, diffraction theory and using drag and inertia properties with Morrison approximation. The mooring system is defined in the model in the same way as for the models in chapter 4. During the experimentation both regular and irregular wave tests were performed. The regular wave tests were designed to produce motion characteristics for the WEC. The irregular wave tests are designed to indicate the response of the WEC during operational conditions.

### **5.5.1 Regular Wave Comparison**

The wave field for the regular waves can be simulated with a high degree of agreement in both the frequency and time domain using a linear wave theory. To compare the agreement between the numerical models and the simulations it is convenient to look at the response of the system using an RAO plot. This is done by normalising the response of the WEC system to the wave field and plotting it against the wave period. This produces coupled RAO's which have the implication that they do not conform the theory of an amplitude operator. An RAO can be applied to many different wave heights due to the

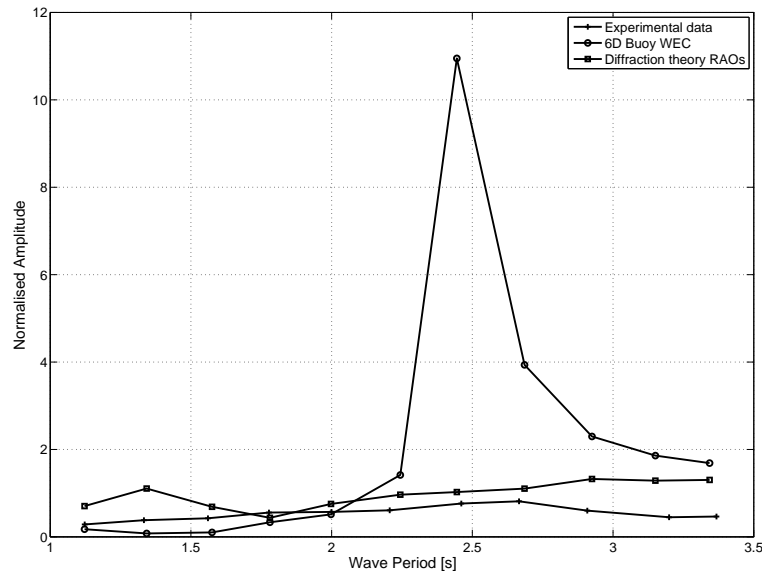


Figure 5.14: Comparison of Surge RAOs

assumption that it is possible to linearise the response amplitude at a given wave period to the wave height. Coupled RAO's cannot be assumed to be linear with respect to the wave height, as the tension characteristics and the hydrodynamic parameters of the coupled system change with the excursion of the device from the still water position. This is something that can be emphasised by the work by Vickers and Johanning (2009) where the damping in the system due to forced oscillations changed over different pre-tensions. The pre-tension in the mooring line during one cycle can be seen as the tension in the line due to the mean operating position, which will be different depending on the wave field. Also from the tests on the fibre ropes in Chapter 3 the load extension properties are seen to be non-linear making this another source of non-linearity in the response at different excursions. However since the wave climate used is similar it allows a direct comparison of the response of the experimental data to the numerical simulations. The RAOs are calculated using the same methodology as in section 5.2 in chapter 3. At steady operating condition the response of the WEC is analysed against the wave height. Figures 5.14 to 5.16 show the comparison of the coupled RAOs from the numerical simulation using the 6 degree of freedom buoy and the diffraction theory approximations for the body of the WEC with the experimental RAOs.

The numerical simulations show an over prediction of the response of the system to

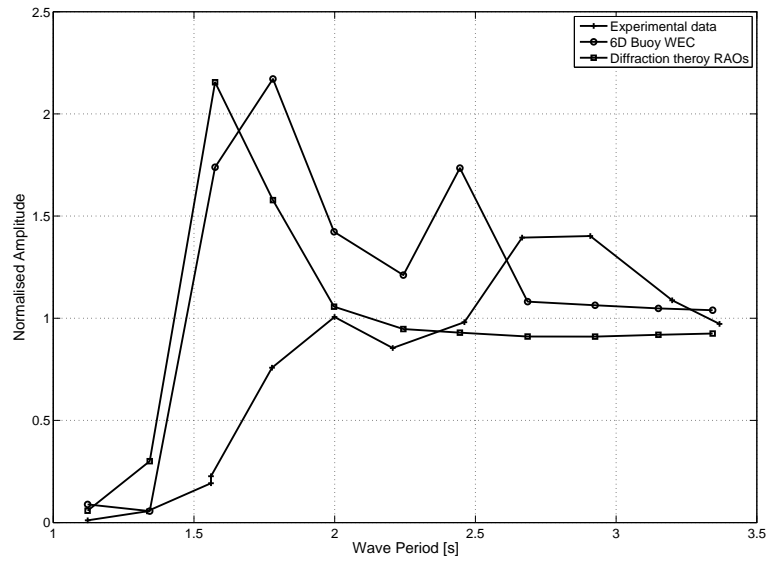


Figure 5.15: Comparison of Heave RAOs

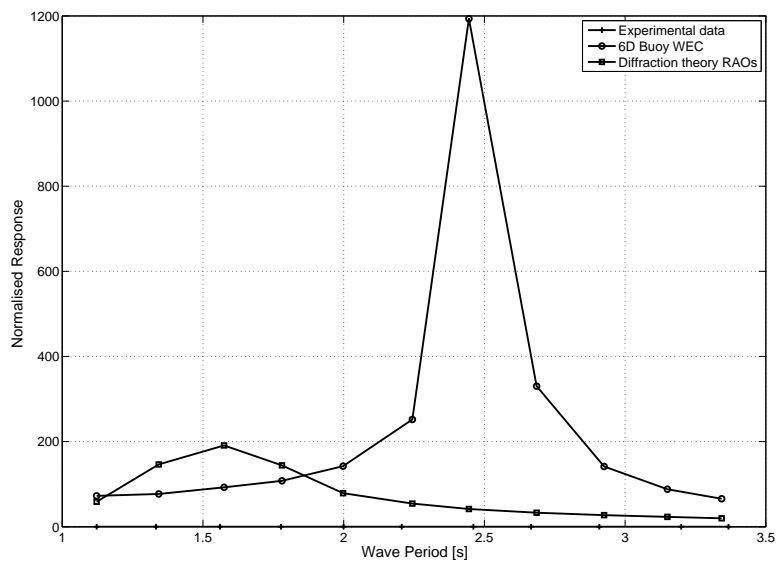


Figure 5.16: Comparison of Pitch RAOs

all wave periods for all the degrees of freedom. This would clearly have an effect on the mooring line tension prediction and over predictions in the motion of the WEC could lead to ill-informed design choices being made. Any disparity between the prediction and the experimental data in the comparison of the motion modes of surge and pitch could be due to the coupling of the motion response of the WEC body and mooring system. The heave motion of the WEC is restricted a lot less by the mooring system and experimental results for the heave RAOs using the soft mooring system could be used to calibrate the numerical RAO output to better represent the response of the WEC. Figure 5.17 shows the numerical RAO output from WAMIT for the heave motion where an additional linear damping of  $100\text{N}/(\text{m}/\text{s})$  has been included in the model. This brings the peak response down to something closer to the experimental result indicating that the over prediction from the numerical model could be controlled. Applying this damping value to the time domain model allows the effect of this on the coupled system to be compared (figures 5.19 to 5.20). This added damping has decreased the peak in the heave motion response prediction compared with the diffraction theory output with no additional damping. This change in the model parameters has however increased the response in pitch at 1.57 seconds resulting in the model prediction being further from the experimental results. This is due to the coupled nature of the response of the motion modes of the system. A reduction in the heave motion of the device would allow the mooring system greater freedom allowing more scope in other degrees of freedom.

### 5.5.2 Irregular wave comparison

The method used for the generation of the irregular wave signals means that the instantaneous water surface elevation are not the same for the experimental and numerical data in the time domain. This is because the phase relationships of the individual wave components are not conserved in the definition of the wave field. This produces an input wave field that is statistically similar in the frequency domain but not in the time domain. This means that event comparison in the time domain is not possible. To summarise the data from the simulations in a similar way as the comparison in chapter 4, the maximum, minimum and mean values for the motion of the WEC body and the tensions in the mooring line for test 3030 are presented in table 5.2.

For all the tests results shown in table 5.2 the diffraction theory is generally a closer

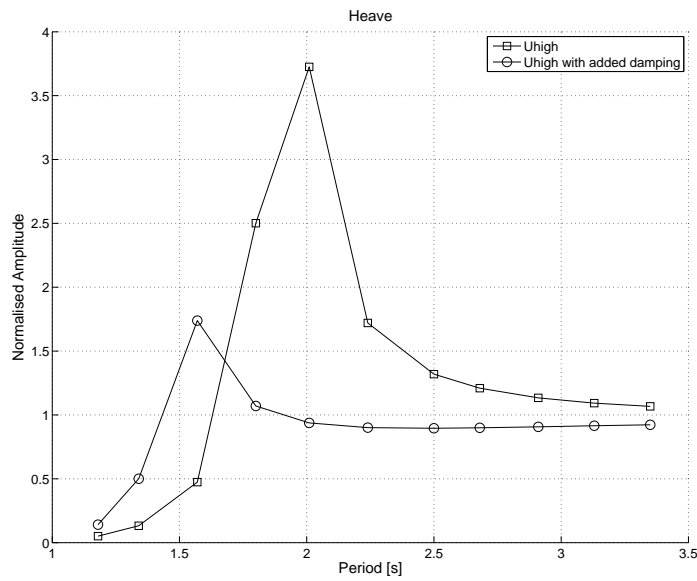


Figure 5.17: Comparison between highest resolution geometry model with and without additional linear damping

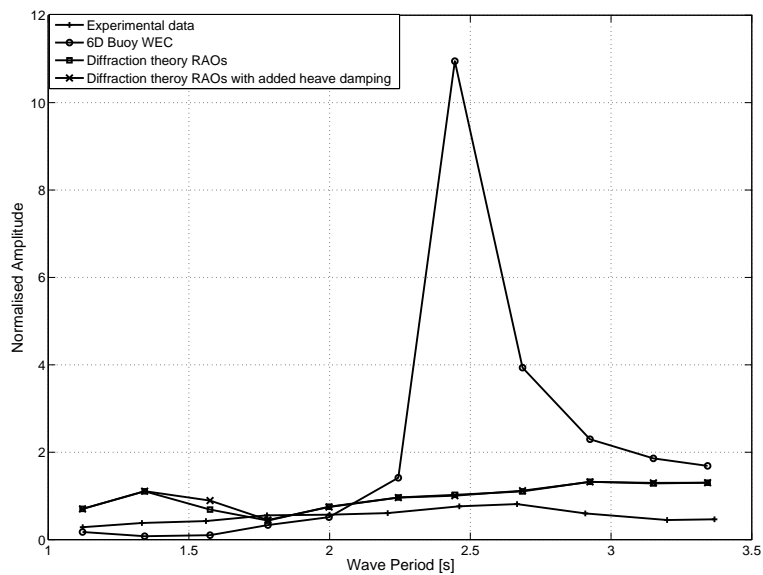


Figure 5.18: Comparison of Surge RAOs



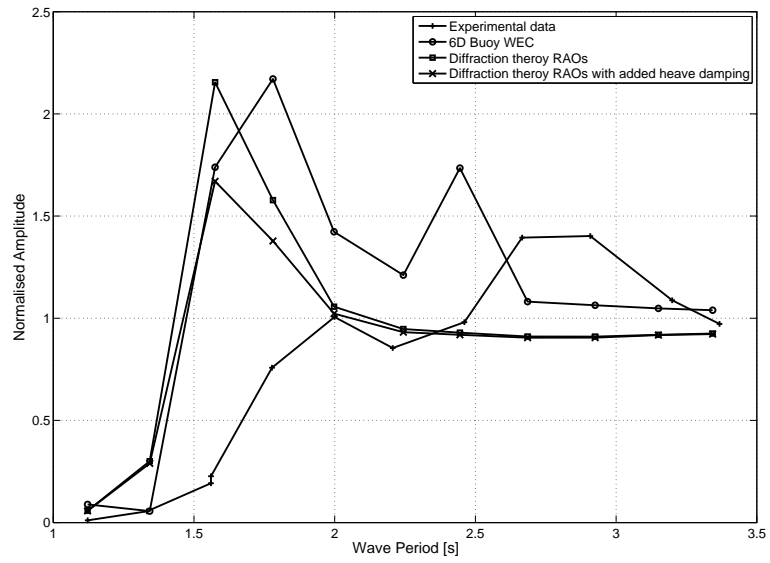


Figure 5.19: Comparison of Heave RAOs

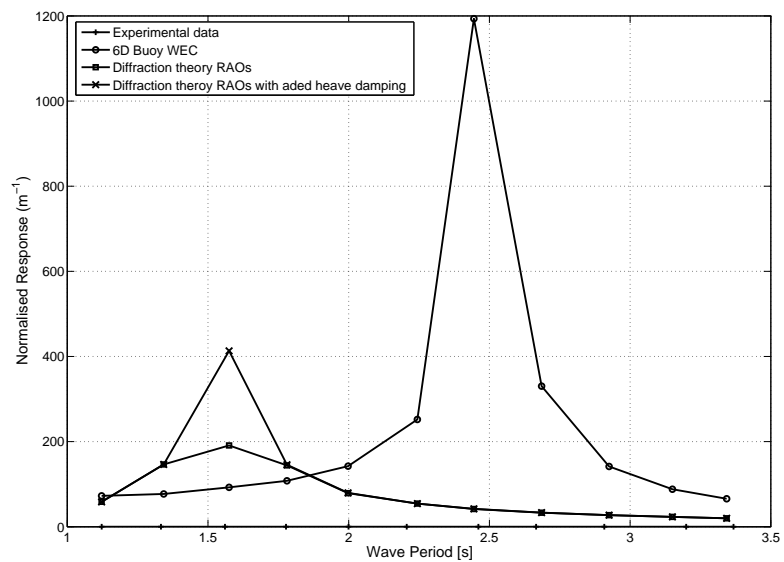


Figure 5.20: Comparison of Pitch RAOs

Table 5.2: Maximum, Minimum and Mean results for test 3030

Motion mode Load cell position	Parameter [m/kN]	Experimental data	6D buoy data	Diffraction theory data	Diffraction theory data with additional damping
Surge	max	0.3738	1.0382	0.9445	0.9038
	min	-0.3445	-1.7042	-0.8230	-0.8007
	mean	-0.0025	-0.0970	-0.1598	-0.0831
Sway	max	0.1976	1.2878	0.5692	0.1864
	min	-0.2489	-1.1133	-0.6034	-0.2132
	mean	0.0006	0.2117	0.0073	0.0010
Heave	max	0.1020	-0.3835	0.3284	0.1479
	min	-0.1233	-1.1829	-0.2916	-0.1313
	mean	-0.0050	-0.7243	0.0012	0.0020
Roll	max	16.9840	49.8191	11.6157	6.5659
	min	-16.8120	-48.3155	-11.7218	-7.0819
	mean	-0.0572	1.0026	0.0191	0.0015
Pitch	max	19.1359	51.3994	33.6564	21.2428
	min	-28.2970	-62.6748	-30.7119	-19.2948
	mean	-2.6516	0.4428	0.3231	0.0743
Yaw	max	2.5529	83.6644	40.8289	44.6453
	min	-9.3653	-78.4971	-40.0996	-25.9227
	mean	-2.8375	-0.0312	1.8513	1.5463
BowA	max	0.1647	0.9141	0.3643	0.0798
	min	-0.0008	$-6 * 10^{-6}$	$2.7 * 10^{-6}$	$-1.74 * 10^{-06}$
	mean	0.0114	0.0279	0.0054	0.0024
BowB	max	0.1592	0.9228	0.3754	0.0866
	min	-0.0028	-0.0004	0.0006	-0.0004
	mean	0.0056	0.0311	0.0826	0.0047
PortA	max	0.0139	0.3877	0.4985	0.0210
	min	-0.0016	$-7 * 10^{-6}$	$5.9 * 10^{-6}$	$-1.73 * 10^{-06}$
	mean	0.0006	0.0144	0.0015	0.0008
PortB	max	0.0454	0.3988	0.1226	0.0254
	min	0.0388	-0.0058	0.0129	-0.0001
	mean	0.0000	0.0178	0.0026	0.0017
StarboardA	max	0.0179	0.2788	0.5397	0.0146
	min	-0.0018	$-8 * 10^{-6}$	$-5.3 * 10^{-6}$	$-1.54 * 10^{-06}$
	mean	0.0016	0.0123	0.0012	0.0008
StarboardB	max	0.0102	0.2616	0.1257	0.0221
	min	-0.0010	-0.0005	0.0005	-0.0002
	mean	0.0006	0.0283	0.0022	0.0019

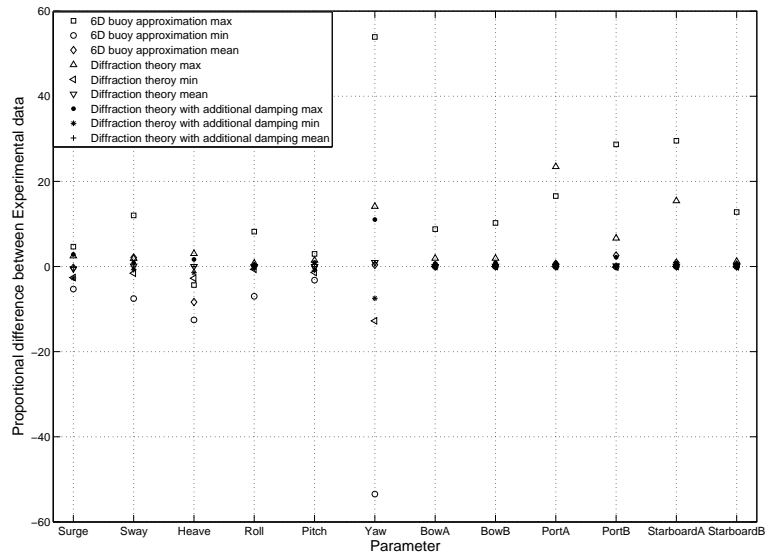


Figure 5.21: Average difference between experimental data and numerical data of the motion and tension results for all tests

approximation to the experimental data. As a comparison to the simpler models of the mooring system only the error in the maximum predicted tension in the bow mooring line is evaluated to be 4.5% and 1.4% for the 6D buoy approximation and vessel approximation using RAOs respectively. This error is less than that for the previous model and is argued to be a result of coupled interaction of the system where the floating body is restricted by the properties of the mooring. In the previous tests the motion of the body was prescribed and the mooring did not restrict this motion.

The argument for the diffraction model is backed up when looking at the proportional difference between the simulations and the experimental data for all the test cases. This is done by dividing the maximum, minimum and mean of the simulation data with the maximum, minimum and mean of the experimental data for each test, and then averaging the differences of the individual parameters of all tests and plotting them as shown in figure 5.21. This method of analysis does not completely describe the performance of the simulation against the experimental data. The reason for this is that it is quite possible that two time history signals which are very different can have the same maximum, mean and minimum.

To get a more complete assessment of the performance of the numerical model it

is necessary look at the distribution of the response by calculating an estimate of the probability density. To compute the probability density estimate of the data for the motion of the WEC or the tension in the mooring lines an estimate based on the kernel function is applied using a window parameter that is a function based on the number of points in the data. The density is evaluated at 100 equally spaced points which cover the range of the data. Figures 5.22 and 5.23 shows the probability density plot of the motion response of the WEC body and the tension in the mooring lines respectively. From the probability density plot it is possible to determine the mode position of the different degrees of freedom. The mode is identified as the peak or the highest point on the plot.

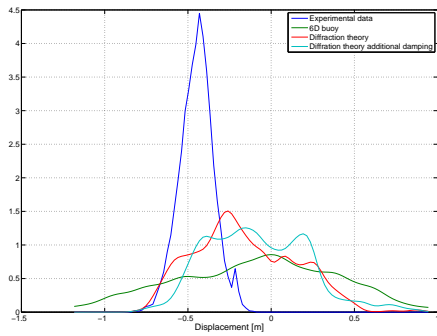
For this comparison it is considered to be less important to compare the motions of the system in the sway, roll and yaw, as the wave direction is head on  $0^\circ$ . Due the symmetry that exists in the numerical definitions of the WEC body there would be no cross coupling between the different motion modes. This means that any motion in the sway direction would not come directly from the wave loading but could be a result of the iterative solver reaching a solution for slack condition. The slack condition could force the model to test solutions for the line position or the buoy in the sway direction.

Generally it is clear that the motion response of the numerical models, both 6 degree of freedom model and diffraction theory model, have a much wider spread of displacement than the experimental data. The peak visible in the experimental data shows that the motion response is dominated around the mode value more so than the simulations. In the surge motion the simulations have a much higher probability of the motion reaching extreme values than the experimental data. This translates to the predictions showing the WEC having more freedom or to be restrained less than is the case for the experimental situation. Evident in the motion response for the surge motion, the mode value differs between the experimental result and the numerical approximations. This mode value represents the operating position or dynamic equilibrium position of the WEC system during the test. The mode position in the surge motion mode for the experimental shows that the device operates further from the still water position than the simulations predict. Also there is a much lower probability in the peak displacement regions. The probability density plot for the diffraction theory shows closer agreement than the 6 degree of freedom buoy, in the fact that the probability for the extremes is lower and the peak (mode) is closer to that of the experimental data.

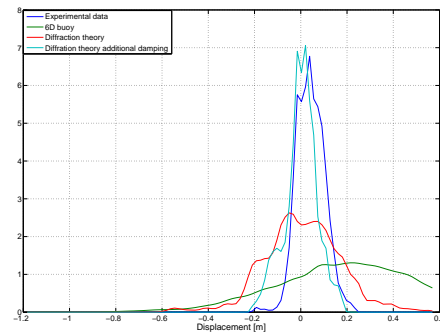
The heave mode of motion has a distribution about zero. Zero here being the still water position defined by the buoyancy of the system as one would expect. For this mode of motion the 6 degree of freedom buoy makes a better approximation over the range of positions. This is shown by the distribution of the heave motion having a higher probability of being in a position close to the operating position. The probability distribution for the diffraction theory shows higher probability than both the experimental data and the 6 degree of freedom buoy data at more extreme positions away from the still water position. Of interest is the fact that it is not apparent in figure 5.21 that the 6 degree of freedom buoy could be said to be performing better in the case of heave. The inclusion of the added liner damping to the diffraction model in the heave motion mode has reduced the probability of the extreme positions. The agreement between the experimental data and the prediction from the diffraction theory with the additional damping is better than the other numerical predictions.

The distribution of rotational position in pitch shows an operating magnitude of around  $-2^\circ$ . This indicates that the wave action causes the WEC body to have a non-zero dynamic operating equilibrium position. This is not reflected in the simulations where the operating position is zero. The range of the angle in pitch for the numerical simulation is greater than the range in the experimental data. This shows that the numerical simulations predict more extreme excitation in the pitch motion than is apparent from the experimental data. For this motion the diffraction theory provides a better comparison with the experimental data.

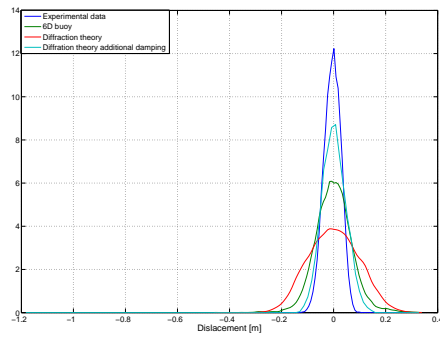
The response in all motion modes will be a combination of wave frequency motion and resonant period oscillation. To identify the frequencies at which the different oscillations occur, it is necessary to perform a frequency domain analysis. By calculating the spectral energy density over the frequency range of the resonant periods for the motion and the wave period of the input wave field, it should be possible to assess the distribution of the energy. The comparison of the spectral density for the wave field from test 3030 is shown in figure 5.24, where the numerical simulation wave field will be the same for the 6 degree of freedom buoy and the diffraction theory model. This comparison shows a close agreement between the wave fields where the range of frequencies match. The spectra for the experimental data is smoother and contains fewer peaks than the numerical wave field. The reason for the less smooth trace for the numerical simulation is the fact that the



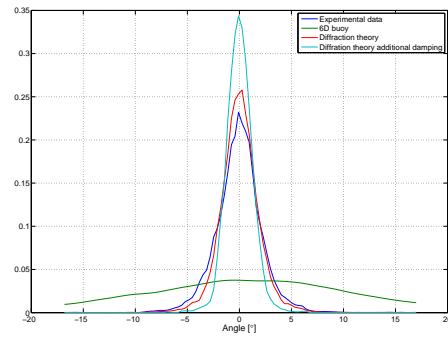
(a) Surge



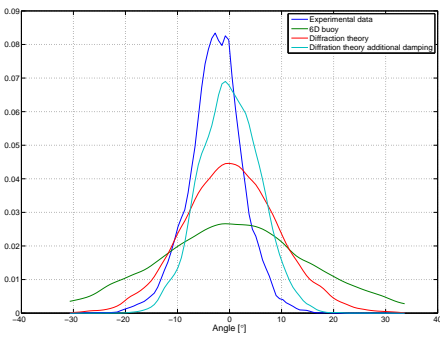
(b) Sway



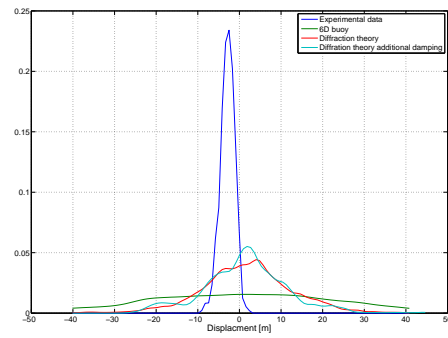
(c) Heave



(d) Roll

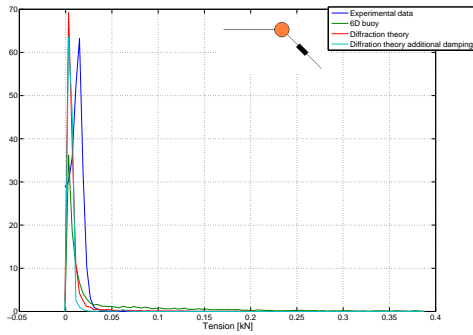


(e) Pitch

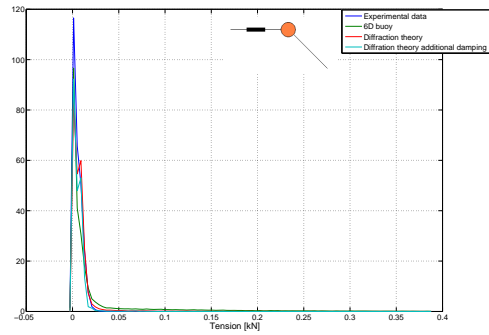


(f) Yaw

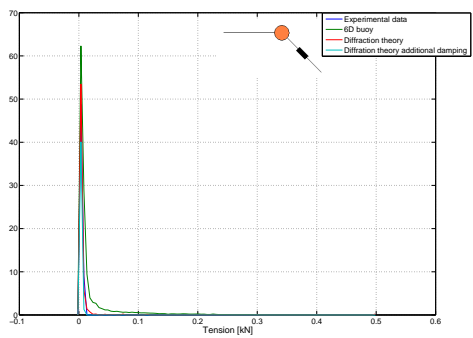
Figure 5.22: Probability density estimate for the motion response of the WEC for test 3030



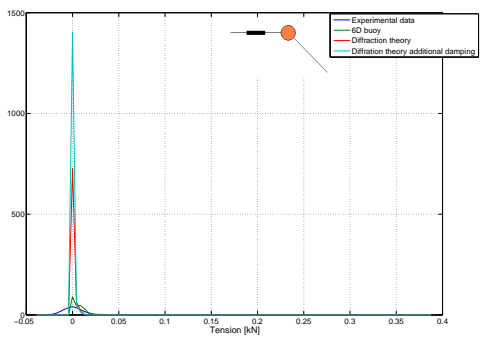
(a) BowA



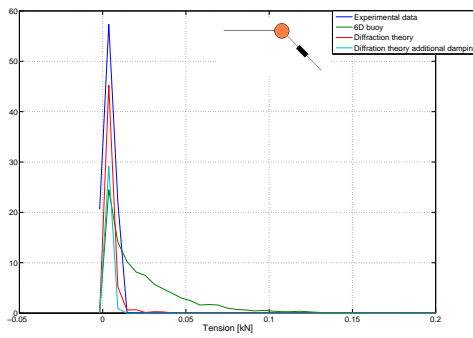
(b) BowB



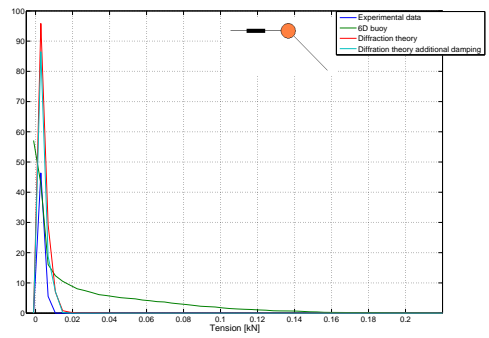
(c) PortA



(d) PortB



(e) StarboardA



(f) StarboardB

Figure 5.23: Probability density estimate for the Tension in the mooring line for test 3030

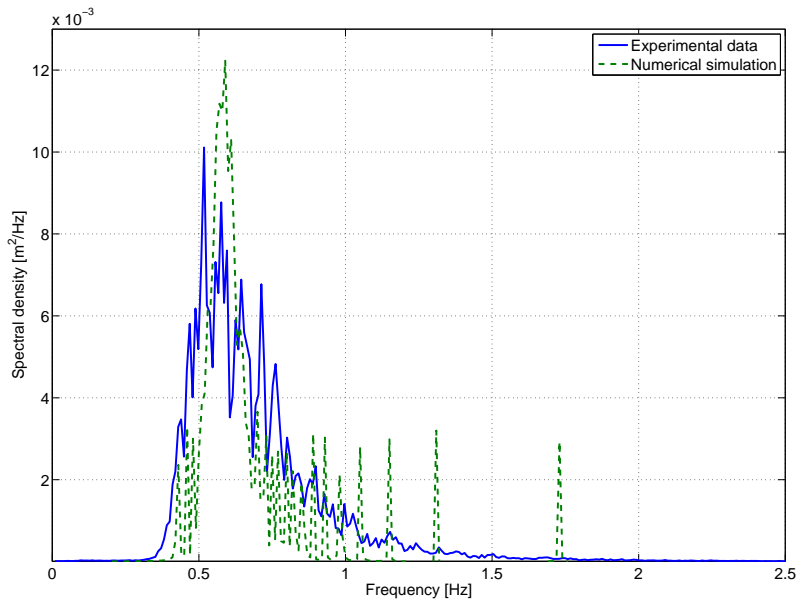


Figure 5.24: Comparison of spectral density of the wave field between the experimental and numerical data

numerical wave field is defined by 15 individual wave components. This means that the energy in the wave field is not spread over as many wave components as the experimental data. Instead it is divided over the 15 different wave components. This explains the outlying peaks above 1 Hz as the energy for that part of the spectrum is almost focused at the 4 different wave component frequencies that can be seen.

The experimental wave field will have been created in a similar way to the numerical approximation, where a finite number of wave components make up the spectrum. The signal is then passed to the wave makers that transfer this to the water. At this point the waves in the tank interact with each other as well as the sides and bottom of the tank itself and anything else floating in the tank. The signal is then read by the wave probe which is subject to background noise caused by electromagnetic interference. All of this creates a more analogue signal with respect to the spectra as opposed to the digital type signal of the numerical simulations where the discrete wave components are preserved.

The spectral density for the motion response of the WEC in the experimental tests and the numerical simulations is shown in figures 5.25 and 5.26, which show the response in the two frequency ranges. This is identified as the wave frequency range and the resonant period range for the particular motion mode. The resonant periods of the system for the



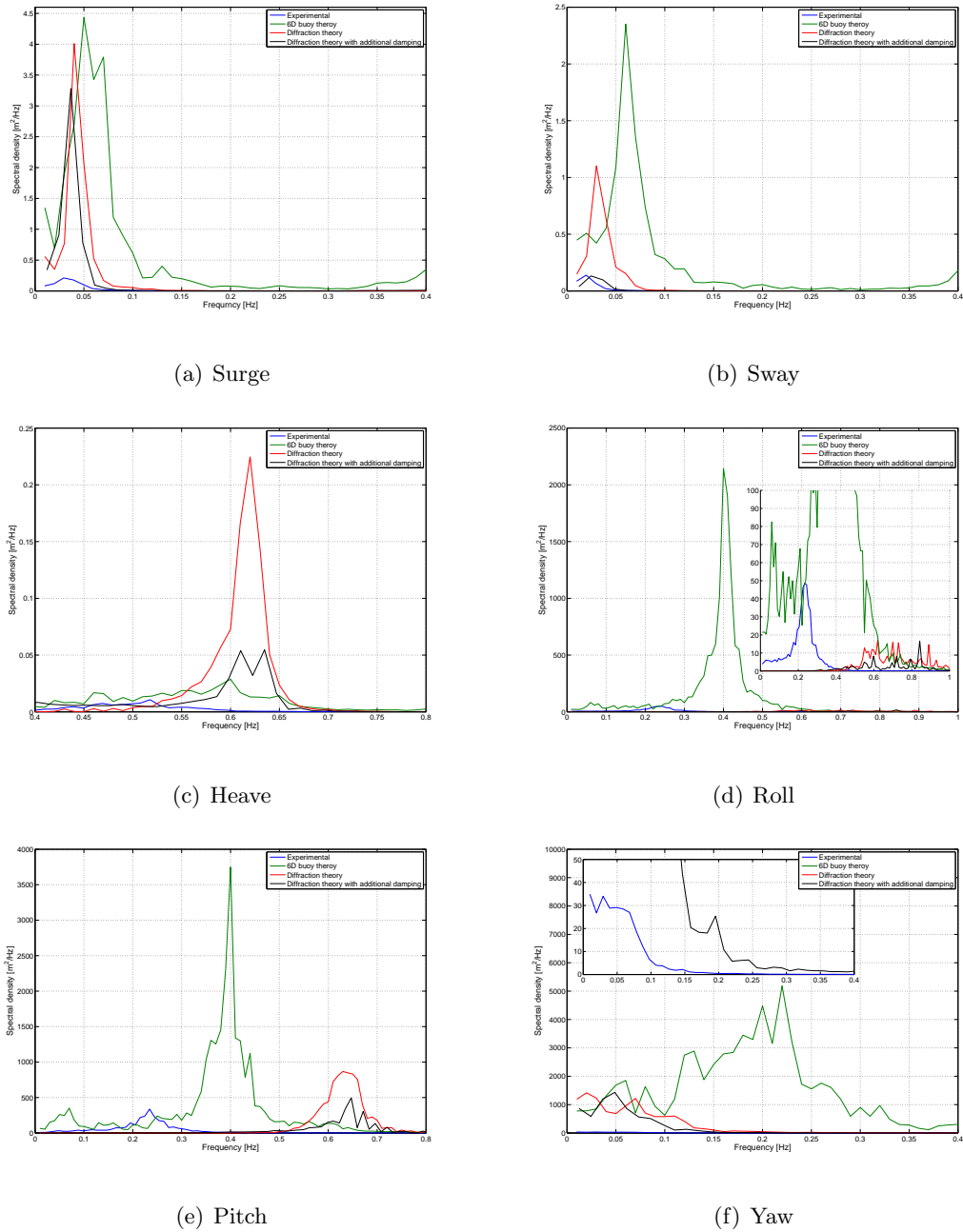


Figure 5.25: Spectral density of motion of the WEC body over resonant frequency range

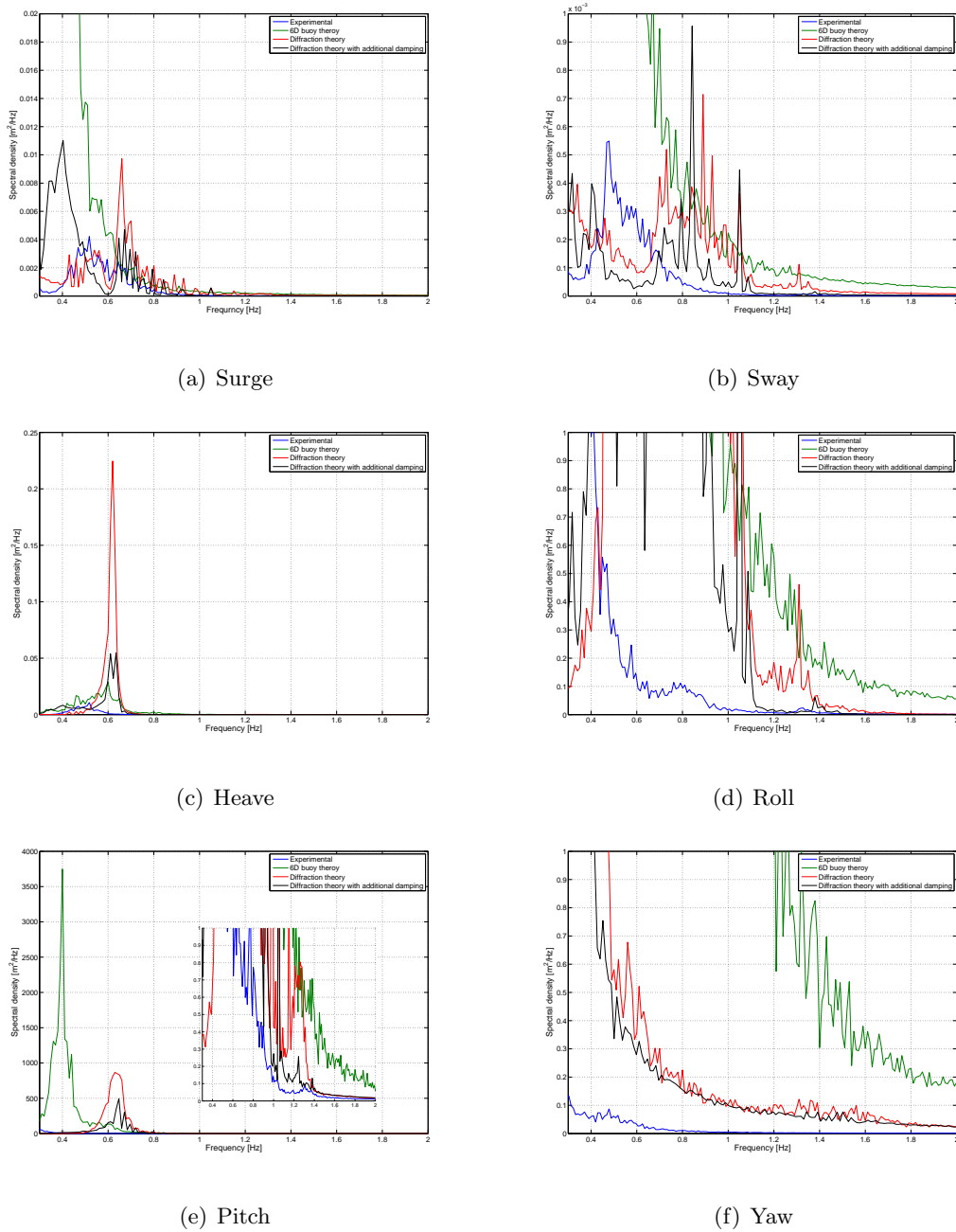


Figure 5.26: Spectral density of motion of the WEC body over wave frequency range

Table 5.3: Comparison of the natural periods of the system

Motion mode	6D buoy	Diffraction Theory	Experimental
Surge	20	30	32
Sway	25.1	30	36
Heave	1.6	1.61	1.75
Roll	2.4	1.1	3.98
Pitch	2.4	1.54	4.12
Yaw	8.5	17.5	12.7

numerical simulation and the experimental data have been calculated using a time domain analysis using the decaying method and are shown in table 5.3. The peak spectral density for the different motion modes coincides with the natural periods in the table except for the sway motion mode for the 6 degree of freedom buoy theory model. In the decay simulation the natural period is 20s whereas there is a large response at the frequency of 0.06Hz or 16.6s.

The spectral density of the motion response over the resonant frequency range is smoother than the spectral density of the response over the wave frequency range. This could be due to the fact that the wave spectra (figure 5.24) for the numerical simulations is not smooth due to the small number of wave components, therefore the wave frequency response for the motion of the WEC body will show this as the energy from the wave is directly transferred to the WEC body at the wave frequency. The resonant effect is set up by the wave action but not however at the wave frequency but at a frequency determined by the stiffness and damping of the system in each degree of freedom and as such does not show such a peaky signal.

The magnitude of the spectral density could be used as a measure of the agreement between the numerical simulations and experimental data. From figures 5.25 and 5.26 it appears that the numerical simulation prediction of the spectral density for the motion response of the WEC is higher for all frequencies. At the resonant periods for the WEC, the response predicted by the diffraction theory is a closer approximation for all the motion modes except the Heave motion. Over the wave frequency range the numerical prediction of the spectral density shows a much more noisy signal. The spectral density plot of the experimental data is also noisy but the magnitude is lower for all degrees of freedom. The

frequencies over which the energy is concentrated for the experiments and simulations is not consistent. The energy in the wave spectra (figure 5.24) shows that the simulation wave field has a peak at a slightly higher frequency of 0.59Hz compared to the peak at 0.52Hz for the experimental data.

The wave frequency range plots (figure 5.26) show a concentration of energy that could be said to not coincide with the wave excitation. The pitch motion plot in figure 5.26 shows that the 6D buoy has a large amount of energy around a frequency of 0.4Hz whereas the diffraction theory and the experimental data show the peaks to be around 0.5Hz. This and other shifts in the peaks in the spectral density could be due to excitation caused by the marker buoy response.

Assessing the level of agreement between the experimental data and the numerical simulations based on the spectral density could be misleading. As mentioned above, the comparison of the wave input spectra showed a difference on the smoothness due to the reduced number of wave components as a result of the compromise between computation time and detail. This means that the WEC is not excited to the same level as the experimental situation over the whole frequency range. This means that the spectral density representation may show the response of the WEC is concentrated around the frequencies of the wave component. If the numerical wave field has a lower excitation at a given frequency the response would be less, however the excitation may be increased at a different frequency making the wave field statistically similar. This means that the magnitude of the spectral density could be very different, depending the resolution of the Fourier transform performed to produce the wave field from the wave statistics.

An initial thought would be that the response in the frequency domain could be normalised to the wave field catering for the difference in the wave input. This makes the assumption that the magnitude of the response is linear with respect to the wave height. The issue with coupled moored system is that the response amplitude of the system is not linear with respect to the wave height. The coupled system response is a result of the hydrodynamics of the floating body and the mooring system together. The floating body response can be linearised with respect to the wave height, however when the body is coupled to the mooring system, this assumption is no longer valid. The mooring systems restoring force is non-linear with excursion due to the configuration and the material properties. Also due to the irregular wave field the motion response of the WEC body is

not uniform. This means that the response of the WEC would depend on the motion and position of the WEC at the point where a particular wave event occurred. With sinusoidal waves the motion and position response of the WEC to a singular wave frequency when the WEC is in a stable equilibrium would be the same for every wave event. This means that in simple terms the response of the system to a 1m wave would not be twice that of the response of the system to a 0.5m wave.

CHAPTER

6

CONCLUSIONS

The main aim of this project has been to investigate the uncertainties in the numerical modelling of wave energy converters. The reason behind this is to aid the design process by indicating the level applicability of the industrial standards and methods used in offshore oil and gas industry to a WEC problem. The implementation of the standards is to apply time domain, fully dynamic numerical modelling methods. This was intended to evaluate the issues of using numerical models in the prediction of the response of a floating WEC. The performance would be judged against experimentation of the same device. This would lead to a level of validation of the numerical modelling technique for this application. This chapter will explain the results of the comparison between the numerical and experimental investigation and go on to suggest avenues for further work.

The objective of the experimental work in this project was to provide a data set of the response of a floating WEC device during operation. The experimental work would also be required to provide information on the properties of the system. The experiments conducted at the MarinTek centre in Trondheim under the HydraLab III initiative produced data describing the response of the WEC in simulated irregular and regular sea states. The results included the 6 degrees of freedom of the floating body as well as the tension in the mooring lines during the tests. This is a valuable asset to research as it provides data set of the motion of a WEC during operational conditions. This data set has been used in this project as a case study to compare the performance of the numerical analysis to. Also the data has been used by Thies et al. (2012) to assess the reliability of mooring components as well as work on the reliability on umbilical power cables with the device (Thies et al. (2011)). The system documentation tests performed at the Heriot-Watt basin in Edinburgh allowed the characteristics of the system to be evaluated. These tests allowed the normalised response of the device to be evaluated as well as the natural periods of the system in all six degrees of freedom. These results add to the data set of results from the tests at the MarinTek centre. As well as the system documentation tests on the floating WEC system the material properties of the mooring line material were evaluated using load extension tests.

Numerical prediction in the design phase of a WEC device offers a low cost option of informing the designer as to the performance of a WEC concept. The industrial software packages WAMIT and OrcaFlex were used to model the WEC system used in the experimental work. The numerical analysis had two cases, one where the mooring line only is

the subject of the calculation and one where the floating body response and the mooring line are the subject in the coupled analysis. Also the implementation of the industrial standards from institutes such as the DNV for a WEC device is demonstrated. These included the drag and added mass properties which were defined for each component and scaled from the data provided in the DNV codes.

The predicted mooring line tension output from the numerical simulation in which the motion response of the WEC was prescribed from the experimental data showed fairly good agreement. The numerical models predicted the mean trend of the tension as well as the extreme snatch loadings. While magnitude of the predictions differ from the experimental data, the maximum instantaneous error was evaluated to be an over prediction of around 16 times the experimental tension. This error however was generally observed during the lower tension situations. During the higher loadings the error was evaluated to be 26% of the measured tension.

For this model the calculation for the tension in the mooring line is based on the definition of the mooring line system only. This data comes from the characterisation of the stiffness of the mooring material and the definition of the marker buoy.

As discussed in Chapter 4 there remains a large degree of uncertainty over the elongation properties of the mooring line. The motion of marker buoy was not measured during the experiments due to the fact that it was often submerged which causes problems for the motion tracking equipment. As the position of these marker buoys was measured no validation can be done on the numerical approximation of their response to the wave field or the effect they have on the tension response and indeed the motion response of the system. Further error could come from the definition of the Hydrodynamic parameters of the mooring line and the way in which the line moves through the water during the tests. This draws back to the initial discussion in Chapter 2 where the comparison between quasi-static and dynamic analysis was made. The experimental measurement of the mooring lines during testing is limited to the tension. The motion of the line through the water is not measured and therefore validation of the dynamic analysis for the mooring line cannot be conducted.

A refinement of the numerical model included the prediction of the motion response of the WEC body to the wave field and the mooring system in a coupled analysis. The



results from the model allowed a comparison of the motion response of the WEC body as well as the tension in the mooring lines. The comparison of the model using regular wave inputs is done using RAO theory as the wave input for the model and the experiments are the same. This comparison is done for the motion of the WEC body using the normalised response. This produced RAOs for the coupled system at the different wave periods. The agreement for the motion modes of Surge and Heave showed a close agreement for both modelling method (Morison theory and diffraction theory), where the closer approximation was from the diffraction theory. The pitch motion mode prediction showed an over prediction for both numerical methods. The inclusion of linear damping in the calculation of the numerical RAOs allowed them to be calibrated to the experimental data showing that over-prediction could be controlled with better understanding of the input criteria especially with relation to the damping of the system. This damping was included in the coupled model which improved the coupled RAO reducing the over prediction of the normalised response.

The irregular wave tests used wave spectra to define the wave input. One of the main issues in this comparison is that the tension in the mooring lines, the motion of the WEC and the water surface elevation would be different between the numerical simulation and the experimental data in the time domain. This led to a comparison where the distribution of the position and the mooring line tension was compared. This allowed the freedom of the device to be commented on in terms of how far it drifted from the still water equilibrium point. This gave an insight in to which of the modelling methods could produce a better approximation of the response of the system. Similar to the regular wave analysis the diffraction theory model produced a better approximation using the motion of the WEC and the tension in the mooring lines as an indicator. From the distribution of the position of the WEC the numerical models can be seen to predict more extreme motions indicating the system is allowed greater excursion. For the tension in the mooring lines, a similar trend in terms of the spread of the tension is observed. Over prediction in the motion response of the WEC can be explained to a degree by the comparison of the input RAOs. This over prediction clearly causes excessive mooring line tension predictions shown in the data.

The results were then analysed in the frequency domain where the identification could be made of the response of the system at the wave excitation frequency and the resonant

periods of the different motion modes of the system. The correlation of the natural periods of the numerical models and the experimental system for the translation motion modes was fairly close with bigger disagreement between the results for the rotational motions.

The main outcome from this work shows that the numerical methods available primarily for the use in the offshore oil and gas industry can be used to make a good first approximation for the response of a WEC. However the selection of mooring line materials based on this result could lead to gross over engineering of the load capacities of the lines. This would then have an effect on the response of the system, as WEC systems motion responses (and thus their power conversion efficiency) are sensitive to changes in properties such as stiffness and damping attributed to different mooring line types. This could therefore reduce the efficiency of the device as sub-optimal mooring configurations could be used.

Another outcome of this work came through in the discussion of the frequency domain analysis. The motion results of the numerical simulations could not be compared to the experimental data in the time domain. This led to the frequency domain analysis where the spectral density was calculated at different frequencies. The temptation is then to normalise this response to the spectral density of the input wave field and compare the numerical and experimental data. This assumes that the relationship between the response amplitude of the system and the amplitude of the wave field is linear. Whilst it is acceptable to linearise the response of the floating body, the coupled system of WEC and mooring cannot be linearised. This emphasises the requirement of time domain analysis and modelling of moored floating WEC systems over frequency domain analysis. It is therefore important for the numerical methods to accurately characterise the hydrodynamic properties of WEC systems to ensure reliable prediction of motion response and power capture efficiency.

## 6.1 Further work

Addressing the main points from the previous discussions in terms of how this work could be taken forward leads to the following suggestions for further work to better understand the uncertainties for the modelling of a moored wave energy converter:

- **Definition of mooring line mechanical properties** - In Chapter 2 it was discussed that the stiffness characteristics of a fibre rope mooring line would be a combination of non-time dependent stiffness and time dependent stiffness. The characterisation of the mooring line used in the models in this work only included the non-time dependent stiffness that was evaluated in a quasi-static way in Chapter 3. From the work by Flory et al. (2004) a model of a fibre rope mooring limb including both the dynamic and quasi-static stiffness of the line. The result of this would be a higher stiffness. The numerical models used in this project could be modified by the use of external functions to include a more complex definition of the stiffness of the mooring line. This could include the effect of accumulated elastic stretch of the mooring line which serves to characterise the mooring line retaining some strain due to a relatively quick load cycle.
- **Mooring line hydrodynamic definition** - The dynamic analysis conducted here clearly has the advantage over a quasi-static analysis in that the motion of the line through the water is not uniform and the numerical prediction can approximate the implication on the tension as a result of this. The issue of this is that the motion of the line in the water is not measured and therefore no validation is conducted on this. The drag and added mass (defined in the model using coefficients) is heavily dependent on the Reynolds and KC number which would vary throughout the test. The non-uniformity of the motion of the line has been outlined as the cause of snatch loadings which have been predicted here in the numerical models however the magnitude of the predictions was higher than that experienced in the experimental work. If experimental tests of a similar fashion of those conducted in the work here were to be performed where the motion of the mooring line is measured at intervals along the line during a test, validation of the mooring line model could be better conducted. This would also present the opportunity to measure the motion of the marker buoy which would allow further validation to the models in this work. This would require motion tracking of components of the mooring system which are submerged during the test as well as portions of the limb which are partly submerged.
- **Second order drift motion validation** - The work in this project went to lengths to validate the first order response of the WEC body to different wave climates. The results of the irregular wave tests showed that the position of the WEC body was predicted by the numerical simulations to vary more often from the mode position

than the experiments showed. This could be due to the numerical approximation of the second order drift forces calculated by WAMIT and included in the model as quadratic transfer functions (QTFs) not being accurate. To validate the QTFs, a completely unrestrained WEC would need to be tested where the WEC could be allowed to drift until it had reached a stable operating response situation to a regular wave field. The first order motions could be removed isolating the second order motions of the WEC and a comparison to WAMIT outputs could be made. This could aid in the calibration of the WEC model reducing some of the errors in the prediction of the motion response of the WEC.

- **Validation of techniques using further data sets** - The issue of addressing the uncertainties of modelling moored floating WECs is complicated by the possible variety of different mooring configurations designed to cater for the different operating principals of WECs. This project has assessed the applicability of the industrial standards used in the oil and gas industry to an OWC type device. The mooring limbs included a floating marker buoy in the line that was identified as a possible source of error. Different mooring systems will include different components that will have issues leading to uncertainty when they are approximated with numerical models. A similar analysis conducted here of different mooring systems could provide useful validation of modelling techniques on otherwise untested mooring configurations. This would require further data sets of moored devices from an installation that could simulate real sea conditions or a facility that could be installed in real sea conditions. Such a facility exists in the form of the South West Mooring Test Facility (SWMFT). This device has been developed at the University of Exeter at the Cornwall campus. The SWMTF is a 2.9m, 3,300kg buoy deployed in Falmouth bay in water depths of 27m. The buoy is equipped with:

- Six-axis inertial sensing system, 'MotionPack'
- Tri-axis Load Cell (3 off)
- In-line Load Cell (3 off)
- Vishay CEA-06-26OUR-350 strain rosettes
- Tilt-compensated flux-gate compass
- Temperature Sensor
- Trimble 57001-51-46 DGPS RTK rover

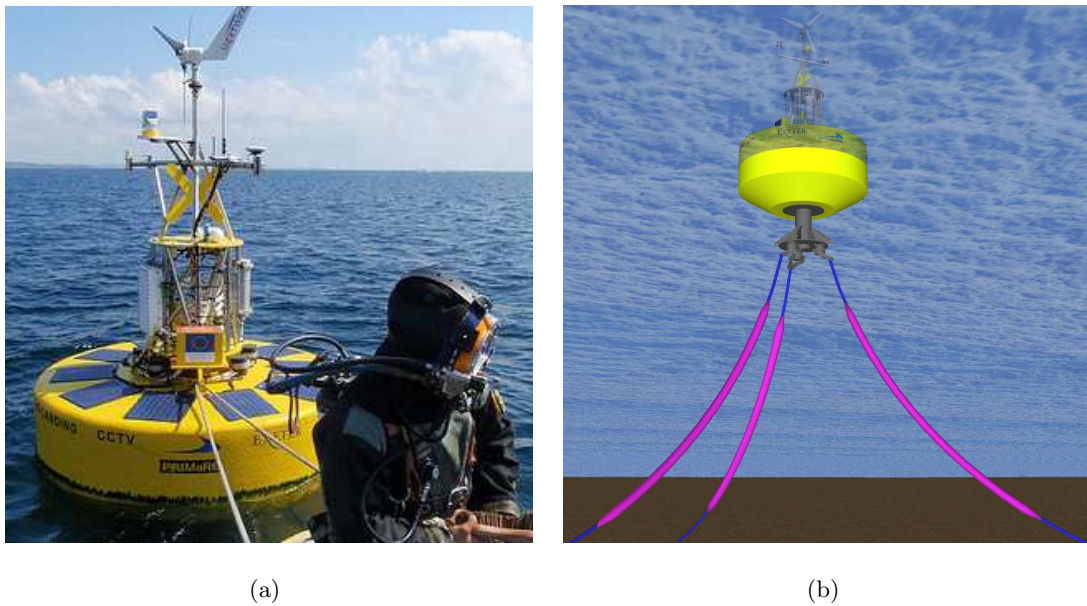


Figure 6.1: South West Mooring Test Facility

- WindSonic wind sensor
- Aanderaa 3919 conductivity sensor

This facility would allow different types of moorings to be implemented and analysed in real sea conditions at large scale. This could allow the validation of the modelling techniques for different mooring systems and different mooring materials as well as provide case studies for other research such as the inclusion of experimentally derived damping properties in to numerical models.

- **Inclusion of power take off system** - One of the main issues facing the modelling of all wave energy converters, compared with a floating moored body such as a platform, is the complication of the power take off system. The power take off system converts the motion energy imparted to the device from the waves to another useful form of energy. This means that energy will be taken from the system which adds a source of damping reducing the motion response of the system. The inclusion of the PTO would require the modelling of various different systems depending on the type of device. For example the OWC device in this project used an orifice plate to simulate the resistance of a turbine. Other devices may use hydraulic pistons and pumps and some may have direct drive electric generators. Modelling the different PTO methods would allow an approximation to be made as to the energy production from the device as well as the inclusion of the PTO as a source of damping on the

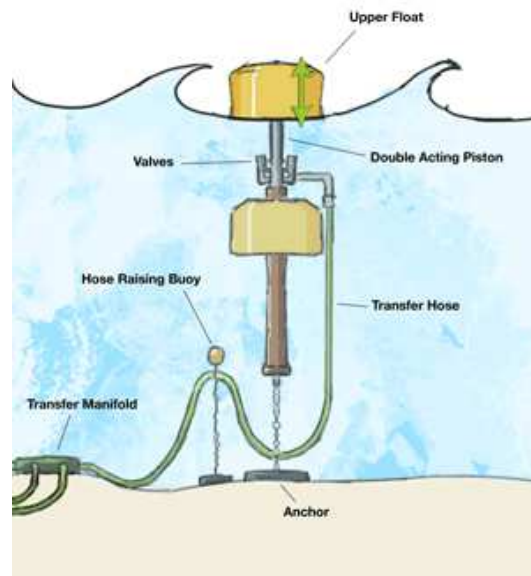


Figure 6.2: SeaRaser device Ecotricity (2012)

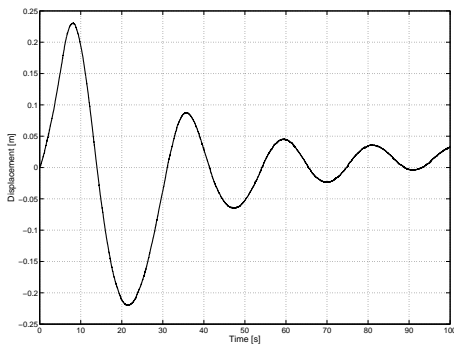
motion response. This would allow optimisation of the moored WEC system in terms of the power capture efficiency.

Work at the University of Exeter by Baptiste Chardon on the SeaRaser (figure 6.2) device has led to the creation of a numerical model of the device using many of the methods presented in this project. This device is a point absorber device designed to operate a pumping system to pump seawater to a shoreline generator. The PTO system has been characterised in this model as a damper and included in the numerical model using an external function. This is being done from a design point and as such there is not yet a physical device to validate the result. The device is to be installed however, in Falmouth bay. The device will be installed at the Fab Test site which is a site overseen by the University of Exeter specifically for the testing of wave energy devices. The operation of this device could provide some validation of this method as an option for including the PTO for other systems.

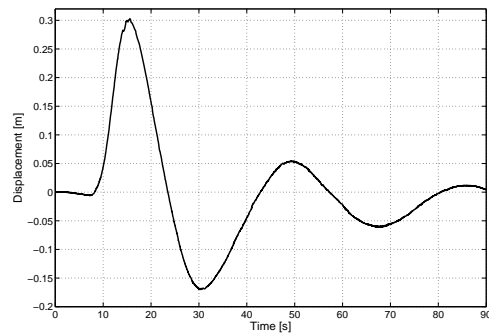
APPENDIX

A

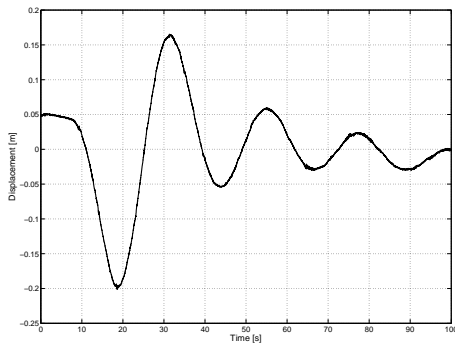
HERIOT-WATT TEST RESULTS



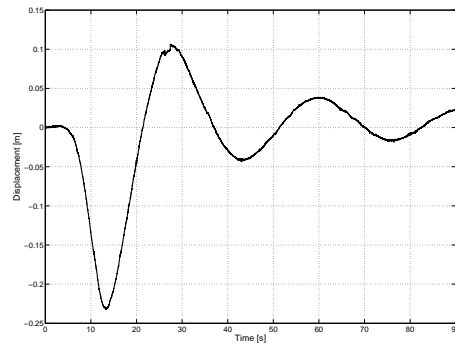
(a) Decay test time history for the surge motion with test moorings



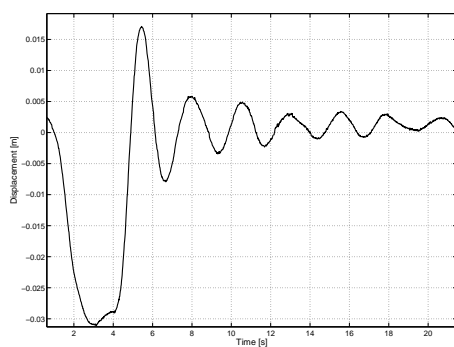
(b) Decay test time history for the surge motion with horizontal moorings



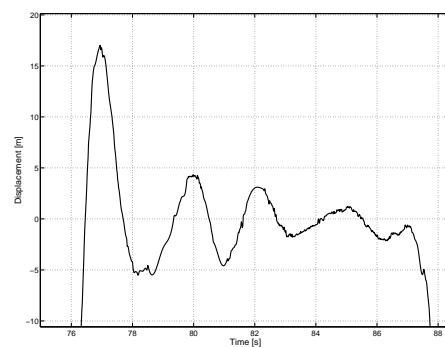
(c) Decay test time history for the sway motion with test moorings



(d) Decay test time history for the sway motion with horizontal moorings



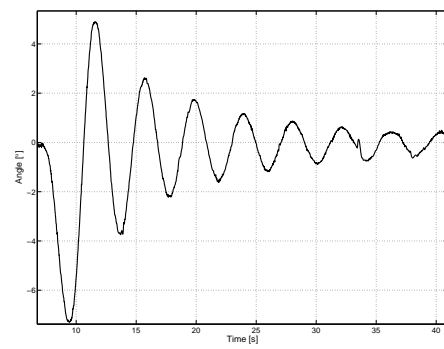
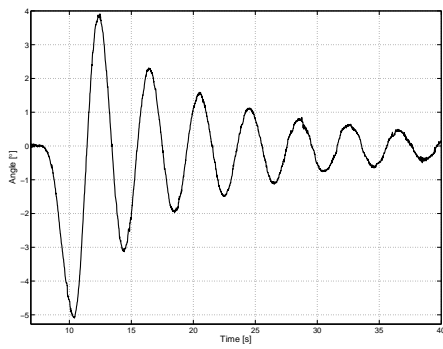
(e) Decay test time history for the heave motion with test moorings



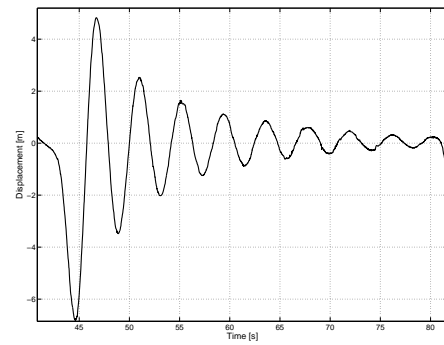
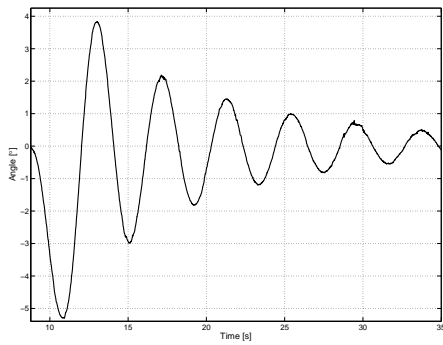
(f) Decay test time history for the heave motion with horizontal moorings

Figure A.1: Translational motion mode decay time histories for the test carried out at Heriot-Watt

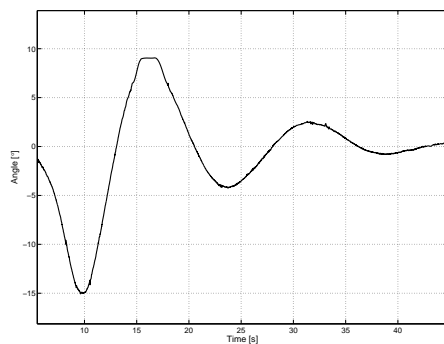
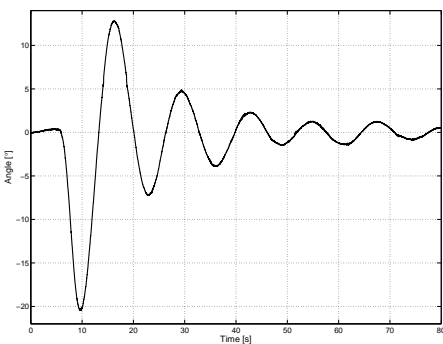




(a) Decay test time history for the roll motion with test moorings (b) Decay test time history for the roll motion with horizontal moorings

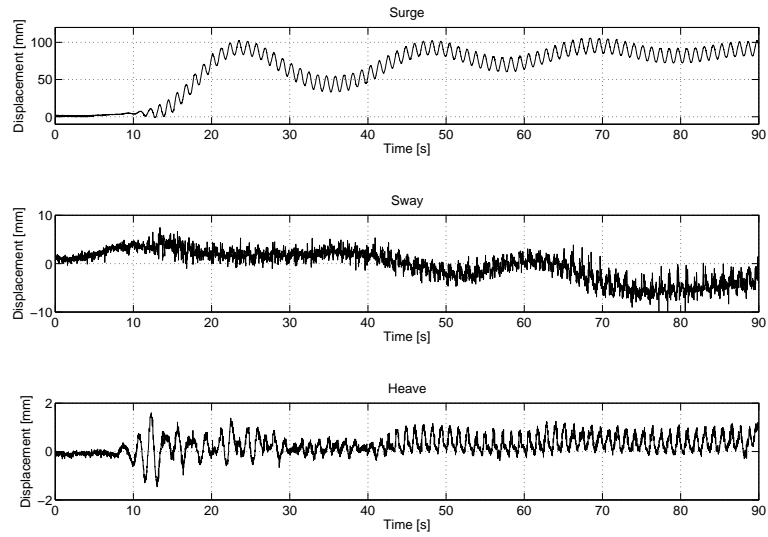


(c) Decay test time history for the pitch motion with test moorings (d) Decay test time history for the pitch motion with horizontal moorings

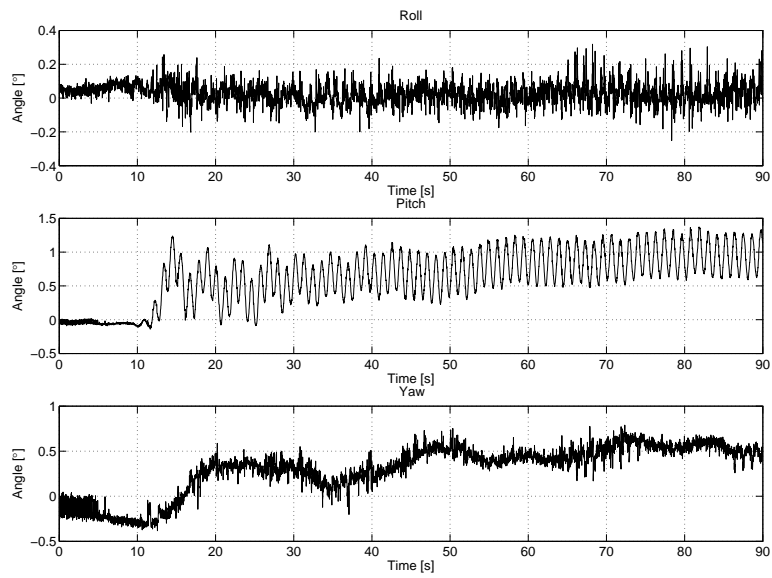


(e) Decay test time history for the yaw motion with test moorings (f) Decay test time history for the yaw motion with horizontal moorings

Figure A.2: Rotational motion mode decay time histories for the test carried out at Heriot-Watt



(a) Translational motion results from RAO test



(b) Rotational motion results from RAOtest

Figure A.3: Motion results for RAO tests

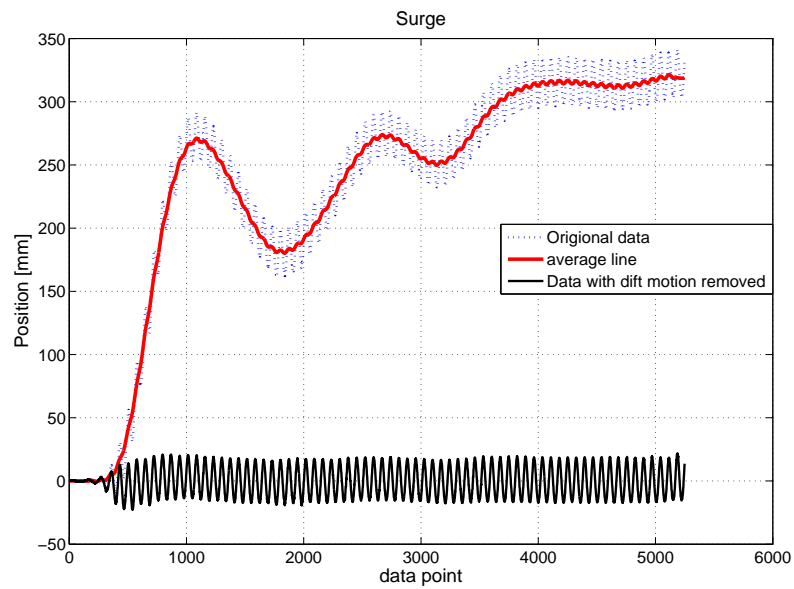
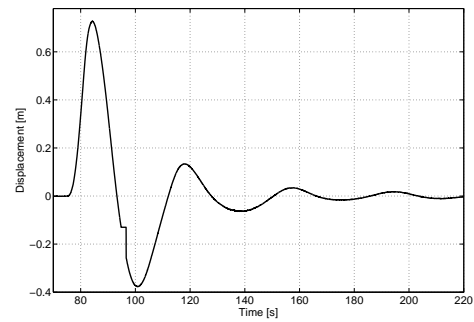
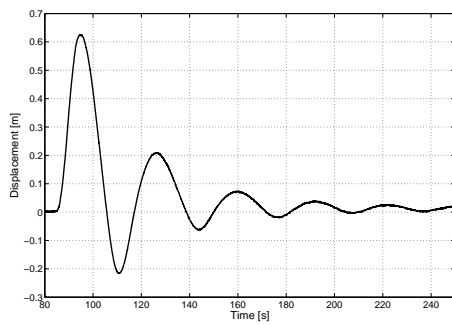


Figure A.4: Applying a moving average to the surge motion and subtracting from the data to remove drift motion

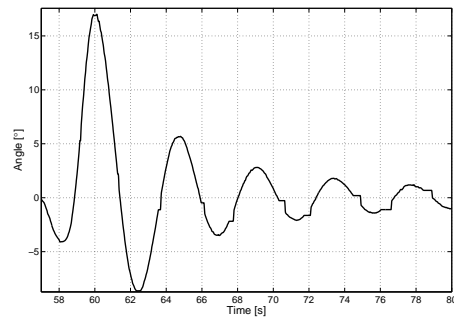
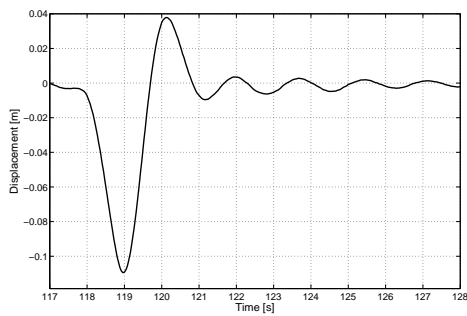
APPENDIX

B

TRONDHEIM MARINTEK TEST  
RESULTS

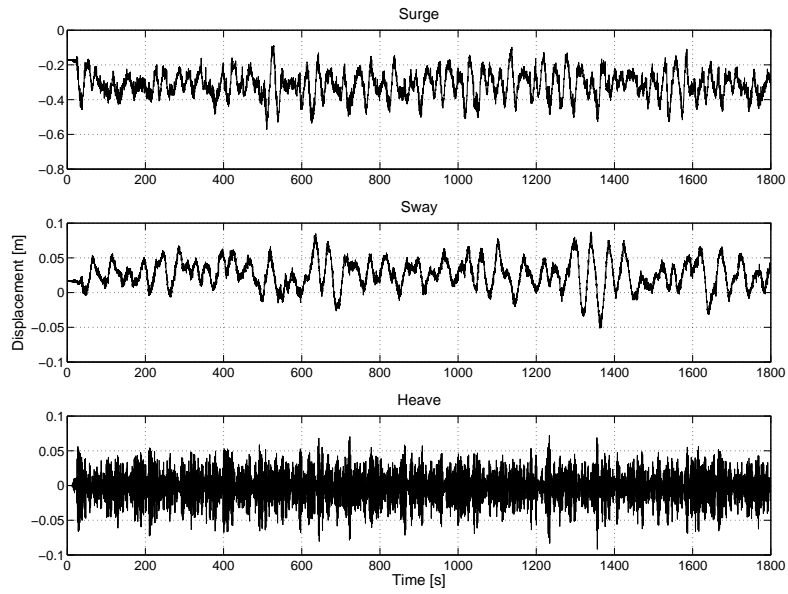


(a) Decay test time history for the Surge motion with test moorings (b) Decay test time history for the sway motion with test moorings

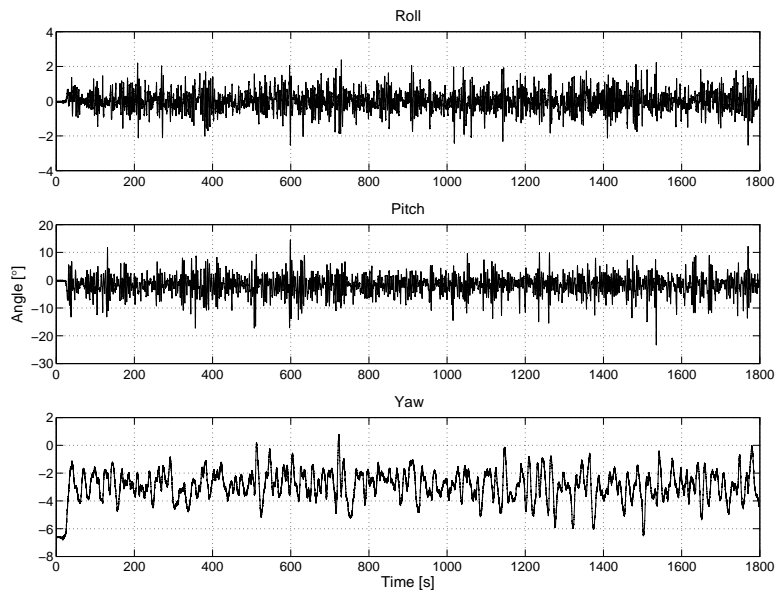


(c) Decay test time history for the heave motion with test moorings (d) Decay test time history for the pitch motion with test moorings

Figure B.1: Decay time histories for different motion modes for the test carried out at MarinTek

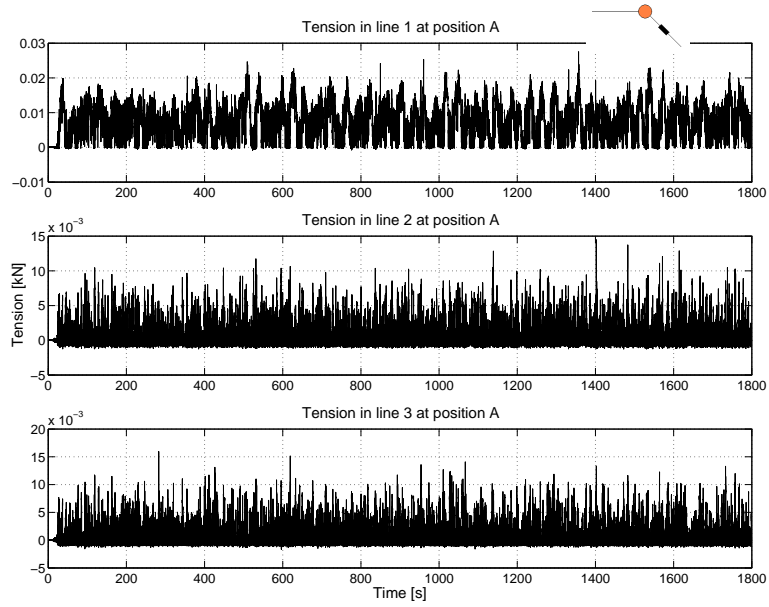


(a) Translational motions for test 3000

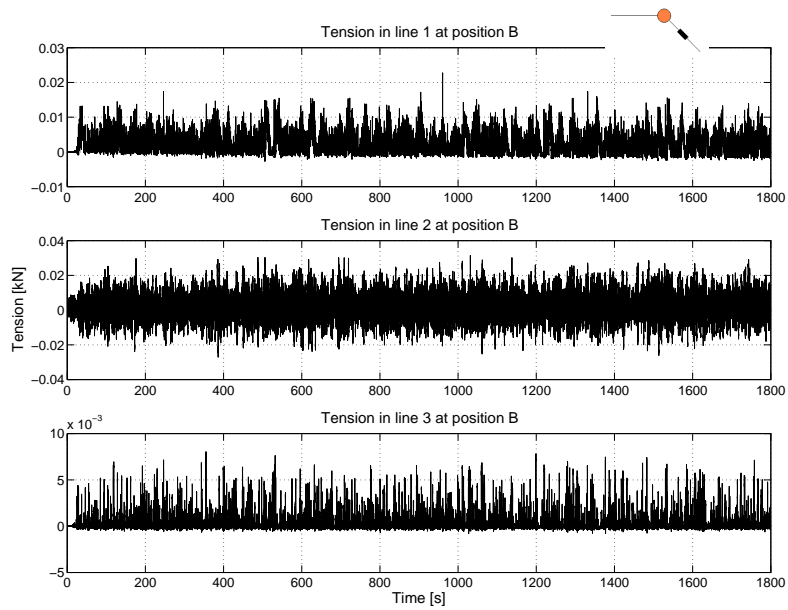


(b) Rotational motions for test 3000

Figure B.2: Motion response for test 3000

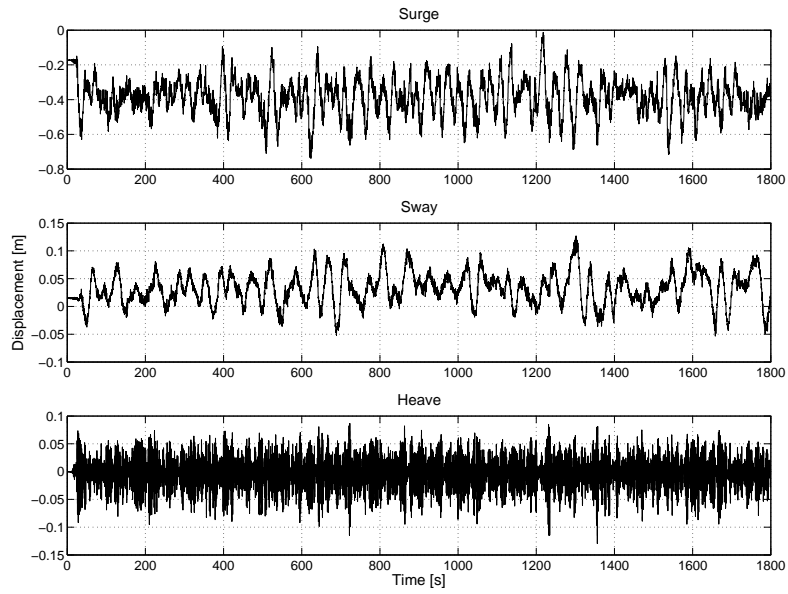


(a) Tension in mooring lines at position A for test 3000

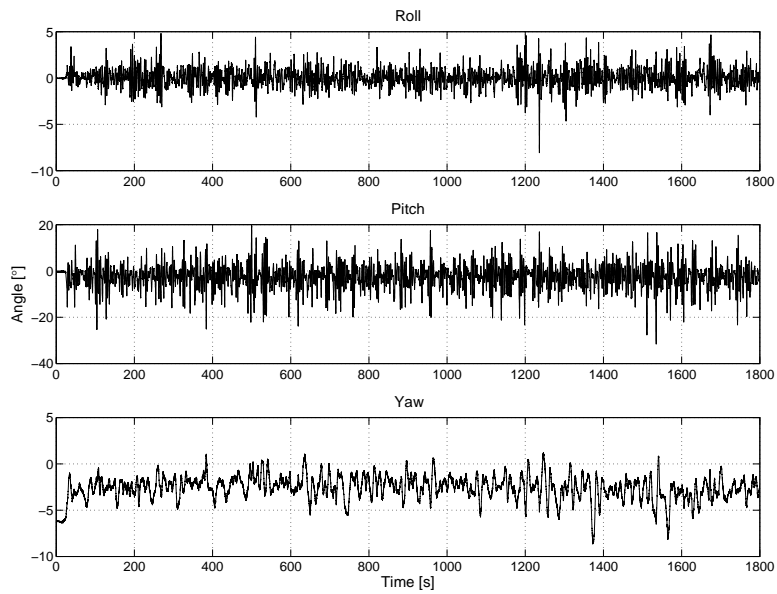


(b) Tensions in mooring lines at position B for test 3000

Figure B.3: Tension results for test 3000



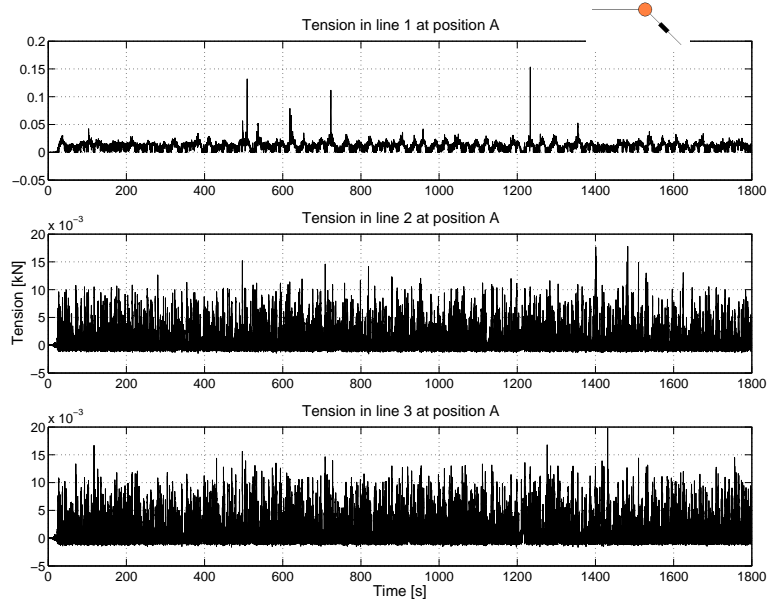
(a) Translational motions for test 3010



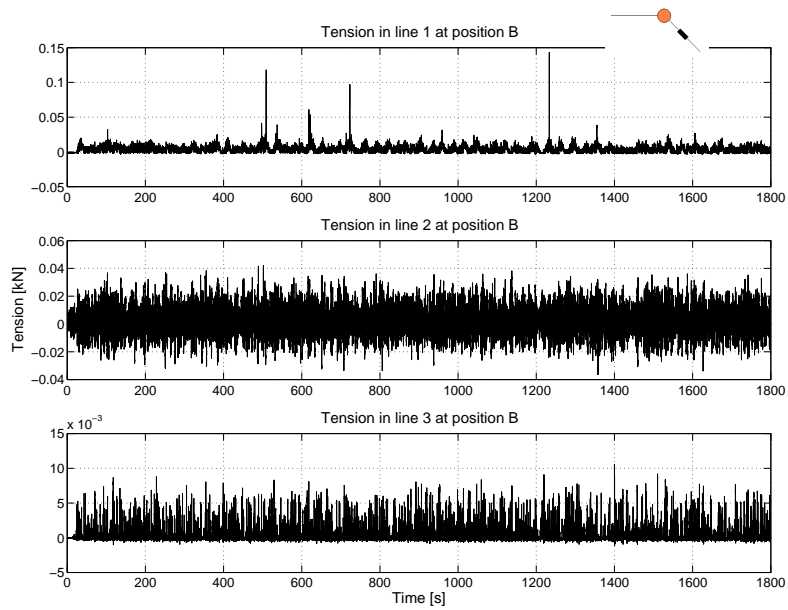
(b) Rotational motions for test 3010

Figure B.4: Motion results for test 3010



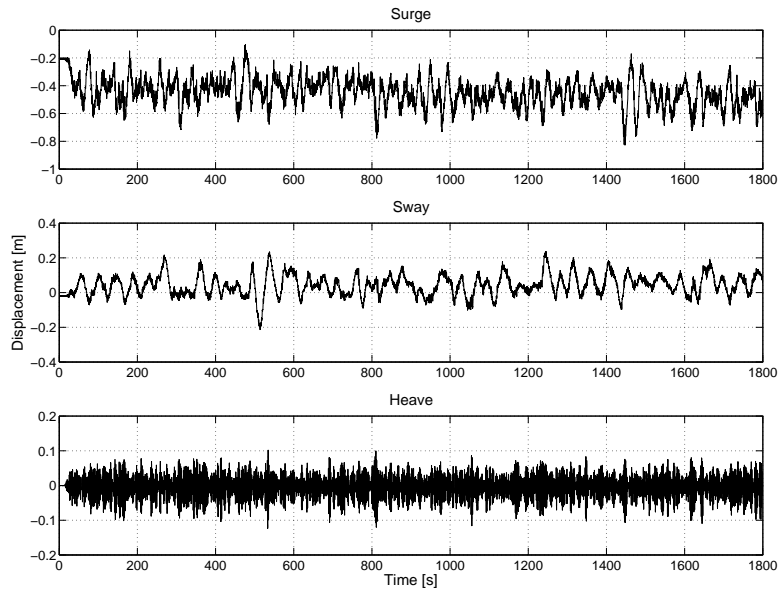


(a) Tension in mooring lines at position A for test 3010

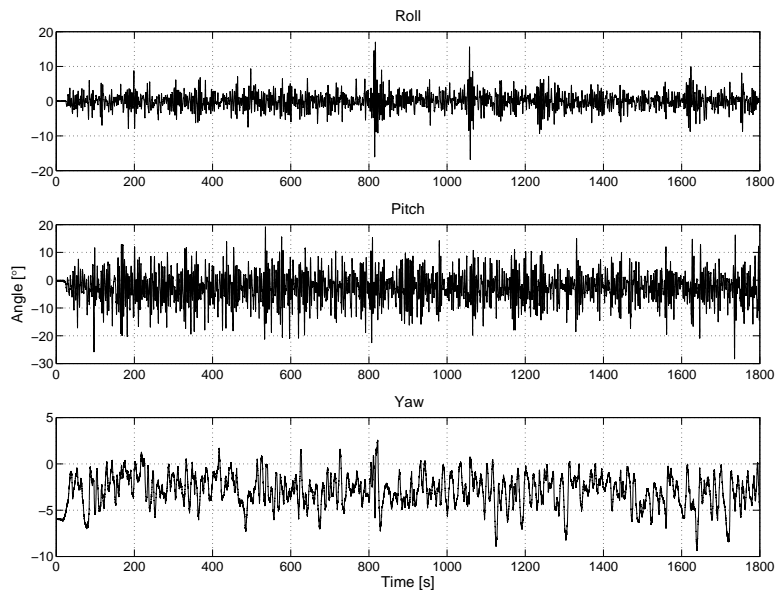


(b) Tensions in mooring lines at position B for test 3010

Figure B.5: Tension results for test 3010

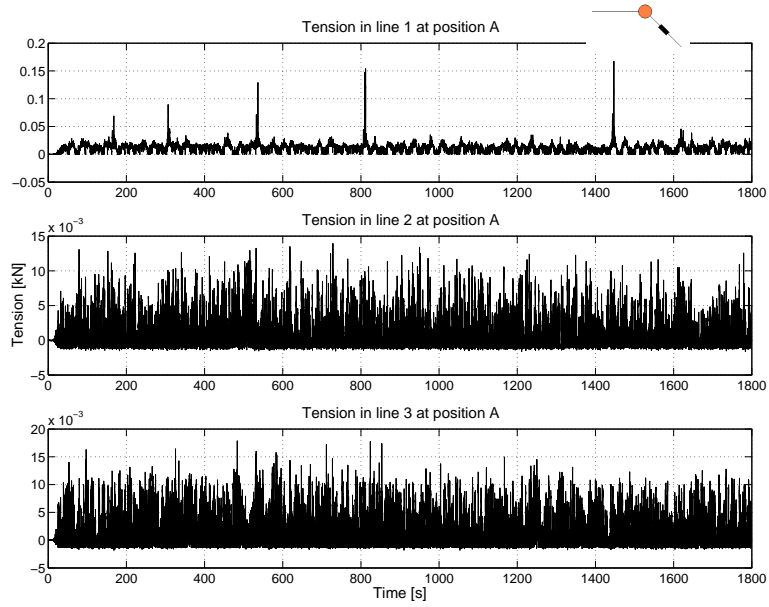


(a) Translational motions for test 3030

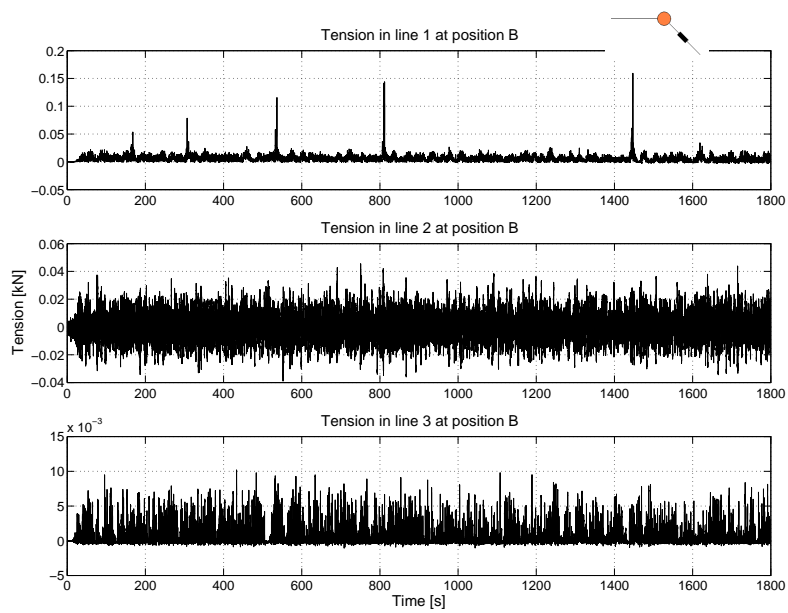


(b) Rotational motions for test 3030

Figure B.6: Motion results for test 3030

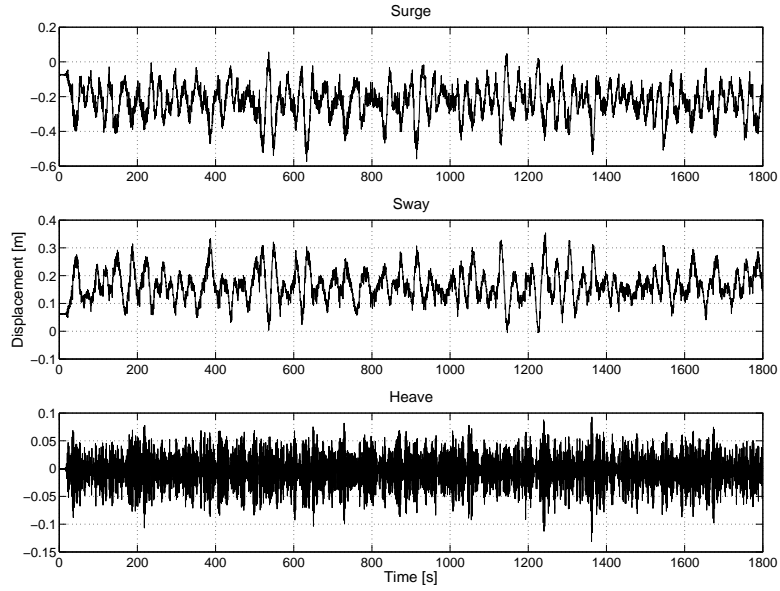


(a) Tension in mooring lines at position A for test 3030

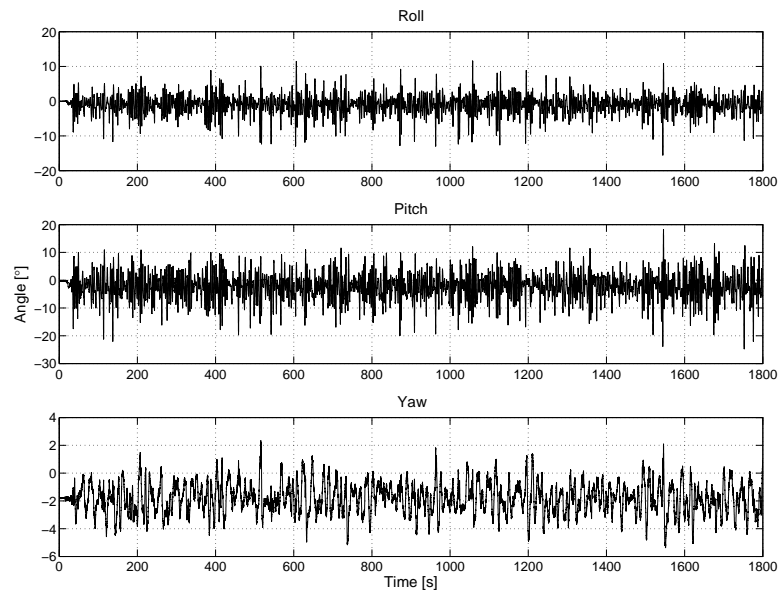


(b) Tensions in mooring lines at position B for test 3030

Figure B.7: Tension results for test 3030

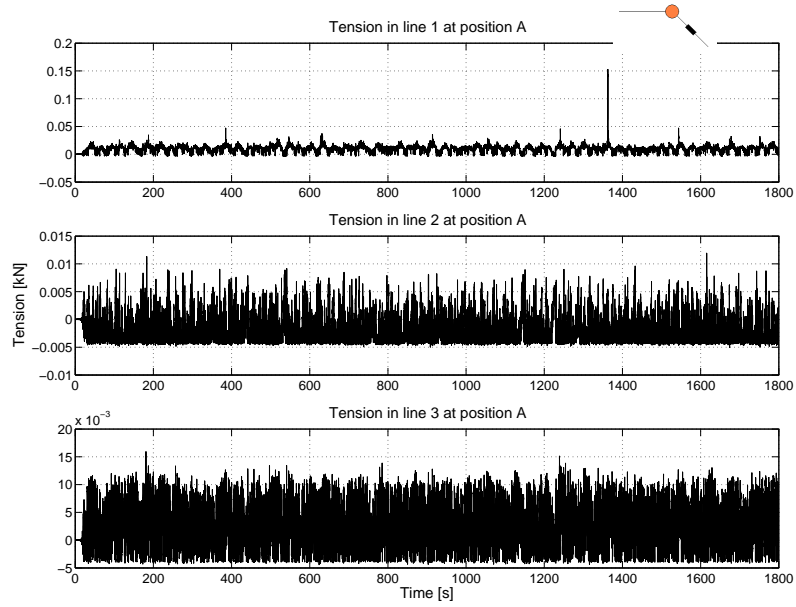


(a) Translational motions for test 3041

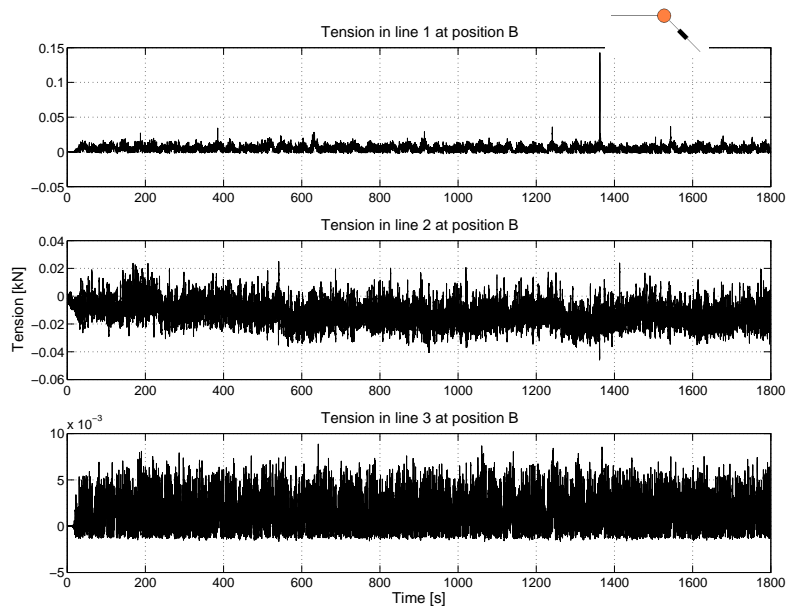


(b) Rotational motions for test 3041

Figure B.8: Motion results for test 3041



(a) Tension in mooring lines at position A for test 3041



(b) Tensions in mooring lines at position B for test 3041

Figure B.9: Tension results for test 3041

APPENDIX

C

RAOS

### C.1 RAOs

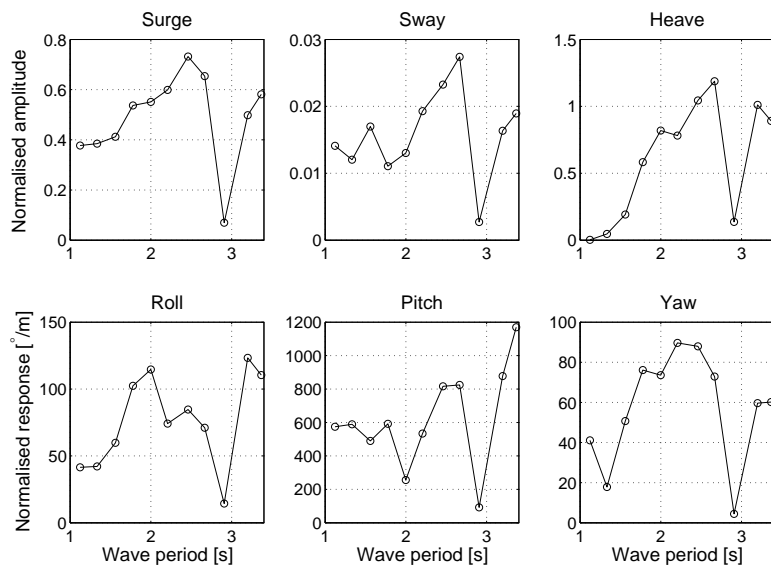


Figure C.1: RAO for WEC with moorings with wave paddle set to 100% gain

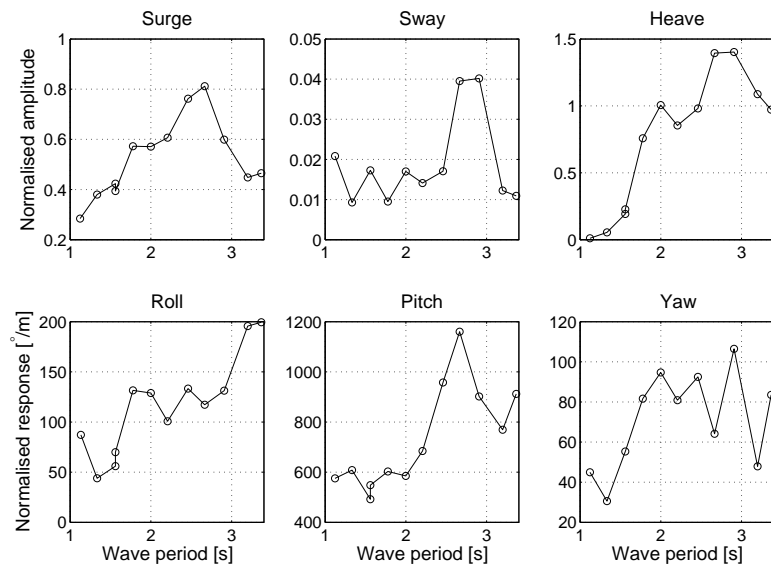


Figure C.2: RAO for WEC with moorings with wave paddle set to 50% gain

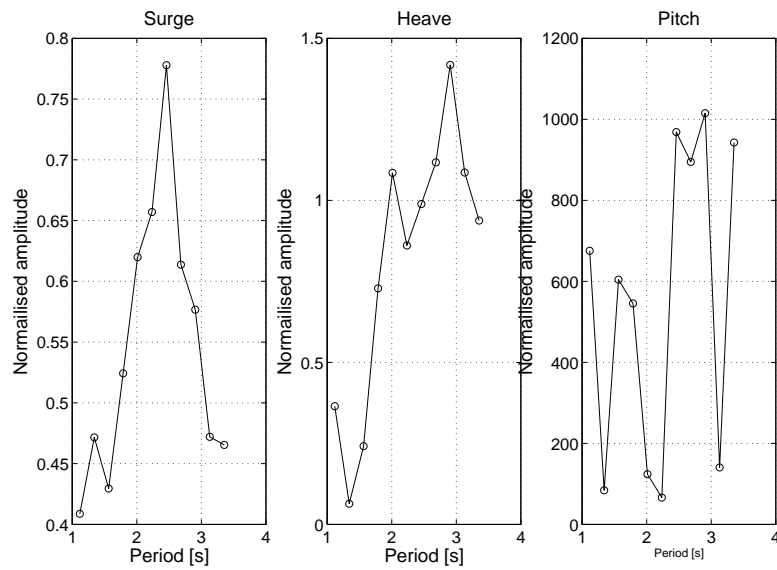


Figure C.3: RAO for WEC with soft mooring with wave paddle set to 50% gain

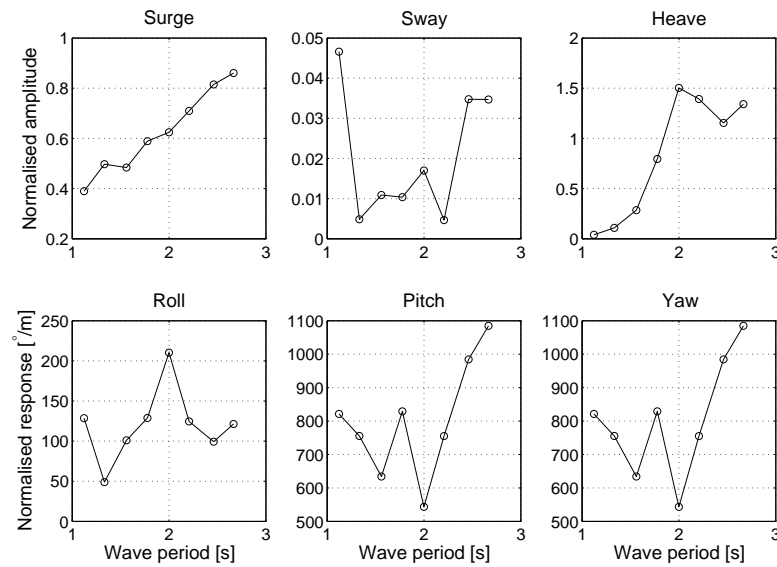


Figure C.4: RAO for WEC with soft mooring and closed orifice with wave paddle set to 50% gain



APPENDIX

D

GEOMETRIC DATA FILE FOR  
TRONDHEIM WEC

### D.0.1 Functions defining Shapes

The following function creates a disc used as a part of the model:

```

function [datafile] = GDFdisc(Radius,depth,type)
%% GDFdisc
%%%%%%%%%%%%%%%%%%%%%%%%%%%%%%%%%%%%%%%%%%%%%%%%%%%%%%%%%%%%%%%%%%%%%%%%
% GDFdisc creates a datafile containing corner coordinates for panels of a
%disc to be used in a GDF file. the inputs are as follows:
%
%                               Radius = outer radius of the cylinder
%
%                               depth  = is the depth that the disc
%                               will be in the model in relation to
%                               the water surface
%
%                               Type   = This defines weather the disc
%                               will be facing up or down where 2=up
%                               and 2=down
% Input the variables as follows:- output=GDFdisc(Radius,depth,type)

%% define constants
% first the range of angle theta the section of the shape is to be
% evaluated is defined. by default it is a quarter.
theta=(0:pi/32:(pi/2))';
x=[];
y=[];
for i=1:length(theta);
R=(0:Radius/8:Radius)';
x1=R*sin(theta(i));
y1=R*cos(theta(i));
x=[x,x1];
y=[y,y1];
end

```

```

datafile=[];

if type==1
%% Create Panels for down ward facing cylinder

for j=1:length(x)-1;
    for i=1:length(R)-1;
        xs=[x(i,j);x(i,j+1);x(i+1,j+1);x(i+1,j)];
        ys=[y(i,j);y(i,j+1);y(i+1,j+1);y(i+1,j)];
        zs=[-depth;-depth;-depth;-depth];
        datafile=[datafile;[ys,xs,zs]];
    end
end

else if type==2

    %% Create panels for upward facing cylinder
for j=1:length(x)-1;
    for i=1:length(R)-1;
        xs=[x(i+1,j);x(i+1,j+1);x(i,j+1);x(i,j)];
        ys=[y(i+1,j);y(i+1,j+1);y(i,j+1);y(i,j)];
        zs=[-depth;-depth;-depth;-depth];
        datafile=[datafile;[ys,xs,zs]];
    end
end
end
end

plot3(datafile(:,1),datafile(:,2),datafile(:,3))

```

The following function creates a cylinder wall used as part of the model:

```

function [datafile] = GDFcylrwall(Radius,draft,thickness,type)
%% GDFcylrwall
%%%%%%%%%%%%%%%%%%%%%%%%%%%%%%%%%%%%%%%%%%%%%%%%%%%%%%%%%%%%%%%%%%%%%%%%
% GDFcylrwall creates a variable "datafile" containing corner coordinates
%for panels of a cylinder wall to be used in a GDF file. The corners of the
%panels are defined using a right hand cartesian system to define the
%dirctionallity of the panel
%
%       The inputs are as follows:
%
%                               Radius = outer radius of the cylinder
%
%                               draft  = is the depth of the lowest point
%                               of the wall
%
%                               Type   = This defines weather the wet
%                               face of the wall is facing out or in
%                               where 1=out and 2=in
%
%
%Input variables as follows:-output=GDFcylrwall(Radius,draft,thickness,type)
%%%%%%%%%%%%%%%%%%%%%%%%%%%%%%%%%%%%%%%%%%%%%%%%%%%%%%%%%%%%%%%%%%%%%%%%

%% Define ranges
% First the range of angle theta the section of the shape is to be
% evaluated over is defined.

theta=(0:pi/32:(pi/2))';

x=[];
y=[];
z=(-draft:((thickness)/10):(-draft+thickness))';

```

```

%% Create data points for the cylinder
%The data points for the cylinder are created using the  $x=R*\sin(\theta)$  and
% $y=R*\cos(\theta)$  and the z coordinate is defined later.

for i=1:length(theta);
R=(0:Radius/8:Radius)';
x1=R*sin(theta(i));
y1=R*cos(theta(i));
x=[x,x1];
y=[y,y1];
end
datafile=[];

if type==1
%% Create outward facing wall
% The data points are selected in a clockwise fashion to define that the
% wall is facing out.

B=length(R);
for j=1:length(x)-1;
    for i=1:length(z)-1;
        xs=[x(B,j);x(B,j+1);x(B,j+1);x(B,j)];
        ys=[y(B,j);y(B,j+1);y(B,j+1);y(B,j)];
        zs=[z(i);z(i);z(i+1);z(i+1)];
        datafile=[datafile;[ys,xs,zs]];
    end
end

%% Create inward facing wall
% The data points are selected in a anti-clockwise fashion to define that the
% wall is facing out.

else if type==2

```

```

B=length(R);
for j=1:length(x)-1;
    for i=1:length(z)-1;
        xs=[x(B,j);x(B,j+1);x(B,j+1);x(B,j)];
        ys=[y(B,j);y(B,j+1);y(B,j+1);y(B,j)];
        zs=[z(i+1);z(i+1);z(i);z(i)];
        datafile=[datafile;[ys,xs,zs]];
    end
end
end
end
end
plot3(datafile(:,1),datafile(:,2),datafile(:,3))

```

The following function creates a ring used as part of the model:

```

function[datafile] = GDFring(outerR,innerR,depth,type)
%% GDFring
%%%%%%%%%%%%%%%%%%%%%%%%%%%%%%%%%%%%%%%%%%%%%%%%%%%%%%%%%%%%%%%%%%%%%%%%
% GDFring creates a variable "datafile" containing corner coordinates
%for panels of a ring to be used in a GDF file. The corners of the
%panels are defined using a right hand cartesian system to define the
%directionality of the panel
%
%           The inputs are as follows:
%
%           outerR = outer radius of the ring
%
%           innerR = the inner radius of the
%           ring
%
%           depth = is the depth that the disc
%           will be in the model in relation to
%           the water surface
%

```

```

%                                     Type = This defines weather the disc
%                                     will be facing up or down where 1=up
%                                     and 2=down
%
% Input the variables as follows:- output=GDFdisc(Radius,depth,type)
%%%%%%%%%%%%%%%%%%%%%%%%%%%%%%%%%%%%%%%%%%%%%%%%%%%%%%%%%%%%%%%%%%%%%%%%

%% Define ranges
% First the range of angle theta the section of the shape is to be
% evaluated over is defined.

theta=(0:pi/32:(pi/2))';

x=[];

y=[];

%% Create data points for the cylinder
%The data points for the cylinder are created using the x=R*sin(theta) and
%y=R*cos(theta) and the z coordinate is defined by the input depth.

for i=1:length(theta);
R=(innerR:(outerR-innerR)/8:outerR)';
x1=R*sin(theta(i));
y1=R*cos(theta(i));
x=[x,x1];
y=[y,y1];
end
datafile=[];

if type==2
%% Create Panels for down ward facing ring

```

```

    for j=1:length(x)-1;
        for i=1:length(R)-1;
            xs=[x(i,j);x(i,j+1);x(i+1,j+1);x(i+1,j)];
            ys=[y(i,j);y(i,j+1);y(i+1,j+1);y(i+1,j)];
            zs=[-depth;-depth;-depth;-depth];
            datafile=[datafile;[ys,xs,zs]];
        end
    end

else if type==1
%% Create panels for upward facing ring
    for j=1:length(x)-1;
        for i=1:length(R)-1;
            xs=[x(i+1,j);x(i+1,j+1);x(i,j+1);x(i,j)];
            ys=[y(i+1,j);y(i+1,j+1);y(i,j+1);y(i,j)];
            zs=[-depth;-depth;-depth;-depth];
            datafile=[datafile;[ys,xs,zs]];
        end
    end
end
end

end

plot3(datafile(:,1),datafile(:,2),datafile(:,3))

```

The following scriped was used to call the different shape defining functions to make a variable called “ini” which is the final shape to be modeled in WAMIT:

```

figure
hold on
OWC=GDFdisc(0.3,0,2);           % Free surface of the internal OWC

```



```

INC=GDFcyldrwall(0.3,0.4,0.4,2);      % Inner cylinder wall

OUTC=GDFcyldrwall(0.4,0.4,0.4,1);    % Outter cylinder wall

RING=GDFring(0.4,0.3,0.4,2);        % Bottom ring fo the cylinder

TOPP=GDFdisc(0.4,0.7,2);            % Top of damping plate

WALLP=GDFcyldrwall(0.4,0.71,0.01,1); % Thin wall of damping plate

BOTTOMP=GDFdisc(0.4,0.71,1);        % Bottom of damping plate

ini=[INC;OUTC;RING;TOPP;WALLP;BOTTOMP];% Concatonation of the different parts
                                     %of the model

```

The folowing function saves the file named “ini” as a “.gdf” file creating the headers from the inputs as follows:

```

function [] = SaveGDF(datafile,ULEN,GRAV,ISX,ISY,Shape_Name)
%% SaveGDF
%%%%%%%%%%%%%%%%%%%%%%%%%%%%%%%%%%%%%%%%%%%%%%%%%%%%%%%%%%%%%%%%%%%%%%%%
% SaveGDF saves a .gdf file to the workspace containing data from a
% a number of formated shapes concatonated into one file for use with WAMIT
%%%%%%%%%%%%%%%%%%%%%%%%%%%%%%%%%%%%%%%%%%%%%%%%%%%%%%%%%%%%%%%%%%%%%%%%
%
%The inputs of the function are designes to create the shape and the
%headers required by WAMIT as follows:
%
%                                datafile = input x,y,z file of panels
%                                from GDFcreate
%
%                                ULEN = Unit length of coordinates used in relation
%                                to units used for gravity
%
%                                GRAV = Acceleration due gravity in same units as ULEN

```

```

%
%           ISX = Symmetry index (1/0 = symmetric/asymmetric)
%           in the x axis.
%
%           ISY = Symmetry index (1/0 = symmetric/asymmetric)
%           in the y axis
%
%           Shape_Name = this is an 87 character
%           description which also forms the name of the file.
%
%
%
% Input data as follows:- SaveGDF(datafile,ULEN,GRAV,ISX,ISY,header)
%%%%%%%%%%%%%%%%%%%%%%%%%%%%%%%%%%%%%%%%%%%%%%%%%%%%%%%%%%%%%%%%%%%%%%%%
%%%%%%%%%%%%%%%%%%%%%%%%%%%%%%%%%%%%%%%%%%%%%%%%%%%%%%%%%%%%%%%%%%%%%%%%

NEQN=(length(datafile))/4;

fid=fopen([Shape_Name,'.gdf'],'w');
fprintf(fid,'%s\r\n',Shape_Name);
fprintf(fid,'%f %f\r\n%-1.0f %1.0f\r\n%f\r\n',ULEN,GRAV,ISX,ISY,NEQN);
fclose(fid);
fid = fopen([Shape_Name,'.gdf'], 'a');
for i=1:length(datafile);
    fprintf(fid,'%f %f %f\r\n',datafile(i,1),datafile(i,2),datafile(i,3));
end
fclose(fid);
fclose all;

```

APPENDIX

E

NUMERICAL RAOS OF SIMPLE  
CYLINDERS

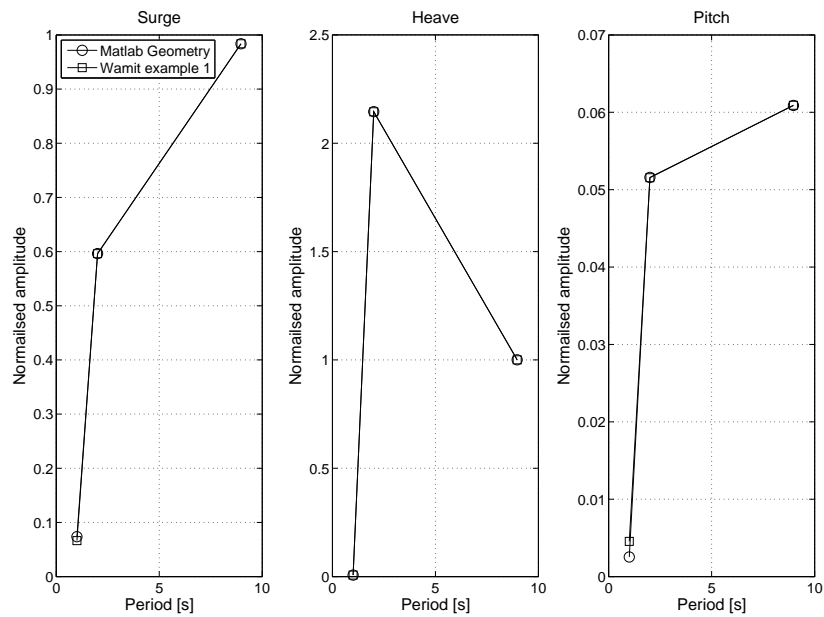


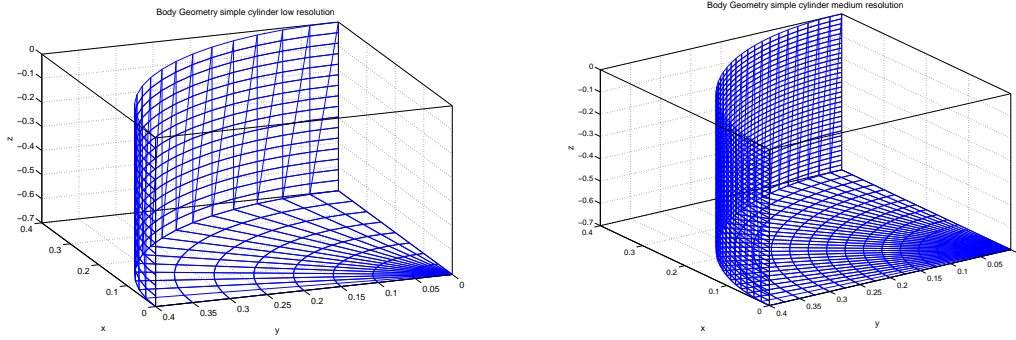
Figure E.1: Comparison of RAO results from WAMIT example 1 and Matlab generated geometry

### E.0.2 Simple Cylinder

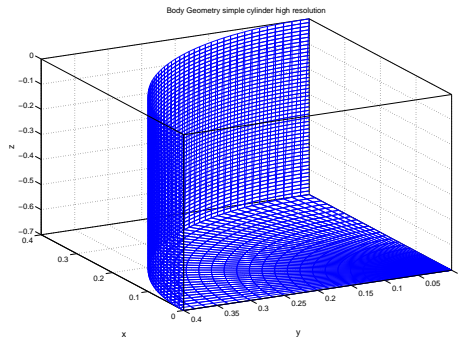
The simple cylinder is a model that can be found in the examples provided by WAMIT. In the example the model uses the lower order method to describe the geometric data. Figure E.1 shows the Response amplitude operators from the WAMIT example model and the model using the MatLab routines to generate the body geometry. The results are the very close in agreement showing that the method of generating the body geometry from the Matlab routines is acceptable.

### E.0.3 Modified simple cylinder

The model size, mass matrix and wave periods for the simulation are modified to reflect the conditions of the experimental work in this project. For this series of runs three different geometry files are used where the resolution of discretisation increases. This means the use of geometric data files consisting of 384, 1536 and 3456 panels for the low, medium and high resolution respectively. Figure E.2 shows the wire frames of the quadrant to be reflected in the x and y axis at the different resolutions. These files were created in Matlab and need to be checked before running them in a simulation to ensure that the panels have



(a) Simple cylinder wire frame geometry with low resolution panellization (b) Simple cylinder wire frame geometry with medium resolution panellization

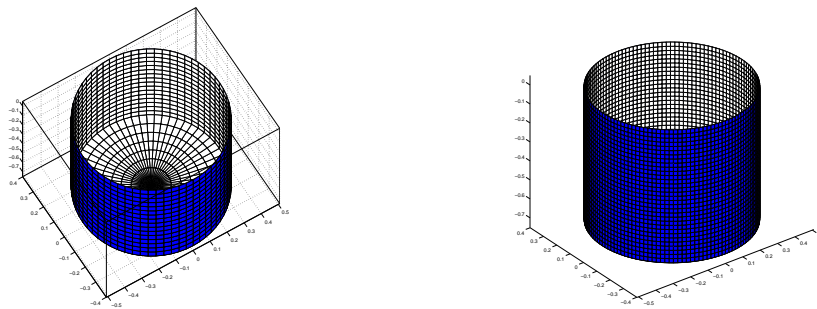


(c) Simple cylinder wire frame geometry with high resolution panellization

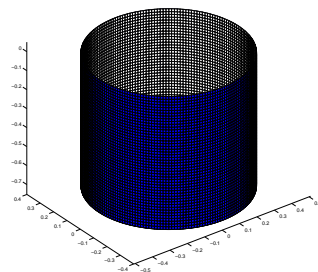
Figure E.2: Wire frame models of the quadrant for simple cylinder geometry

the correct orientation. Figure E.3 shows the geometry reflected in the x and y axis to make the complete shape geometry where the blue colouration indicates the “wet side” of the panels.

Figure E.4 shows a comparison of the RAOs from the models with different discretisation resolution which indicates convergence on the response amplitude of the body. As done by Payne (2006) the error between the simulations and the highest resolution simulation are presented (E.5). The results show good convergence for the cylinder giving confidence in the model. This also indicates the importance of resolution in the penalization of the body geometry.



(a) Simple cylinder geometry with low resolution panellization panel orientation check      (b) Simple cylinder geometry with medium resolution panellization orientation check



(c) Simple cylinder geometry with high resolution panellization orientation check

Figure E.3: Full geometry for simple cylinder model

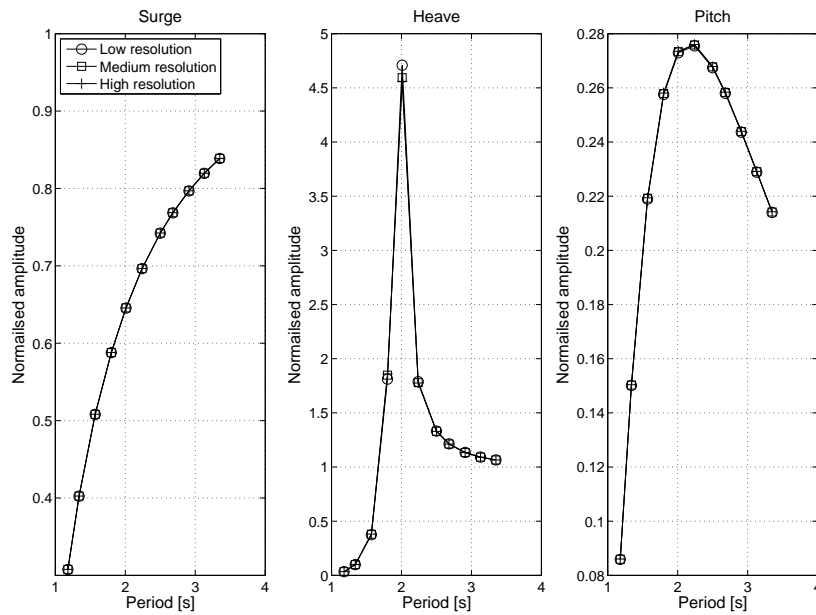


Figure E.4: Comparison of WAMIT calculated RAO's for a cylinder using low medium and high resolution

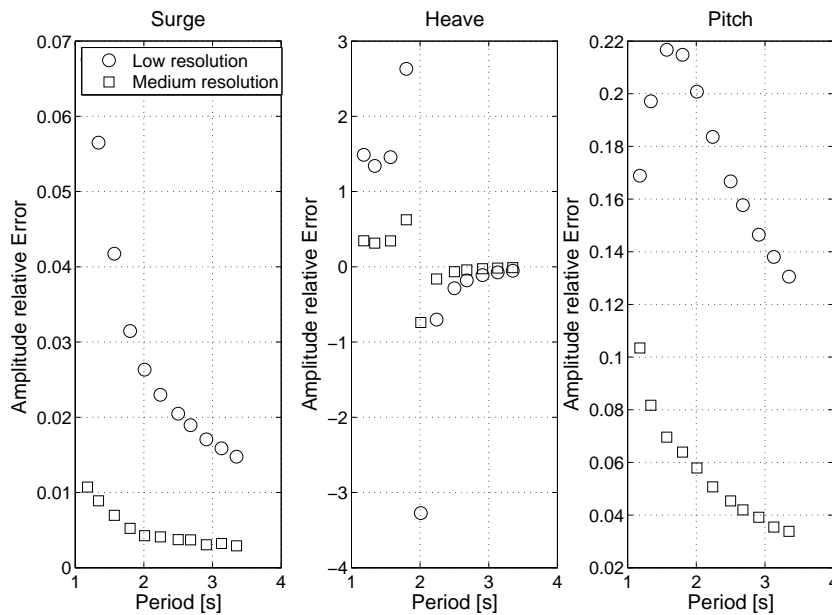


Figure E.5: Percentage error between simulations and the high resolution simulation

# BIBLIOGRAPHY

- Ashton, I., Johanning, L., 2009. Measurement of the effect of power absorption in the lee of a wave energy converter. In: Proceedings of the ASME 28th International Conference on Ocean, Offshore and Arctic Engineering , Honolulu, Hawaii.
- Bartrop, N. D. P., 1998. Floating Structures: a guide for design and analysis (Volume 2). Oilfield Publications Limited.
- Bauduin, C., Naciri, M., 2000. A contribution on quasi-static mooring line damping. Offshore Mechanics and Arctic Engineering 122, 125 – 133.
- British-Standards, 1989. Code of practice for maritime structures: Design of inshore mooring and floating structures. Tech. rep., British Standards Institute.
- Brown, D. T., Mavrakos, S., 1999. Comparative study on mooring line dynamic loading. Marine Structures 12, 131–151.
- Bryden, I., Linfoot, B., 2010. Wave and current testing of an array of wave energy converters. In: Proceedings of the HydraLab III joint user meeting,.
- Chakrabarti., S. K., 2001. Hydrodynamics of offshore structures. WIT Press.
- Chakrabarti, S. K., 2005. Handbook of offshore engineering (Volume 1). ELSEVIER.



- C.H.Lee, 1995. WAMIT theory manual. Massachusetts Institute of Technology, available from [www.wamit.com](http://www.wamit.com).
- Davies, P., Reaud, Y., Dussud, L., Woerther, P., 2011. Mechanical behaviour of hmpe and aramid fibre ropes for deep sea handling operations. *Ocean Engineering* 38, 2208–2214.
- DNV-RP-C205, 2010. Environmental conditions and environmental loads. Tech. rep., DNV.
- DNV-RP-H103, 2011. Modelling and analysis of marine operations. Tech. rep., DNV.
- Ecotricity, 2012. Seamills.  
URL <http://www.ecotricity.co.uk/>
- Faltinsen, O., 1990. Sea loads on ships and offshore structures. Cambridge University Press.
- Fitzgerald, J., 2009. Position mooring of wave energy converters- an engineering study into the mooring of structures in a highly exposed shallow ocean regime, within the context of the economics of renewable energy conversion. Ph.D. thesis, Department of Civil and Environmental Engineering Chalmers University of Technology.
- Fitzgerald, J., Bergdahl, L., 2007. Including moorings in the assessment of a generic offshore wave energy converter: A frequency domain approach. *Marine Structures* 21, 23–46.
- Flory, J. F., Ahjem, V., Banfield, S. J., 2007. A new method of testing for change-in-length properties of large fiber-rope deepwater mooring lines. In: *Offshore Technology Conference*, Houston, Texas.
- Flory, J. F., Banfield, S. P., Petruska, D. J., 2004. Defining, measuring and calculating the properties of fibre rope deepwater moorings. In: *Offshore Technology Conference*, Houston, Texas U.S.A.
- Halrow, 2006. Wave hub development and design phase coastal processes study report. Tech. rep., Halrow group ltd.
- Harris, R. E., Johanning, L., Wolfram, J., 2004. Mooring systems for wave energy converters: A review of design issues and choices. In: *3rd International Conference on Marine Renewable Energy*.

- Haver, S. K., 2010. Lecture in “design of offshore structures”, ntnu, trondheim.
- Huse, E., 1991a. Methods for numerical prediction of mooring line damping. Tech. rep., MarinTek, Trondheim.
- Huse, E., 1991b. New developments in prediction of mooring system damping. In: Offshore Technology Conference, Houston, Texas.
- Huse, E., Matsumoto, K., 1988. Practical estimation of mooring line damping. In: Offshore Technology Conference, Houston, Texas.
- Johanning, L., Smith, G. H., 2005. Towards design standards for wec moorings. In: European Wave and Tidal Energy Conference, Glasgow.
- Johanning, L., Smith, G. H., 2006. Comparison of simulation and test results for a generic moored wec using a catenary mooring arrangement. In: International conference OCEAN ENERGY.
- Johanning, L., Smith, G. H., 2008a. Improved measurement technologies for floating wave energy converter (wec) mooring arrangements. *International Journal of the Society for Underwater Technology* 27,N.o4, 1–10.
- Johanning, L., Smith, G. H., 2008b. Station keeping study for wec devices including compliant chain, compliant hybrid and taut arrangement. In: Offshore Mechanics and Arctic Engineering.
- Johanning, L., Smith, G. H., Bullen, C., 2007a. Large scale mooring line experiments and comparison with a fully dynamic simulation program with importance to wec installation. In: International Offshore and Polar Engineering Conference Lisbon, Portugal.
- Johanning, L., Smith, G. H., Wolfram, J., 2006a. Interaction between mooring line damping and response frequency as a result of stiffness alteration in surge. In: Offshore Mechanics and Arctic Energy (OMAE), Hamburg, Germany.
- Johanning, L., Smith, G. H., Wolfram, J., 2006b. Mooring design approach for wave energy converters. *Proceedings of the I MECH E Part M* 220, 159–174.
- Johanning, L., Smith, G. H., Wolfram, J., 2007b. Measurements of static and dynamic mooring line damping and their importance for floating wec devices. *Ocean Engineering* 34, 1918–1934.

- Johanning, L., Wolfram, J., 2005. Challenging tasks on moorings for floating wecs. In: International Symposium on Fluid Machinery for Wave and Tidal Energy: State of the Art and New Developments, London, Uk.
- Johanning, L., Wolfram, J., Smith, G. H., Harris, R. E., 2006c. Importance of mooring line damping for wec's. Tech. rep., Heriot-Watt University, Edingburgh, UK.
- Kitney, N., Brown, D. T., 2001. Experimental investigation of mooring line loading using large and small scale models. *Offshore Mechanics and Arctic Engineering* 123, 1–9.
- Lee, C. H., Newman, J. N., Nielsen, F. G., Lee:1996. Wave interactions with an oscillating water column. In: International Offshores and Polar Engineering Conference, LA,.
- Liu, Y., Bergdahl, L., 1999. On combination formulae for the extremes of wave-frequency and low-frequency responses. *Applied Ocean Research* 21, 41–46.
- Loukogeorgaki, E., Angelides, D. C., 2005. Stiffness of mooring lines and performance of floating breakwater in three dimensions. *Applied Ocean Research* 27, 187–209.
- Marlow, ropes, E. E., 2006. Extension data. Tech. rep., [www.marlowropes.com](http://www.marlowropes.com).
- MetOffice, 2008. Atlas of uk marine renewable energy resources - a strategic environmental assessment report. Tech. rep., ABPmer and The Met Office and Proudman Oceanographic Laboratory.
- OS-E301, D., 2001. Position mooring. Tech. rep., DNV.
- Parkin, P., Taylor, J. R. M., 2005. Tank power capture measurements on a free-floating slope ips buoy. In: 6th European Wave and Tidal Energy Conference Glasgow UK.
- Payne, G. S., 2006. Numerical modeling of a sloped wave energy device. Ph.D. thesis, University of Edinburgh.
- Rapaka, E. V., Natarjan, R., Neelamani, S., 2004. Experimental investigation on the dynamic response of a moored wave energy device under regular sea waves. *Ocean Engineering* 31, 725–743.
- Sumer, B., Fredsøe, J., 2006. Hydrodynamics around cylindrical structures - revised edition. World Scientific Publishing.Co.Pte.Ltd.

- Thies, P. R., Johanning, L., Smith, G. H., 2011. Assessing loading regimes and failure modes of marine power cables in marine energy applications. In: *Advances in Risk and Reliability Technology Symposium*, Stratford-upon-Avon, UK.
- Thies, P. R., Johanning, L., Smith, G. H., 2012. Lifecycle fatigue load spectrum estimation for mooring lines of a floating marine energy converter. In: *ASME 2012 31st International Conference on Ocean, Offshore and Arctic Engineering (OMAE)*, Rio De Janeiro, Brazil, 1st - 6th Jul 2012.
- Thorpe, T. W., 1999. An overview of wave energy technologies: Status performance and costs. In: *Wave Power - Moving Towards Commercial Viability*, IMECHE Seminar, London, UK.
- Trust, C., 2005. Guidelines on design and operation of wave energy converters. Tech. rep., Carbon Trust.
- Tucker, M. J., Pitt, E. G., 2001. *Waves in ocean engineering*. Elsevier.
- Vickers, A. W., Johanning, L., 2009. Comparison of damping properties for three different mooring arrangements. In: *8th European Wave and Tidal Energy Conference*, Upsala, Sweden.
- Webster, W. C., 1995. Mooring-induced damping. *Ocean Engineering* 22 (6), 571–591.